POLITECNICO DI MILANO

Scuola di Ingegneria Industriale e dell'Informazione
Corso di Laurea Magistrale in Ingegneria Biomedica

POLITECNICO
MILANO 1863

Design and implementation of a robotic prototype for the control of a flexible ureteroscope

Relatore: Prof. Elena De Momi
Correlatore: Prof. Álvaro Gutiérrez Martín

Tesi di laurea di:

Federico Nasi Matr. 878729

Anno Accademico 2017 – 2018

CONTENTS

List of Figures

List of Tables

Sommario

La presenza di calcoli nel sistema urinario umano è diventato un problema di notevole entità con alti livelli di diffusione in gran parte del mondo occidentale e in Italia. Diverse soluzioni tecnologiche sono state sviluppate nel corso degli anni per la cura e il trattamento di questa patologia. Negli ultimi anni la tecnica maggiormente diffusa e consigliata dagli urologi è la uretroscopia flessibile. Questa è una tecnica mininvasiva che consiste nell'inserimento di uno strumento chirurgico (uretroscopio) attraverso orifizi naturali, in questo caso l'uretra, per raggiungere le parti più profonde del sistema urinario (ureteri e reni) dove si localizzano i calcoli. Problemi ergonomici e posturali sono stati riscontrati nei chirurghi che attuano questo tipo di tecnica nel quotidiano, creando disturbi e lesioni permanenti nel personale sanitario. Grazie allo sviluppo della robotica chirurgica si sono sviluppate perciò soluzioni che prevedono il controllo dell'uretroscopio attraverso un sistema robotico.

Il progetto LITHOS, nel quale si colloca questo lavoro di tesi, prevede lo sviluppo di un sistema di controllo robotico per un uretroscopio commerciale, con la finalità di risolvere i problemi ergonomici riscontrati e favorire la diffusione di questa promettente tecnica.

Lo scopo principale di questo lavoro è quello di progettare e creare un prototipo di sistema robotico per il controllo di un uretroscopio, che consenta ai chirurghi di operare a distanza e in una posizione comoda, annullando il rischio di lesioni muscolari o esposizioni alle radiazioni.

Durante questa tesi di laura, l'autore ha progettato e sviluppato le diverse parti meccaniche che si collegano all'uretroscopio, configurato l'hardware per la gestione dei motori che muovono le diverse parti meccaniche, implementato il firmware che controlla i motori e il software ad uso dell'utente. Questo sistema ha tre gradi di libertà, e ogni singolo grado necessita la progettazione di soluzioni meccaniche per il controllo di quel preciso movimento. Inoltre, si è reso necessario progettare un sistema di controllo per lo strumento che possa consentire all'utente di realizzare i movimenti preposti da una posizione ergonomicamente vantaggiosa. Il prototipo è stato progettato in ogni sua parte meccanica e hardware e si sono sviluppati firmware per la comunicazione tra i vari elementi del dispositivo e la raccolta di dati.

Viene inoltre progettata una prima interfaccia grafica che rende possibile all'utente il monitoraggio delle prestazioni del robot.

Un'analisi statistica sul prototipo finito è stata necessaria per studiare le prestazioni e riscontrare problemi sulle soluzioni tecnologiche implementate. Il prototipo deve infatti rispettare alcune specifiche base, circa il suo range di movimento e la sua precisione. Sono stati perciò calcolati o stimati i range di movimento che ciascuno grado di libertà può eseguire e la precisione con il quale questi movimenti avvengono. Si richiedeva che il cavo dell'uretroscopio potesse

percorrere l’intero sistema urinario, circa 50/55 cm. Un range di 51,5 cm viene ottenuto. Inoltre, lo strumento doveva poter ruotare di 360° intorno al proprio asse e la leva che controlla il movimento della punta deve potere traslare di 90°. Valori oltre i 360° e vicini ai 90° vengono ottenuti per questi movimenti. L’accuratezza inoltre viene valutata per ogni grado di libertà, ottenendo valori di 0,51 cm per il movimento di inserimento del cavo endoscopico, 0,38° per la rotazione dello strumento intorno al proprio asse, 4,67° per il movimento della leva di controllo della punta. Valori che possono ritenersi migliorati o vicini rispetto alla precisione ottenibile con il controllo manuale dello strumento. L’analisi statistica ha portato inoltre alla scoperta e allo studio di alcune problematiche, dovute alla tecnologia meccanica progettata.
Parole chiave: uretroscopia flessibile, robotica chirurgica, disegno meccanico, periferica di controllo, comunicazione seriale, interfaccia grafica utente, range di movimento, precisione di movimento.

Abstract

Kidney stones in the human urinary system has become a notable problem with high levels of diffusion in most of the western world and in Italy. Several technological solutions have been developed over the years for the treatment of this pathology. In recent years the most widespread technique recommended by urologists is flexible urethroscopy. It is a minimally invasive technique which consists in inserting a surgical instrument (ureteroscope) through natural orifices, in this case the urethra, to reach the deepest parts of the urinary system (ureters and kidneys) where the kidney stones are located. Ergonomics and postural problems have been found in surgeons who exploit this technique in everyday work, creating ailments and permanent injuries in clinicians. Thanks to the development of surgical robotics, solutions have been developed that involve the control of the ureteroscope through a robotic system.

The LITHOS project, where this master's thesis is framed, involves the development of a robotic control system for a commercial ureteroscope, with the aim of solving the ergonomic problems encountered and favouring the diffusion of this promising technique.

The main purpose of this work is to design and implement a prototype robotic system for the control of an ureteroscope, which allows the surgeons to remotely operate in a comfortable position without the risk of muscle injuries and exposures to radiation.

During this MSc Thesis, the author has designed, developed and implemented the mechanical design to attach to the ureteroscope, configured the hardware to be connected to the motors that attached to the mechanical parts, implemented the firmware controlling the motors and the software on the computer for the surgeons testing. This system has three degrees of freedom, and every single degree of freedom requires the design of mechanical solutions to control that movement. Furthermore, it was necessary to design a control system for the instrument that could allow the user to perform the movements in an ergonomically advantageous position. The prototype has been designed in all its mechanical and hardware parts and firmware has been developed for the communication between the elements of the device and the data collection.

A first graphical interface has also been designed that makes it possible for the user to monitor the performance of the robot.

A statistical analysis on the finished prototype was necessary to study the performance and find problems on the implemented technological solutions. In fact, the prototype must comply with some basic specifications, about its range of motion and its precision. The ranges of movement that each degree of freedom can perform, and the precision of these movements have been evaluated. The ureteroscope cable was required to travel the entire urinary system, about 50/55 cm. A range of 51,5 cm was obtained. Furthermore, the instrument had to rotate

360 ° around its longitudinal axis and the lever that controls the movement of the tip must be able to travel 90 °. Values over 360 ° and about 90° have been obtained for these movements. The accuracy is also evaluated for each movement, obtaining values of 0,51 cm for the insertion movement of the endoscopic cable, 0,38 ° for the rotation of the instrument around its own axis, 4,67 ° for the movement of the lever of tip control. Values that can be considered improved or close to the ones achievable with manual control of the instrument. The statistical analysis has also led to the discovery and study of some problems due to the designed mechanical technology.
Keywords: flexible urethroscopy, surgical robotics, mechanical design, control peripheral, serial communication, graphic user interface, movement range, movement precision.

Chapter 1: Introduction

1.1 Clinical Scenario

1.1.1 Urinary Lithiasis

Urinary Lithiasis is a medical condition defined as the formation of calculi in the urinary tract. This pathology has a high incidence nowadays in the world: according to the last studies, in the U.S.A the 10.6% of the man and the 7.1% of the woman are affected by the presence of stones before the age 70 (Scales, Smith, Hanley, Saigal, & Project Urologic Diseases in America, 2012). In Italy, it affects the 4.53% of the male population and the 3.78% of the female (Prezioso, et al., 2014). The diffusion of this pathology in other countries has been reported in the last year, as a proof of its incidence (Heers & Turney, (2016)) (Hesse, Brändle, Wilbert, Köhrmann, & Alken, 2003) (Yasui, Iguchi, Suzuki, & Kohri, 2008). Moreover, the paediatric incidence of this pathology has considerably increased in the last years (Routh, Graham, & Nelson, 2010) (Sas, Hulsey, Shatat, & Orak, 2010) (Dwyer, et al., 2012) (Edvardsson, Ingvarsdottir, Palsson, & Indridason, 2018)

Even though the number of patients that dies for reason related with urinary lithiasis is very small, this disease is cause of problem in everyday life:

- Nephritic colic: intense lumbar pain, caused by the blockage of the exit of urine from the kidney, which can spread to the anterior abdomen and genitals. It is usually intermittent and associated with nausea, vomiting, sweating and a feeling of abdominal swelling.
- Haematuria: appearance of blood in the urine, caused by the lesions of the calculus in the urinary tract.
- Urinary infections: that can be caused by the appearance of the stone or can be the cause of it.

Moreover, the probability of recurrence of the disease a second time after the first stone is quite high (40% by 5 years, 75% by 20 years) (Worcester & Coe, 2010)

The causes of the increasing diffusion of this pathology are not yet fully clear and still under discussion. The morbidity is certainly influenced by age, by gender, by regional position, by lifestyle and eating habits of people. In Italy, for example, the highest prevalence rate of urolithiasis was reported in Campania and Sicily (Tab. 1.1) with a geographic distribution showing higher prevalence and incidences in Southern regions. This can be easily explained, by the well documented knowledge that the incidence of urinary stones is higher in countries with warm or hot climates, probably due to low urinary output and scant fluid intake. It is also possible note how the prevalence grows with increasing age, and it reaches the highest value in group age 65-74 age (Tab. 1.2).

Moreover, a higher incidence on the male population in most of the cases has been found. (Prezioso, et al., 2014).

Region	***Total***		***Male***		***Female***	
	N	**1000*	*N*	**1000*	*N*	**1000*
Piemonte/Aosta	2237	3.63	1241	4.17	996	3.12
Liguria	*1104*	*3.71*	*634*	*4.50*	*470*	*2.99*
Lombardia	*4412*	*3.13*	*2547*	*3.68*	*1866*	*2.60*
Trentino/FVG	*1216*	*2.62*	*699*	*3.15*	*517*	*2.13*
Veneto	*2119*	*2.92*	*1222*	*3.48*	*897*	*2.40*
Emilia Romagna	*2486*	*4.57*	*1436*	*5.65*	*1050*	*3.62*
Toscana	*1576*	*3.75*	*1063*	*4.71*	*693*	*2.86*
Umbria	*960*	*3.82*	*592*	*4.94*	*368*	*2.80*
Marche	*1334*	*5.53*	*770*	*6.29*	*564*	*4.45*
Lazio	*3160*	*3.95*	*1635*	*4.33*	*1525*	*3.62*
Abruzzo/Molise	*136*	*4.39*	*659*	*4.70*	*647*	*4.12*
Campania	*4718*	*6.08*	*2105*	*5.67*	*2613*	*6.46*
Puglia	*3072*	*4.69*	*1461*	*4.61*	*1611*	*4.76*
Basilicata/Calabria	*2107*	*5.11*	*977*	*4.87*	*1130*	*5.34*
Sicilia	*4355*	*5.34*	*2135*	*5.50*	*2220*	*5.19*
Sardegna	*966*	*4.26*	*446*	*4.14*	*520*	*4.37*
Total	*37316*	*4.14*	*19626*	*4.53*	*17690*	*3.78*

Table 1.1 Prevalence of urolithiasis in Italian living population by region and gender (Prezioso, et al., 2014).

Age	***Total***		***Male***		***Female***	
	N	**1000*	*N*	**1000*	*N*	**1000*
15-24	*601*	*0.65*	*236*	*0.49*	*365*	*0.83*
25-34	*2303*	*1.89*	*928*	*1.52*	*1375*	*2.27*
35-44	*4903*	*3.05*	*2384*	*2.99*	*2519*	*3.10*
45-54	*7381*	*4.51*	*3941*	*4.91*	*3440*	*4.12*
55-64	*8012*	*5.92*	*4562*	*6.90*	*3450*	*4.99*
65-74	*7646*	*6.71*	*4355*	*8.02*	*3291*	*5.51*
75-84	*5142*	*6.35*	*2633*	*7.91*	*2509*	*5.27*
>85	*1328*	*4.12*	*587*	*5.74*	*741*	*3.37*

Table 1.2 Prevalence of urolithiasis in Italian living population by age and gender (Prezioso, et al., 2014).

Genetic factors, global warming, climate factors are also associated with the risk of suffering the insurgence of stones and it is hypothesized that the environmental factors have a main role in the recent diffusion of the pathology. (Sofia & Walter, 2016) (Sorokin, et al., 2017)

1.2 Current clinical Solution

Usually the 95% of the stones located in the ureters are expelled spontaneously between 3 and 4 weeks after their appearance. Otherwise, different techniques can be exploited to treat and eliminate the calculi or to promote their elimination through the urine.

The more common techniques for the treatment of kidney stones are here reported:

- Extracorporeal shock-wave lithotripsy (SWL) is a minimally invasive technique that exploit a machine that produce focused shock waves (short pulses of high energy sound waves). These waves are transmitted to the stone through the skin. When the waves impact the calculi, the energy of the shock fragments them into smaller pieces, that can easily exit with the urine (Fig. 1.1). The advantages of this technique are the low risk of complications and the no need for an anaesthesia. The disadvantages are that it just breaks the calculi into smaller pieces, without removing them. Some days or weeks are necessary to complete remove them through the urine, with the risk of renal colic. In some case more than a session of shock waves is requested to break the largest stones. (European Association of Urology, 2019b)

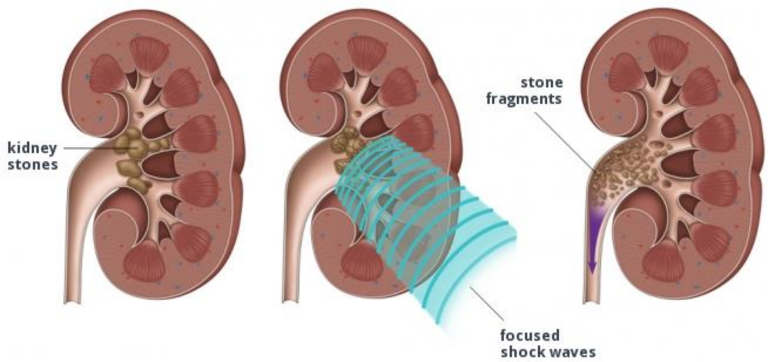

Figure 1.1 SWL application with fragmentation of kidney stones (European Association of Urology, 2019b).

- Percutaneous nephrolithotomy (PNL) is a minimally invasive technique, in which the calculi are removed directly from the kidney, thanks to a tubular medical instrument called nephoscopy. This technique is normally used when the kidneys stones are too large (bigger than 2 cm) to be break by a shock waves, too numerous, or too difficult to be reach by ureteroscope. The nephroscope is inserted through the skin, so a general anaesthesia is required. Compared with the other techniques (SWL, URS) is more invasive and it presents a higher risk of complications as fever and bleeding. It is used only in extreme cases, when other techniques cannot perform the task. (European Association of Urology, 2019a)

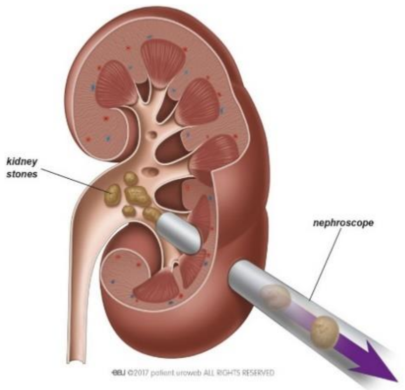

Figure 1.2 A Nephroscope used to remove stones directly from the kidney (European Association of Urology, 2019a).

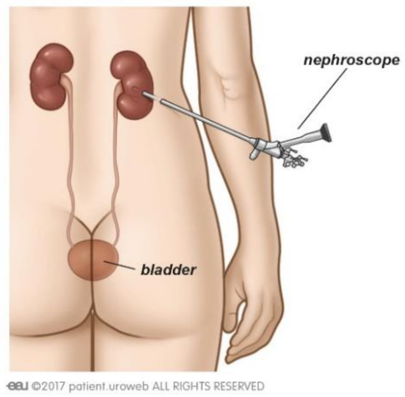

Figure 1.3 Stone fragments removed with a nephroscope (European Association of Urology, 2019a).

- Open surgery is an invasive procedure used just in critical cases. The urinary tract is accessed through an incision in the patient skin. It requires a general anaesthesia. The kidney stones are directly treated and removed by surgeons. This procedure should be avoided in most cases. It can be considered just in exceptional occasion for those patients in whom a reasonable number of less invasive procedures would not be useful. Other case in which it can be taken in account include complex stone situation and anatomical abnormalities (Alivizatos & Skolarikos, 2006)

- Ureteroscopy (URS) is a minimally invasive technique for the fragmentation and the elimination of kidney stones, located in the ureters or kidneys that is performed with a flexible tubular instrumentation (ureteroscope). It is introduced thought the urinary system (urethra, bladder, ureter) until the area of interest is reached. This instrumentation has different channel that can be exploited to perform the operation. Usually a fibre optic is inserted to allow the surgeon to drive the ureteroscope in the urinary system and localize the targets. A special stone basket is used to pulled out directly the kidney stones. In case they are too large, a laser fibre is used to break the stone into smaller pieces. The smallest fragments are eliminated with the urine. Both laser fibre and stone basket are inserted thanks to the ureteroscope. (European Association of Urology, 2019c)

URS is a safe and effective treatment option for kidney and ureteral stones and is particularly indicated for renal stones smaller than 2 centimetres and. For larger calculations, it offers an alternative of similar efficacy to percutaneous approaches. (Aboumarzouk, Monga, Kata, Traxer, & Somani, 2012) Although it requires anaesthesia and it is more invasive than SWL, it offers considerable advantages, since it can eliminate almost all the pieces of the calculations without the need for the patient to eliminate them late and considerably reduces the risk of appearance of second calculations.

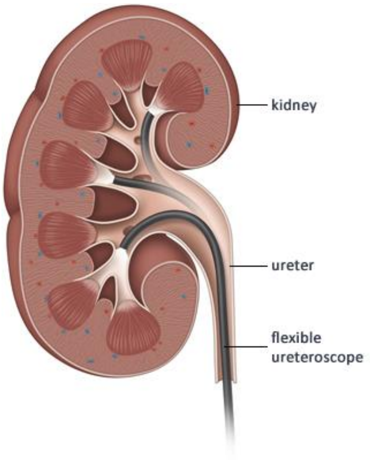

Figure 1.4 An ureteroscope allows the surgeon to reach every area of the kidney (European Association of Urology, 2019c).

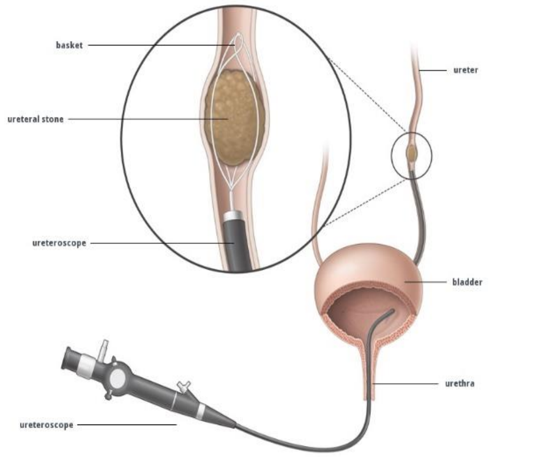

Figure 1.5 An ureteroscope cross the urinary system to reach the working zone. In the circle it is put in evidence the basket stone used to extract the calculi (Toowoombaurology, 2019).

Treatment decisions are made individually according to stone size, location, and (if known) composition, as well as patient preference and local expertise.
According to the latest recommendations of European Association of Urology, the guidelines for the treatment of kidney stones are moving towards endourologic procedures, such as URS and PNL, versus SWL (Türk, et al., 2016)
In the same way the urolithiasis treatment is evolving all over the world. (Geraghty, Jones, & Somani, 2017). Considering the four main techniques described above, it has been seen how the open surgery technique and SWL have a negative trend in terms of share of total treatments and how the PNL remains stable. Above all, it revealed an exponential spread of the URS.

1.2.1 Flexible Ureteroscopy (fURS)

The ureteroscope was used for the first time for a surgical operation in 1912 by Young. Since that moment, this instrument has undergone many changes and improvements. The endoscopes evolved from rigid, to semi-rigid, to flexible instrument. The first use of flexible ureteroscope (fURS) was done by Marshall in 1964. The first intraoperative view solution was based on thin lenses (Nitze design), then substituted by glass rods (Hopkins design). Nowadays optical fibre technology is exploited. Thanks to this technology was easier to design new semi-rigid and flexible solution. Progress of flexible ureteroscopy was closely related to the development of flexible fibre optic.

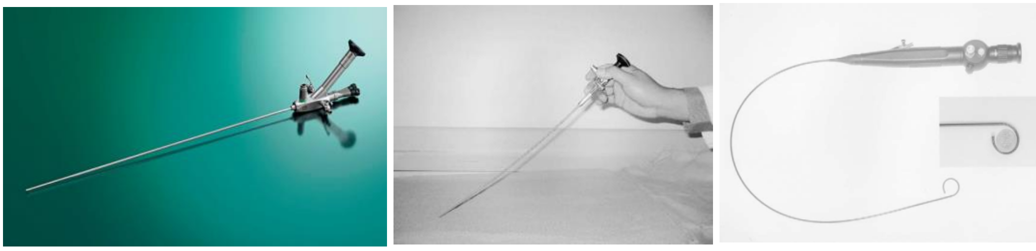

Figure 1.6 A rigid (left) (Nickbrookurology, 2019), a semirigid(centre), a flexible(right) ureteroscope (Basillote, Lee, Eichel, & Clayman, 2005).

Recently some kind of digital flexible and rigid ureteroscopes have been developed and released. They integrate a digital camera chip (CCD or CMOS technology), mounted on the tip, which improved the image quality and resulted in lighter-weight equipment due to the integration of the light-cable and camera within the endoscope. Unfortunately, digital flexible ureteroscopes have a larger diameter than the conventional fibre optic flexible counterparts and their use was associated with increased need for placement of an ureteral access sheath, which is associated with a higher risk of ureteral injuries.
Another important step in the evolution of the instrument was the introduction of an active mobile tip that can be controlled by the surgeon with a mechanism on the handle of the ureteroscope. It introduces the possibility of deflecting the distal part of the instrument, facilitating the movement inside the urinary system.
Technological advances have led to the implementation of miniaturized flexible ureteroscope with a diameter that can reach 6.0 Fr and working channels of 3.6 Fr. This improvement still increased the endoscope manoeuvrability and clinical applicability. Moreover, the ureteroscope miniaturization has improved the effectiveness of the instrument, leading to an increase in the average durability of it. Due to its natural fragility and high repair and replacement costs, the durability has become a main aspect to be considered.
The inclusion of holmium laser was also a great enhancement of this technology in order to allow intracorporeal lithotripsy, so the fragmentation of the largest

stones. Fragmentation of calculi is produced by a photothermal reaction with the crystalline matrix of calculi. By not relying upon shock-wave generation for stone fragmentation, the photothermal reaction produces stone dust rather than fragments, effectively removing a moderate volume of the stone. This kind of lithotripsy was associated with shorter operation time and postoperative hospitalization period.

Another important characteristic of the ureteroscope is the possibly to use surgical working instrument through its channels. These include a variety of stone-graspers and baskets, electrodes, cup biopsy forceps, and intraluminal lithotripsy devices even though three-pronged stone-grasping forceps are the safest and more used instruments for removing calculi with the flexible ureteroscope.

The channels are also used to permit an adequate water irrigation of the operating area, that can improve visibility and may facilitate treatment of the stones.

FURS is usually combinate with fluoroscopy, a radiology technique to obtain real time images of the anatomy of the patients, based on X-ray principles. It allows to better follow the position of the ureteroscope inside the human urinary system. (Basillote, Lee, Eichel, & Clayman, 2005) (Buscarini & Conlin, 2008) (Alenezi & Denstedt, 2015)

It is easy to understand how the role of fURS in the management of urolithiasis has expanded greatly during the last decades thanks to the advancing equipment technology and surgical techniques.

Increased ureteroscopic skills and experience together with miniaturization of flexible ureteroscopes have led to an associated high safety margin for fURS. For these reasons nowadays fURS plays a key role in the management of urolithiasis (Alenezi & Denstedt, 2015) (Breda, Ogunyemi, Leppert, Lam, & Schulam, 2008)

Despite its wide diffusion and the benefit for the patients compared to the other existing techniques (It is minimally invasive, it does not need further openings on the skin, better recovery times, better efficiency ...) some problems have been found, especially regarding the surgeon and the medical staff.

Firstly, it is important to point out as this technique is not easy to be performed and it requires highly specialized surgeons and medical equipe, trained in the handling of the ureteroscope.

As said, the endourologist needs a medical team specialized to perform this operation. They help the surgeon in some important procedures, as insertion and advance of the laser fibres or baskets and perform the irrigation while holding the endoscope and focusing on the target. In Table 1.3 are summarized all the different operative actions and by who they are performed. It is possible to see how the surgeon must performs many non-comfortable actions as the activation of several devices by foot pedal, such as those for digital fluoroscopy, laser lithotripsy, or irrigation. (Saglam, et al., 2014)

Moreover, the surgeons must keep a standing position for the time needed for the intervention, holding the ureteroscope up and turning the head to look at the endoscopy and radiography screens (Fig. 1.7).
For the same reason can occur the surgeon need a help to sustain the ureteroscope in the final part of the procedure.
Many studies were conduct about the ergonomic problems recorded in the surgeons during endourological procedures and ureteroscopy. They reported many physical complaints about endourological practice and, above all, the diffusion of hand, wrist and neck problems, which in some cases can lead to tendinitis In the most of the case these problems are more common among endourologists that works with the URS (Elkoushy & Andonian, 2011) (Healy, Pak, Cleary, Colon-Herdman, & Bagley, 2011)
Although URS procedures significantly benefit patients in terms of decreased recovery times and improved outcomes, they contribute to mental fatigue and musculoskeletal problems among surgeons. (Miller, Benden, Pickens, Shipp, & Zheng, 2012)

Operative Action	Extremity required	Performed by
Insertion of ureteroscope	Fingers of both hands (at glans and instrument)	Surgeon
Deflection of ureteroscope	Hand holding hand piece and thumb; fingers of the other hand at meatus	Surgeon
Rotation of ureteroscope	Hand holding hand piece; fingers of the other hand at meatus	Surgeon
Activation of fluoroscopy	Foot	Surgeon or radio technician
Movement of table or C-arm	Foot or hand	Radio technician (surgeon)
Control of irrigation		Nurse or assistant
Syringe	Hand	
Mechanical device	Foot	
Pump device	Finger activation	
Insertion and activation of the Dormia basket and grasper	Finger and hand	Nurse or assistant
Insertion of laser fibre	Finger	Nurse or assistant
Setting of laser	Finger	Nurse or technician
Activation of laser	Foot	Surgeon

Table 1.3 Ergonomic requirements for classic flexible ureteroscopy (Saglam, et al., 2014)**.**

Figure 1.7 Urologist surgeon must keep a standing unnatural posture during traditional URS intervention (Boston Scientific Urology, 2019)

Therefore, the fURS forces surgeons to work near the X-ray machines used to acquire the intra-operative images, with the consequent exposure to ionizing radiation, which could be a risk factor for the development of cancer for the entire medical equipment.
FURS is associated with a radiation exposure of the operator of the range of 1.7-56μSv (Saglam, et al., 2014) This amount is less than 2% of permissible annual limits of equivalent dose to the extremities. Nevertheless, medical personnel should be aware of scatter radiation risks and minimize radiation exposure when involved in fluoroscopic screening procedures, especially in cases where many procedures are performed every year (Hellawell, Mutch, Thevendran, Wells, & Morgan, 2005). In addition, the possibility of damaging the instruments is very high, which requires frequent replenishments of material that can be expensive for the hospital.
In this promising but problematic context, robotics has been proposed as a possible solution to the problems encountered, leading to further development and diffusion of the fURS.
In this application context the idea of this thesis was born, in which, starting from the approach developed in the LITHOS project, a robotic prototype has been developed for the control of a flexible ureteroscope. The LITHOS project proposes the design and development of a new tele-controlled robotic system for the URS. In this way, the benefits introduced by this technique can be exploited and the main problems of ergonomic posture and proximity to x-ray machine can be solved. The final system is based on a multifunctional collaborative robot located in the patient site for the ureteroscope manipulation and a control panel where the surgeon can tele-control the system. This panel shows the stereoscopic vision of the endoscope and the images obtained from the fluoroscopy.

Chapter 2: State of Art and Objectives of the work

2.1 Robotized Flexible Ureteroscopy

2.1.1 Introduction to Minimally Invasive and Robot Assisted Surgery

In the last decades the robotic-assisted surgery (RAS) has substituted the traditional techniques in many medical areas.
Some year before, Mouret, 1987, performed the first laparoscopic cholecystectomy, starting one the most significant change in surgical practice, the minimally invasive surgery (MIS). The minimally invasive surgery is performed through small incisions or trocars, leading to many advantages over traditional open surgery: shorter recovering periods, minor postoperative complications, less scarring, shorter hospital stays, reduced pain and lower morbidity rate. Also, some drawbacks are relevant: complication during the operation can occur, requiring passing to a traditional technique, the longer learning curve of the new techniques for the surgeons, the longer operating time, the higher cost of the equipment, the smaller field of view and the loss of tactile perception and surgeon dexterity. (Jaffray, 2005) (Fuchs, 2002). Thanks to the cited advantages, MIS and non-invasive surgery, rapidly expanded in many medical areas, providing a valid alternative to the traditional open surgery. (Smithers, Gotley, Martin, & Thomas, 2007) (Guillotreau, et al., 2009).
As explicated in the first chapter for the URS, also for most of the MIS techniques one of the main disadvantages is the occurrence of ergonomic problems on surgeons (Miller, Benden, Pickens, Shipp, & Zheng, 2012) (Sari, Nieboer, Vierhout, Stegeman, & Kluivers, 2010)
The robotic assisted surgery development, accomplished by a continuous improvement of video-endoscopy technology and of medical images, dramatically influenced MIS, introducing console-based manipulators that can perform MIS procedures with higher precision, improving the surgeon dexterity (Fuchs, 2002) (Mack, 2001). Moreover, a computer interface in command of a mechanical robot allows the surgeon to obtain a better visual and a better and more stable control of the instrument manipulation, to modulate amplitude of surgical motions by downscaling and stabilization, to work at a distance from the patient. (Cadiere, et al., 2001). Above all, surgeons' working conditions are greatly improved from an ergonomic point of view, compared to the traditional MIS internventions. Even thought, in some cases the time to complete the task is longer using telerobotic technique, this solution provides a much more

confortable enviroment, reducing the mental stress. An improvement of the postural condtion during surgery can also help to avoid any loss of quality of the intervention due to tiredness or stress caused on the surgeon by the lack of working comfort. (Saglam, et al., 2014) (Geavlete B. , et al., 2016a) (Lee, Rafiq, Merrell, Ackerman, & Dennerlein, 2005). The feasibility of robot assisted minimally invasive surgery has been proof in many medical areas, demostrating that phisical and cognitive ergonomics with robotic procedures is significantly less challanging compared with the traditional tecniques. It has been seen how robotics is a safe alternative, offering improved perioperative outcomes and similar cost, even if a well-structured training in always necessary to maximize the benefits.
(Cadiere, et al., 2001) (Coronado, Herraiz, Magrina, Fasero, & Vidart, 2012) (Pigazzi, Ellenhorn, Ballantyne, & Paz, 2006) (Lee, et al., 2014).

2.1.2 Surgical robots

Different types of robots for MIS are available on the market or under development, with different specifications and characteristics that make them specific for laparoscopy, catheterization or endoscopy.
Some examples are here reported, correlated with application under analysis. The main features and concepts exploited by the robots developed for fURS are highlighted yet.

- The DaVinci Surgical System (Intuitive Surgical Inc, CA, USA): It is composed by four computer-manipulated arms, located in the operative site that replicate identically the movement performed by the surgeon in the control console. The arms support wristed instrumentation (EndoWrist; Intuitive Surgical, Inc.), which allow seven degrees of freedom, tremor filtration and high resolution. The console is the site where the specialist remains comfortable seat during the intervention. It is provided by stereoscopic view, hand and pedals for the control of the slave. It is has been demonstrated that DaVinci offers many advantages; among them that people without any surgical experience can learn to perform standardized tasks more easily and more accurately with the aid of the da Vinci robotic system, as compared with traditional manually assisted laparoscopic techniques. (Hubens, Coveliers, Balliu, Ruppert, & Vaneerdeweg, 2003) (Maeso, et al., 2010)

Figure 2.1 The components of DaVinci Surgical System (Intuitive Surgical Inc, CA, USA) (Simorov, Otte, Kopietz, & Oleynikov, 2012).

- The TELELAP ALF-X surgical system (SOFAR S.p.A., ALF-X Surgical Robotics Department, Milan, Italy): It offers a different approach respect the DaVinci System for MIS. It is composed by a a control unit with easy-to-use interface and 3 or 4 manipulators arms, that can not support wristed instrumentation. Nevertheless, it introduces the haptic feedback sensation that could improve surgical experience, making it more reliable, an eye-tracking camera and a high degree of configuration versatility. (Gidaro, Buscarini, Ruiz, Stark, & Labruzzo, 2012)
  Its applicability in different areas has been reported, offering benefit over other minimally invasive surgical tecgniques. (Alletti, et al., 2015) (Fanfani, et al., 2016) (Fanfani, et al., 2015).

Figure 2.2 The TELELAP ALF-X surgical system (SOFAR S.p.A., ALF-X Surgical Robotics Department, Milan, Italy) (Fanfani, et al., 2015).

- The RAVEN Surgical System (University of Washington, WA, USA): It is a minimally invasive robot system that introduce the possibility to work in harsh environments. It is equipped with articulated arms that can control different surgical tool as salples, graspers, scissors, clip appliers with 6

DOF. The brushless motor that run the arms, are mounted outside the arms themselves. It brings to a smaller and lighter design and a reduced weight, that allow to use the robot in hard condition. The surgeon can control the robot via wireless connection at a distance of 100 m (Simorov, Otte, Kopietz, & Oleynikov, 2012). In a desert environment for three days of intense trials the robot performed precise surgically skills, operating remotely. (Harnett, Doarn, Rosen, Hannaford, & Broderick, 2008) (Lum, et al., 2009).

Figure 2.3 RAVEN Surgical Robot (University of Washington, WA, USA), Operating arms(left), Controllers (right) (Lum, et al., 2009)

- The PAKY (Percutaneous Access to Kidney) device (The Johns Hopkins Medical Institutions, MD, USA). It is a robotic solution designed specifically to replicate PNL technique. The PAKY consists of a passive mechanical arm mounted on the operating table and a radiolucent, sterilized needle which movement is performed by a DC motor, controlled with a joystick. The system utilizes real-time fluoroscopic images provided by a C-arm to align and monitor active needle placement. It has been proved to be an effective and safe system in clinical interventions and in vitro experiments to obtain renal access for nephrolithotomy, also in comparison to standard manual access (Su, et al., 2002) (Cadeddu, Stoianovici, Chen, Moore, & Kavoussi, 1998).

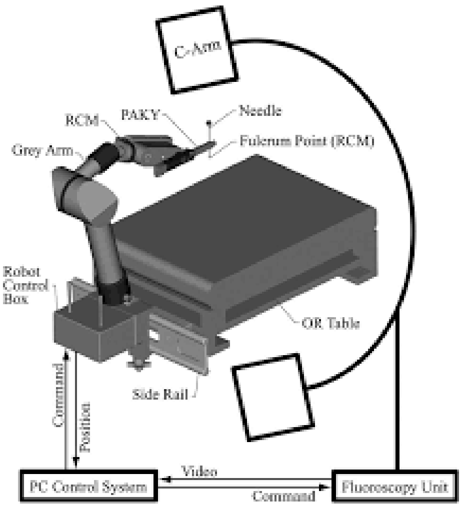

Figure 2.4 Schematization of the PAKY system (Su, et al., 2002).

- The Stereotaxis NIOBE magnetic navigation system (MNS; Stereotaxis, St. Louis, MO). It is an example of robotized system designed for catheter intervention (e.g. Percutaneous coronary intervention (PCI)). It allows an easy and precise navigation of the guidewires by using two permanent magnets located on opposite sides of the patient table to produce a controllable magnetic field that control a small magnet in the distal tip of the catheter. In addition, a computer-controlled system is used to allow truly remote catheter navigation without the need for manual manipulation. Its feasibility and effectiveness in different clinical procedures have been reported. (Ernst, et al., 2004) (Kiemeneij, Patterson, Amoroso, Laarman, & Slagboom, 2008).

Figure 2.5 The Stereotaxis NIOBE magnetic navigation system (MNS; Stereotaxis, St. Louis, MO) (Atrial Fibrillation Center At Hackensack University Medical Center, 2019).

- The Flex System (Medrobotics Corp., MA, USA). It is an example of a robotic technology to steer flexible surgical instrument like endoscope. It is a device specifically developed for transoral robotic surgery (TORS) and in comparison, with other transoral approaches performed with rigid endoscopes and instruments, the Flex Robotic system, using a flexible robotic scope and flexible instruments, allows excellent access to the pharynx, hypopharynx, and parts of the supraglottic larynx.
  The system is composed by five main sections: The Flex Console from where the surgeon can control the system, the Flex Base, an electro mechanical assembly that translate signals from the console into motions, the Flex Disposable, a sterile plastic housing to transfer the motion from the base to the scope, the Table Mounted Stand(TMS), ad adjustable support for the Base and the Disposable, The Flex Cart, used to transport the TMS. Its safety and effectiveness have been demonstrated. (Remacle, et al., 2015) (Mattheis, et al., 2017)

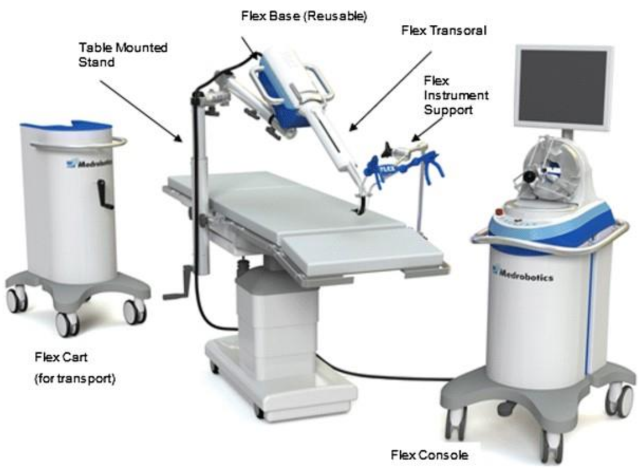

Figure 2.6 The Flex System (Medrobotics Corp., MA, USA) (Remacle, et al., 2015).

- The MASTER. It is a robotic master-slave endosurgical system designed for natural orifice transluminal endoscopic surgery. The control platform allows the bimanual control of two arms, provided with an electrocautery hook and a grasper, with 9 DOF and haptic feedback. Two operators are required for the surgery. The surgeon that controls the master interface and executes the treatment, and the endoscopist that directly moves the endoscope in the target location, favouring an optimal vision of the area. It has been tested in endoscopic sub-mucosal dissections in animal model, giving promising results. (Peters, Armijo, Krause, Choudhury, & Oleynikov, 2018) (Lomanto, Wijerathne, Ho, & Phee, 2015)

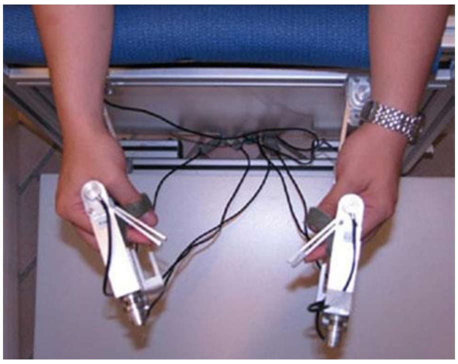

Figure 2.7 The manipulator of the MASTER system (Simorov, Otte, Kopietz, & Oleynikov, 2012).

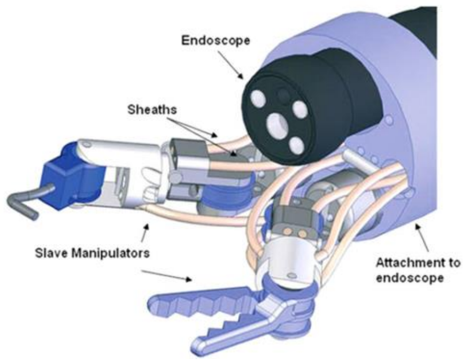

Figure 2.8 The robotic slave and effectors of the MASTER with the endoscope inserted (Peters, Armijo, Krause, Choudhury, & Oleynikov, 2018).

In addition to the examples described, some specific (or that can be uses also for it) robotic solutions have been developed for fURS. In fact, as explained previously, fURS perfectly aligns with this context of minimally invasive endoscopic surgery in which problems have been found, especially on the surgeons' side (postural problems, proximity to x-rays), and where the robotics has been studied and appreciated as a possible and attainable solution, as well as bringing general improvements to the outcome of the surgical intervention. In the following sections the main commercial solutions and those in development are explained in detail.

2.1.3 Avicenna Roboflex (ELMED, Ankara, Turkey)

Since 2010, ELMED (Ankara, Turkey) has been studying and working on a new robot, specifically designed for fURS (Saglam, Kabakci, Koruk, & Tokatli, 2012). The basic idea of the device did not change from the first prototype to the final version. There are two main elements: A manipulator, that holds and moves the flexible ureteroscope, and a console, from which the surgeon can control the robot, using two joysticks and an integrated screen. In the development phase several improvements have been made to the first prototype: the quality of the screen was improved, and its size reduced, the joysticks were redesigned to better control the rotation and deflection of the instrument, the range and accuracy of movement were improved, a central wheel was added to control the fine adjustment of deflection and then integrated with the right joystick.

In its final version the height of the robot can be adjusted according to the size of the patient. The manipulator is fixed directly to a commercial digital endoscope (Karl Storz Flex X2; Olympus URF-V2; Wolf Cobra digital), whose characteristics are then exploited. The robot allows 3 DOF: the bilateral rotation and the advancement/retraction of the ureteroscope that are controlled by a left horizontal joystick, and the deflection of the tip, controlled by the right joystick that integrate a wheel for the fine control. The ranges of movement are 150 mm for insertion/retraction, 220°to each side for the bilateral rotation, 262° to each side for the deflection of the tip. The console is equipped with an adjustable seat and two armrests for the comfort of the operator, as well as two pedals for the activation of the fluoroscopy and the laser-lithotripter. On the screen are shown the endoscopic images and information about the position of the instrument and its velocity, which can be controlled directly from this panel. Moreover, it is possible to check the mechanical insertion of the laser fibre and the irrigation. (Rassweiler, et al., 2018) (Saglam, et al., 2014)

Figure 2.9 Last version of Avicenna Roboflex (Elmed) system, with the left horizontal joystick for insertion and rotation, and right joystick for deflection control (Roboflexusa, 2019).

Figure 2.10 System for fixing the ureteroscope to the mechanical arm (Elmed, 2019).

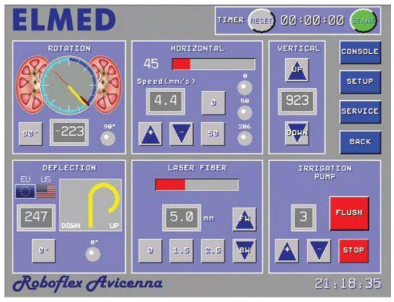

Figure 2.11 The touch screen monitor with various control functions (Elmed, 2019).

As regards the operating technique of the system, an access sheath is used to facilitate the manual insertion of the ureteroscope into the urinary system. After its insertion, it is fixed with two stabilizers to the mechanical arm. Once the stone is localized, it is necessary to retract the system for the safe insertion of the laser fibre. A memory function is then used to return to the working position. In addition to the laser it is possible to exploit a stone basket for the extraction of some fragments that cannot be eliminated with urine.

In these years, it has been continuously developed to implement all the functions necessary to replicate the manual control of the surgeon on the ureteroscope, following the IDEAL protocol for surgical innovation. The IDEAL is framework specially introduced for evaluation of surgical innovations, that divide the development pathway in five steps, Innovation, development, evaluation, assessment and long-term study. (McCulloch, Cook, Altman, Heneghan, & Diener, 2013) (Ergina, Barkun, McCulloch, Cook, & Altman, 2013) (Cook, et al., 2013). Its application to robotic urologic surgery has been reported. (Dahm, Sedrakyan, & McCulloch, 2014) Until now, Avicenna has been tested in the laboratory (IDEAL 1) and 3 clinical trials has been carried out (IDEAL 2).

In these studies, this robot was used on an ever-increasing number of patients, up to 266 (177 males), in the most recent work (Klein, Fiedler, Kabakci, Saglam, & Rassweiler, 2016). In each analysis it has been found a high feasibility and safety in the use of this device in which all the most modern technologies for the treatment of fURS are available. Moreover, a rare case of complications, that force passing to the traditional technique, have been recorded (3 cases out of a total of 414 patients operated in 3 studies).

Geavlete P. et al. evaluated the performance of the robotic-assisted fURS compared with the manual one. They recorded treatment time (51 min vs 50 min)

and fragmentation time (37min vs 39min) similar, but a stone-free rate favouring the robotic approach (92.4 % vs 89.4%). (Geavlete P. , et al., 2016b).
Saglam et al. compared the conventional and robot-assisted fURS using a validated questionnaire concerning ergonomics, and they verified the positive impact of the robot about this main problem. In Table 2.1 is reported a comparison of ergonomics in the two cases. It shows the potentiality of the robotics at the postural level (Saglam, et al., 2014)

Feature	Classic FURS	Robot-Assisted FURS
Position of surgeon	Standing at patient	Sitting with armrest at console
Insertion of instrument	Manually via access sheath	Manually via access sheath
Handling of instrument	With both hands using the hand piece	Using two joysticks
Fine regulation of deflection	Not available	Using central wheel at joystick
Insertion of laser fibre	Manually via working channel	Manually via working channel
Fine movement of laser fibre	Manually via working channel	By pressing on touch screen at console
Activation of laser	Foot pedal (standing) at bedside	Foot pedal (sitting) at console
Adjustment of laser energy	Manually at device	Manually at device
Control of irrigation	By pump at bedside (by nurse)	By pressing on touch screen at console
Movement of table or C-arm	Manually	Manually
Insertion and activation of Dormia basket and grasper	Manually at patient	Manually at patient

Table 2.1 Comparison of ergonomics of classic and robot-assisted fURS (Saglam, et al., 2014).

Avicenna Roboflex is the most advanced and complete device for robotic-assisted fURS. It allows working with the most important commercial ureteroscopes, integrating all the most modern and necessary functions for the fURS. It also allows a range of movement and an accuracy improved compared to the traditional case, as well as a stability that the surgeon will never have. Furthermore, it optimally responds to the postural/ergonomic problem. This results in a shorter learning curve and an improvement in the overall quality of the intervention. In addition, the surgeon is located far from the X-ray machine, also solving the second problem posed for the traditional fURS.
Some features of the device such as the limitation of movements, insertion of the laser fibre in a straight line and the memory function should contribute to a prolongation of the endoscope's life and a lowering of the costs.
Nevertheless, it only provides 3 degrees of freedom and a control console with limited input tools, which reduce the control flexibility and make difficult to track complex trajectories. In addition, the size of the manipulator unit is very large for standard operating room. It does not provide haptic feedback and its functionality in image is limited to the visualization of the endoscopic video, without offering

advanced functionality such as visualization of radiographs and intra-operative navigation. Furthermore, the Avicenna is sold at a very high price, (about € 600,000) which is excessive for most hospitals. Its high price does not always justify its added value as it is an ad hoc robot that can only be used for this application.

2.1.3 Sensei (Hansen Medical Inc, Mountain View, USA)

This system was the first to be used for robot-assisted fURS applications. In 2008, they presented a first application on 5 swine (Desai, et al., 2008). Sensei system is not specifically designed for fURS, but it is a system that was developed for cardiology and angiography and then was converted and adapted for this use.
It introduces an important idea, also taken in account in the LITHOS project: the development of robot that could be used in different applications, and not designed ad hoc for a specific case. This reduces the economic impact of the purchase of the equipment, as it can be exploited in more working areas.
Sensei catheter system (Fig. 2.11) is composed by four main components: a surgeon console, a steerable catheter system, a remote catheter manipulator and an electronic rack, containing computer hardware, power supplies and video distribution unit.
The surgeon console mainly comprises the master input device, a three-dimensional joystick used to remotely control the catheter tip, and displays monitors, that allow the simultaneous visualization of endoscopic and fluoroscopic images. Moreover, it includes a touchscreen monitor dedicated to user interface with various functions and an electronic module for the communication with the electronic rack.
The steerable catheter system (Fig. 2.12) includes an outer catheter (14/12 F) sheath and an inner catheter guide (12/10 F), through which a flexible ureteroscope (7.5 F) has been inserted. Remote manipulation of the catheter system manoeuvres the ureteroscope tip. The working channels of the endoscope, the space between the ureteroscope and the catheter guide and a specific injection channel on the catheter guide are used for the injection and the egress of irrigating fluid or agents of contrast.
The remote catheter manipulator (RCM) is a mechanical arm, fixed to the operating table, that holds the steerable catheter system. Some details were modified to enable attachment of the ureteroscope. A set-up joint is exploited for the optimal positioning. (Rassweiler, et al., 2018) (Desai, et al., 2008)

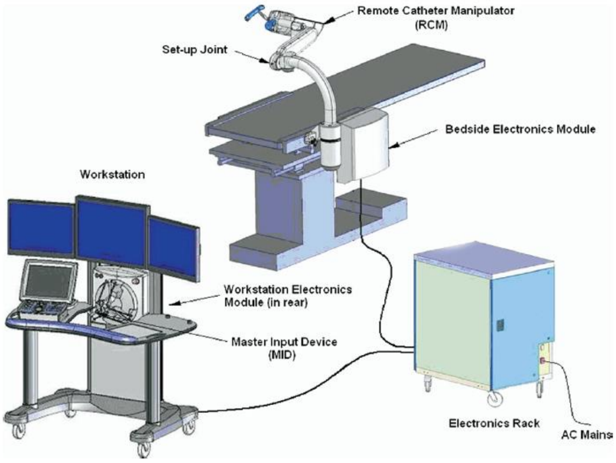

Figure 2.12 Representation of all the components of Sensei system (Hansen Medical Inc, Mountain View, USA) (Desai, et al., 2008).

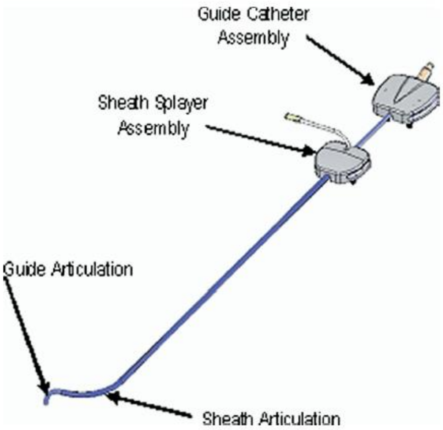

Figure 2.13 Integrated sheath and guide assembly (Desai, et al., 2008).

An external guidewire is necessary to insert manually the steerable catheter in the urinary system. When the catheter is located, the ureteroscope is introduced in the catheter guide and then all the system is mounted on the RCM. At this point is possible to move the ureteroscope in the urinary system and localize the kidney stones that are then treated with holmium laser.

Two studies were conducted by Desai et al. using this system. The specific parameters used to evaluate the feasibility and performance of the system were: need for ureteral dilation to insert the robot in the urinary tract, technical capability and time taken to access each minor calix of the kidneys, reproducibility of access into each minor, ability to fragment intrarenal stones, stability of the system evaluated by ability to robotically “park” the ureteroscope, reproducibility of the auto-retract mechanism evaluated by being able to retract the ureteroscope tip to the original position, evidence of ureteral and pelvicalyceal injury.

Both studies reported quite satisfactory results with a mean operation time of 91 min (60-130 min), higher respect the case of Avicenna Roboflex but still acceptable, a comparable complete disintegration rate and the absence of intraoperative complications that forced to pass to the traditional technique. In addition, Sensei also solves the main problems of the traditional fURS, positioning the surgeon comfortably seated on a console, away from radiation field. Its feasibility and effectiveness have been demonstrated. (Desai, et al., 2008) (Desai, et al., 2011)

Some features like laser and irrigation management from the console, a memory function and the possibility to work with commercial endoscopes are absent. Furthermore, the ureteroscope is only passively controlled. This has been assessed as a possible limitation of this technology solution (Rassweiler, et al., 2018). Nevertheless, the degrees of freedom of movement compared to Avicenna Roboflex are greater (6 vs 4). Further advantage is the simultaneous visualization of endoscopic and fluoroscopic images. Even in this system haptic feedback is not completely implemented.

2.1.4 Robot assistance for manipulating a flexible endoscope developed by Sheikh Zayed Institute for Pediatric Surgery Innovation e Children’s National Health Center (Washington, DC, USA)

Compared to the two previously treated cases, this device has reached only the phase of the creation of a first prototype, with which phantom tests have been performed.

The idea is like the Avicenna Roboflex one, in which an ad-hoc system is designed to attach a commercial ureteroscope to a mechanical arm and drive it.

The device has 3 DOF: insertion (translation), rotation and flexion. Each of these three movements is controlled by a different motor with encoder. Limit switches have been installed for safety reasons and to prevent excessive displacement that could cause damage to the flexible cable of the ureteroscope.

A system of guide rails is used for translator movement. A system of two pulleys to activate the control dials that allows the tip deflection. The rotation is performed by rotating the mechanical arm. The translation has a range of 170 mm, the rotation has a range of ±150 ° and the deflection of about 45 ° (it is the whole range of the control lever that is mapped to the tip flexion of 270°). They are reduced compared to the case of Avicenna Roboflex for what concern the rotation, but still comparable. A Snap-On mechanism is used to be able to easily install and

uninstall the endoscope to the mechanical arm. A rigid annular tube with higher stiffness is used to support the flexible endoscope cable. The Snap-On system and the annular tube are sterilized as they are the parts in contact with the endoscope. Most of the pieces are 3D printed, favouring the creation of a cheap and light device. At first, a 3D mouse and successively a gaming joystick has been used for system control. A special software has been developed to evaluate the efficiency and accuracy of system movements.
Some experiments have been made with this system. In addition to feasibility, usability and ergonomic performance, some other requirements have been evaluated.: velocity to mount the endoscope on the robot; the design should allow the use of a sterile interface to prevent contamination; the design should increase the stiffness of the flexible portion of the ureteroscope for improved manoeuvrability; robotic motor cables should be routed properly to avoid tangling with the light and video cables, and prevent cable breaks due to robot motion; the robotic system should work with existing commercial ureteroscopes.
A comparative analysis with a bladder phantom in which manual and robotic-assisted solutions are compared, was conducted.
In this experimental test the operator must localize some target pre-positioned in the phantom. Much smoother trajectories were recorded for the robotic case, even though the realization time was more than double (362 second vs 145 second). It has also been tested in a phantom kidney in which the operator is able to reach the various targets with dexterity. (Zhang L. , et al., 2013,June) (Zhang L. A., et al., 2014, May).
The proposed design suffers from the same limitations of RoboFlex Avicenna, in terms of a limited mobility freedom and too large size. Its design is ad hoc and does not offer versatility for other types of surgical disciplines, which could cause the need to market it at a very high price to pay for the engineering effort necessary in its design and manufacture. The integration with the images had not yet been treated. This device has not led to more recent developments and results.

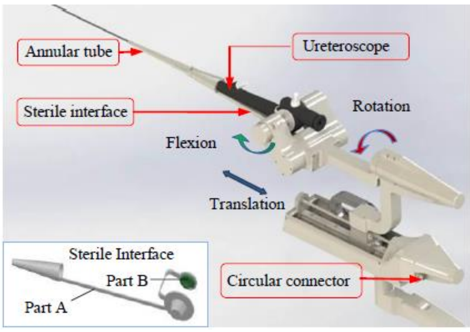

Figure 2.14 Prototype of ureteroscopic robot with all its mechanical parts (Zhang L. A., et al., 2014, May).

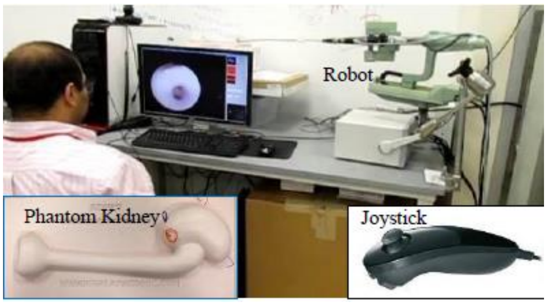

Figure 2.15 Robotic system applied in phantom kidney with the joystick used (Zhang L. A., et al., 2014, May).

2.1 LITHOS Project

LITHOS project arises in this application context. The LITHOS project proposes a solution to a real necessity for the surgeon, improving the postural ergonomic condition and radiological safety. It is based on the creation of a remote tele controlled system composted by a multifunction mechanical arm already existing on the market (KUKA LBR-IIWA), combined with a specific actuator. The actuator must be designed specifically in the development of the project and it should support the endoscope and manage some degrees of freedom of its movement. The combination of degrees of freedom by the multi-function arm and by the specific actuator should increase the flexibility of movement and the possibility to perform more complex trajectories with dexterity and in a stable way. In addition, the specific device (the ureteroscope) may be substituted in order to apply the robot not only in the ureteroscopic field but also in other surgical areas. This would favour a lowering of costs for the health facility, since the same system can be used in different applications. The specific actuator must integrate with endoscopes already available on the market. The mechanical system should be compact, versatile and cheap. A console for the control of the mechanical system must be designed. It allows the surgeon to work comfortably and remotely from the radioactive area.
This system also proposes to include some functions such as:

- The integration with x-ray machines, which must be controllable from the console, on which the radiological images are continuously displayed jointly to the endoscopic ones.
- Laser stabilization and the creation of a laser safety function that allow the laser to shoot only in the right location.
- The possibility to automatically follow the kidney stones and their fragments, thanks to the processing of medical images acquired by the endoscope.
- The real-time display of the endoscope in the radiographic image, through a virtual model avoiding the continuous acquisition of radiographic images. To perform this task SLAM (Simultaneous Localization and Mapping) technique can be exploited. It is process by which a robot moves in an unknown environment, builds the map of that environment and can locate itself within that map.
- Control of the laser, irrigation and contrast agent from the console.

It should improve the overall efficacy of endourological intervention and increase the quality of patient outcomes and the working conditions of the medical team, thus favouring the spread of this promising technique for the treatment of kidney stones.

The main advances compared to the state of the art in LITHOS project are:

- Control: precise control of the ureteroscope with multiple degrees of freedom for tracking curved trajectories within the urinary system, complemented by haptic entry systems that allow a wider range of motion than what is available in the market.
- Versatility: system designed based on a multi-purpose surgical robot, which makes possible its reconfiguration -changing of the actuator- to be used in different surgical applications.
- Price: target price of the product less than half of the direct competing products (€ 600.000), facilitating its acquisition by a wide range of hospitals.
- Intelligence: image processing and navigation modules that provide the system with advanced laser shoot control, fragment tracking and navigation capabilities.
- Portability: compact design and easily transferable between different operating rooms.

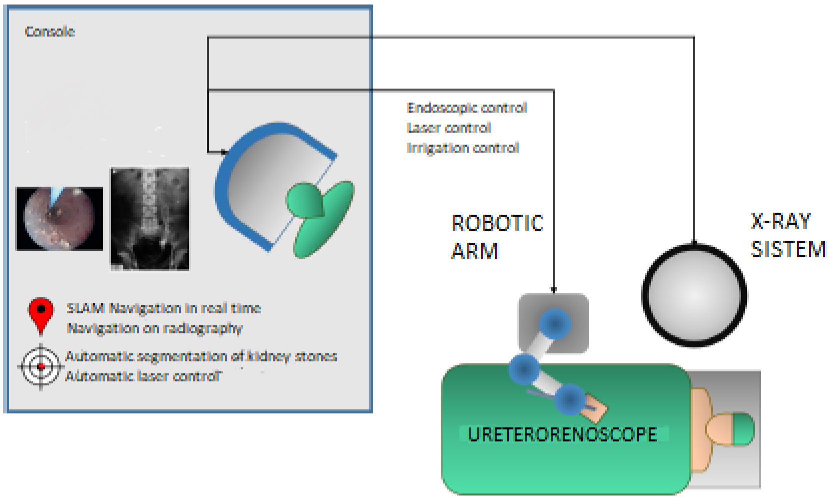

Figure 2.16 Schematic representation of the device that would be developed in LITHOS project.

This project is part of the Spanish state program I + D + I (Investigación, Desarrollo e Innovación Orientada a los Retos de la Sociedad), financed by the Ministry of Economy and Competitiveness.
It is based on a collaboration between a company, ROBOTICSSA (Llanera, Spain), a research center, VICOMTECH-IK4 (San Sebastian, Spain) and a public university, UPM (Universidad Politécnica de Madrid, GBT, Grupo de Bioingegnieria y Telemedicina). The project has been discontinued and nowadays currently interrupted.

Despite of that, the ROBOLABO laboratory (UPM) has continued the investigation in this interesting field of research. In this context this master thesis work has been developed.
The main purpose was to create a first robot prototype that could control a commercial ureteroscope. The mechanical parts were designed and implemented to support the instrument and control its basic movement of the instrument. A control system that allowed the user to perform the different movements was then designed. The prototype had to respect some movement range and precision specifications.

2.2 Aims and objectives of this work

The main purpose of this work is to design and implement a robotic device able to hold a flexible ureteroscope for flexible ureteroscopy (fURS) and control its movement, respecting some limitation of displacement range and motion accuracy.
For this purpose, the project has been divided into three main phases. The first two phases of design and development and a and a final phase of evaluation and analysis.

1. Phase 1, Mechanical design: in this step it is required to design a specific actuator to support and move a commercial ureteroscope (Cobra Vision, Flexible Dual Channel Sensor Ureterorenoscope, Richard Wolf), with three degrees of freedom.
    - Insertion/Retraction movement.
    - Rotation movement around its longitudinal axis.
    - Tip deflection movement.

   Therefore, a hypothetical approach to the specific actuator is studied. It must be specifically designed in LITHOS project. It should be associated with a commercial multifunction arm, in a future development.

2. Phase 2: Control system design: in this phase a firmware must be developed for the integration of a control instrument, which must allow the user to perform the three movements designed in the mechanical phase only using this controller.
   Furthermore, it is planned to implement a first graphical interface that allows the user to monitor data on the position and speed of the different movements.

The cooperation of these two phases must lead to the realization of some technical objectives of the device. It allows to exploit the potentialities of the ureteroscope and to have the same or better performances as in case it is manually controlled.

- Movement range: for each of the three movements a predetermined range of movement must be performed:
    - Insertion / Retraction movement: considering an overall length of the urinary system of about 50 cm (about urethra 20 cm in men, shorter in woman, about 5 cm of bladder, about 25 cm of ureter) (Wikipedia, 2019), the ureteroscope should realize the objective of reaching the final part of the system and the kidney area. For this purpose, the cable of the ureteroscope should travel a stretch of about 50/55cm.
    - Rotation range: the entire rotation range of 360° around its longitudinal axis must be travelled.
    - Deflection range: it is necessary to exploit the whole range of possible movement of the control lever that is used to perform the deflection of the tip. The control lever should travel 90°.

- Precision of movement: it should be comparable or improved compared to the case that the movement is performed in a manual way by the surgeon.

- Stability of the position reached: it is evaluated the ability of the device to maintain a position once reached.

- Total movement: Being able to move with dexterity in an environment that represents human urinary apparatus, reaching certain targets in a time comparable to the case that the endoscope is controlled manually.

3. Phase 3: Experimental evaluation: Data are collected about the movement range and the precisions to verify the realization of the previously set technical objectives. Moreover, some limits of the mechanical pieces designed are discovered and studied.

In the following chapters the mechanical systems and technologies necessary for the development of each movement will be first discussed and analysed.
After that, the control part will be presented, in which the firmware for the communication between the mechanical system and the controller has been designed and the graphic interface developed.
The last part describes the analysis of the data, and the changes at the structural and software level that this caused.

Chapter 3: Mechanical Design

3.1 Introduction to mechanical design

In this section the mechanical parts designed for the realization of the required objectives will be described. For each specific movement a different technological solution has been designed, keeping in mind the final goal that must be achieved. An endoscopic cable drag system will be described. It allows the insertion of this into the human urinary system. A worm gear system to allow the rotation of the instrument and an anchoring system to the tip control lever to allow the deflection of the tip. Every part of the system must be fixed to the ureteroscope, used for this work. Therefore, firstly it is important describe the instrument available in detail. COBRA Vision is a flexible ureterorenoscope, developed by the company Richard Wolf (Knittlingen, Germany) (Fig. 3.1). It is equipped with a working channel, which can be used for irrigation or to insert instruments such as stone basket, a laser channel, a LED for illumination, and a sensor for capturing endoscopic images. An ergonomic handle is present as it is a tool designed for manual control. The tip can be flexed actively using a control lever placed on the handle (Fig. 3.2). The control lever has a range of displacement of 90 °, mapped in an upward and downward deflection of 270 ° of the tip (Fig. 3.3). The length of the cable and so the working range in insertion/retraction is 680mm. (Richard Wolf, 2019)

Figure 3.1 COBRA Vision ureterorenoscope (Richard Wolf, Germany) (Richard Wolf USA, 2019).

Figure 3.2 Control lever for the tip deflection of the COBRA Vision (Richard Wolf, Germany) (Richard Wolf, 2019).

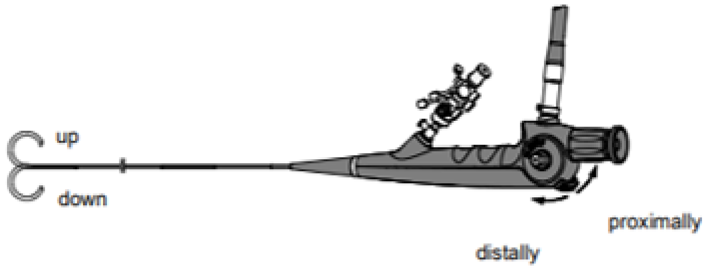

Figure 3.3 Tip deflection upward/downward of COBRA Vision (Richard Wolf, Germany) (Richard Wolf USA, 2019).

Each mechanical part designed in this phase was first projected using Autodesk Inventor, a three-dimensional drawing software. Thanks to this software it is possible to first design every single part alone and then to combine them. It facilitates the work by allowing the visualization of the overall mechanical system necessary for the realization of a mechanical task.

Every single part designed then was 3D printed in plastic material. The printer used was the Prusa i3 Hephestos (Fig. 3.4). The use of the 3D printer allows to evaluate different ideas, to try them, to make mistakes at a low production cost, thanks to the low cost of the material. Furthermore, it accelerates the production and modification of the prototype. At the same time, it allows to print with precision even the most technologically complex parts, such as screw and gear systems. The use of 3D printing is fundamental in this first phase of prototyping where it is common to make mistakes and try different ideas. Some limitations of this technology such as limited use of materials and not enough precision have been found in some applications (Berman, 2012), but they are not relevant problems in this first prototyping phase. Once the mechanical parts have been designed thanks to AutoCAD Inventor, they are saved in. stl format and moved to the management software of the printer, Ultimaker Cura, which allows the setting and preparation of the print.

Figure 3.4 Prusa i3 Hephestos.

A further important step that must be introduced before describing the details of the design of the structures, is how to steer the movements, or rather, which motors are used. In this first prototyping phase, motors already available in the laboratory have been used. Thanks to the final phase of experimental tests, it is possible to evaluate if the motors used were sufficiently powerful and precise to perform the required tasks. When the structure designed for the realization of a movement is working properly and functionally, the change of the motor and the adaptation of the structure to this, is a small problem. Introducing the motors used in this phase is important because the designed structures must hold, in addition to the ureteroscope, also the motors.
Three equal motors have been used, each one to control a different movement. The way in which they have been fixed to the structure will be described in detail in the next sections.
Motor used are: 99:1 Metal Gearmotor 25Dx54L mm HP 12 V with 48 counts per revolution (CPR) encoder, produced by Pololu (Las Vegas, USA). (Fig. 3.6)
This gearmotor consists of a high-power, 12 V brushed DC motor combined with a 98.78:1 metal spur gearbox. The gearbox (Fig. 3.5) is a mechanical device, part of the power transmission, which is used to reduce the speed of the output shaft compared to the input shaft. In the same time, it causes an increase of the output force, with respect to the input one. This motor performs a complete rotation of the output shaft (the one then connected to the mechanical parts) for every 98.78 complete rotations of the input shaft. A high value of this reduction coefficient increases the precision with which the movement of the motor is provided.

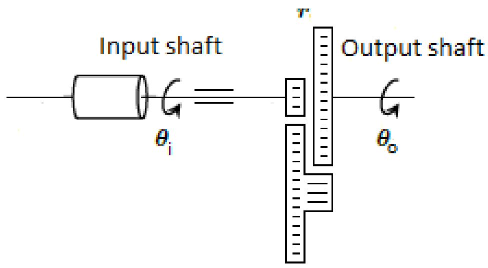

Figure 3.5 Schematic of the motor gearbox. One output rotation (θ_o), corresponds to r, input rotation (θ_i). r=98.78.

It integrates a 48 counts per revolution quadrature (CPR) encoder (Fig. 3.7), based on the hall effect, to measure the number of revolutions of a magnetic disk mounted on the output shaft. The encoder provides a count of 48 for each revolution of the master shaft (input) and then a count of 48(counts provided by the encoder for each internal revolution) multiplied by 98.78(gearbox ratio) for each rotation of the output shaft. So, 4741.44 counts per revolution of the output shaft. It is very important to introduce and describe the meaning of motor counts, measured by these encoders, as it will be the basic measure on which many parameters of the experimental phase will be evaluated.
The gearmotor is cylindrical, with a diameter just under 25 mm, a length of 54 mm, and the D-shaped output shaft is 4 mm in diameter and extends 12.5 mm from the face plate of the gearbox. The D-shaped (Fig. 3.8) is a structure used to connect the motor and the mechanical part that must be moved by the motor. For this reason, every connection between the motor and the mechanical part, have been design taking in account the geometrical characteristic of the D-shaped structure. It is then important to know the shape and the dimensions of the gearmotor to better design the motor support structure. (Pololu, 2019).

Figure 3.6 99:1 Metal gearmotor 25Dx54L mm HP 12 V with a 48 CPR encoder, Pololu (Las Vegas, USA) (Pololu, 2019).

Figure 3.7 Magnetic disk and encoder, integrated in the gearmotor (Pololu, 2019).

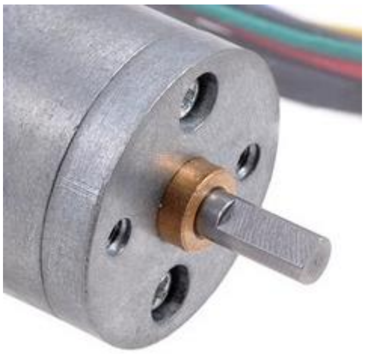

Figure 3.8 D-Shape connector of the gearmotor (Pololu, 2019).

3.2 Movements Implementation

In the following sections will be described the structure designed for the realization of each motion goals.
For each structure some functional and technical characteristics (e.g. the dimensions) have been changed during the development of the device. However, the basic concepts used for each movement have not changed. For this reason, just the finale structure is described, citing the changes made only when significant.
It is also highlighted the different approach used, compared to the devices present in the state of the art that are more similar to this one (Avicenna Roboflex e Sheikh Zayed Institute). Some ideas of possible further development are also described.

3.2.1 Insertion / Retraction movement

The main objective of this type of structure is to move the ureteroscope cable back and forth (Fig. 3.9), allowing:
- Its insertion into the urinary system,
- The exploration of the urinary system in search of kidney stones
- Its retraction when necessary (e.g. to extract a stone or to insert the laser fibre).

It should move for a range long enough to reach the most extreme parts of the urinary system (Movement range about 50/55 cm) (Fig. 3.10), with a good precision, comparable to the manual controlled case. It also should be stable once reached a desired position.

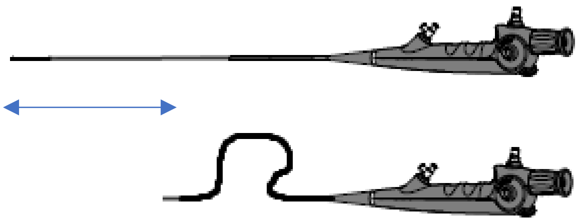

Figure 3.9 Insertion/retraction movement of the cable.

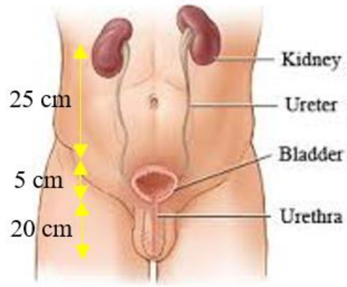

Figure 3.10 Urinary male system. For each part it is reported the length.

When the ureteroscope is controlled manually, the surgeon acts directly on the cable to move it, pushing it or pulling it with the hands.
Starting from the manual application, the idea of the system for the realization of the movement has been developed. The goal was to create a structure that acts directly on the cable, as in the human controlled case, assuming that this kind of control could perform a more precise and stable insertion movement.

In the other cases analysed in the literature a complete translation movement of the entire ureteroscope is exploited, without acting on the cable.
Acting directly on the cable, part of the length of the cable is lost, since the part closest to the connection of the cable to the rest of the endoscope must be inserted into the mechanical system that allows its movement. It implies a reduced possible range of movement. However, the initial part of the cable length cannot be exploited, even in other solutions. In fact, they need a support and directing structure to better steer the movement (Zhang L. A., et al., 2014, May). Even in the human controlled case, part of the cable is kept outside the urinary system to allow the surgeon handling of it.
A drawback of acting directly on the cable is that it can be easily damaged. The ureteroscope and above all the cable are extremely fragile and they can be easily worn out, causing the need for a replacement and an increase in healthcare costs. Some precautions are necessary to deal with this drawback.
Before the description of each single mechanical piece, a schematic representation of the full system for the realization of the movement is reported (Fig. 3.11). The red arrows indicate a physical link between the element. The arrows start or end close to the linking point between the elements. It helps to understand where the mechanical pieces are located on the ureteroscope. The yellow arrows indicate a zoom of a particular mechanical piece. A picture of the result, once all the mechanical pieces had been printed and the ureteroscope mounted in the right way, is also reported (Fig. 3.12)

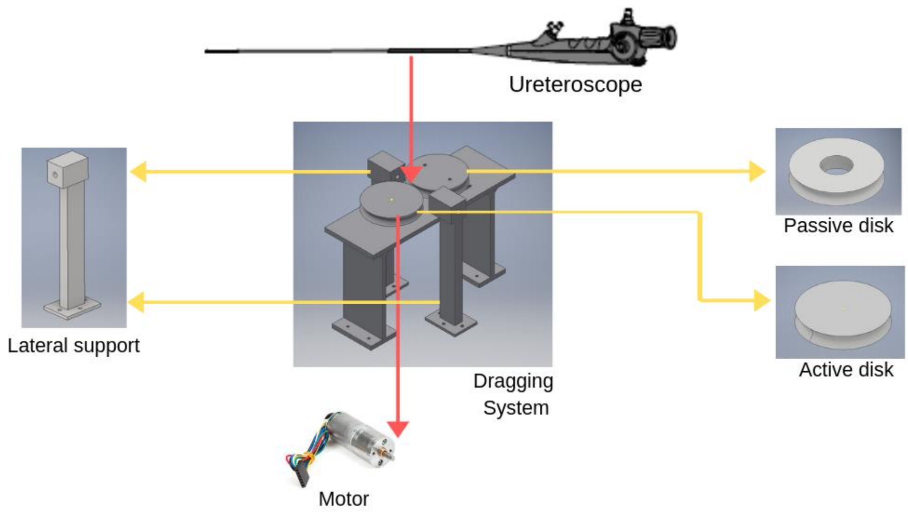

Figure 3.11 Schematization of the technology solution for the insertion/retraction movement. It is basically a drag system, composed by two disk that can push and pull the cable, as the surgeon normally does.

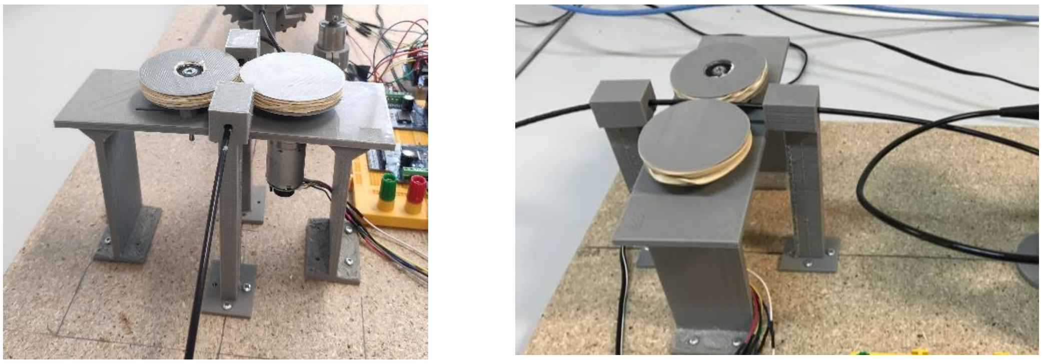

Figure 3.12 The final result of the technology solution for the insertion/retraction movement.

The technology chosen for the realization of this objective is a drag system based on two disks. The first one must be active and driven by the motor. The second one was, at first, stationary and exploitable only as a pivot. This solution led to unsatisfactory results, with objective difficulties in performing the movement. Subsequently, a system with the second disk passively mobile was evaluated. It moves only thanks to the movement of the cable on it. Thanks to this solution an objective improvement of the quality of the movement was found. An additional step that could be evaluated is the addition of two active disks. That would cause the use of two motors, with an increase in costs and the need for perfect synchronization in the movement of these two, or the use of a single motor but the design of a more complex technological solution of movement.

The final structure (Fig. 3.13) has the following characteristics. It consists of two 60 mm diameter disks. The first active disk is attached directly to the motor thanks to a protrusion of the disk (Fig. 3.14, Fig. 3.15) in which it is possible to insert the D-shape connector of the motor and block it with a screw. This type of connection (mechanical part side) will be repeated in all the mechanical-motor connections. The mechanical part side connector consists of a 10 mm protrusion (Fig. 3.14) with three holes. Two holes at the base (Fig. 3.15): A D-shaped hole allows the insertion of the D-shape connector of the motor. A rectangular hole allows the insertion of a mechanical nut.

The last hole is on the lateral surface of the protrusion (Fig. 3.14). It allows the insertion of a screw. The screw enters this hole, passes through the nut, making the system more stable, and pushes against the D-shape connector of the motor. This strategy is used to fix the motor to the mechanical part.

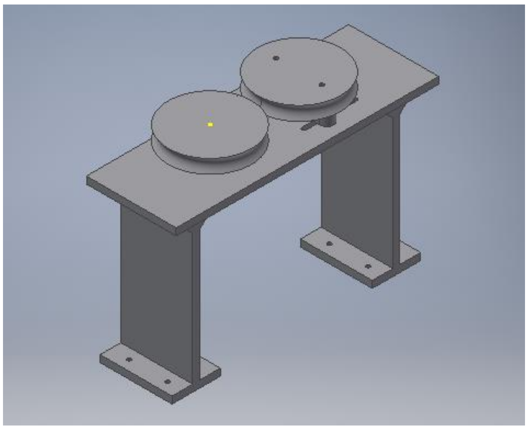

Figure 3.13 Structure for the insertion movement, active disk (right), passive and sliding disk (left), support structure.

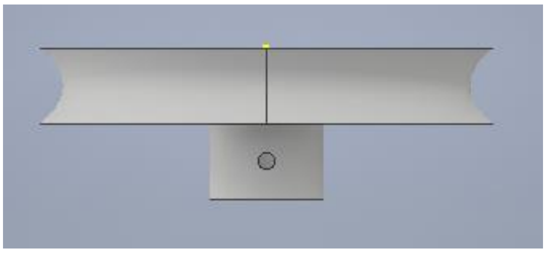

Figure 3.14 Side view of the active disk. It is possible to see the protrusion used for the connection with the motor, and the hole on the lateral surface from which the screw enters.

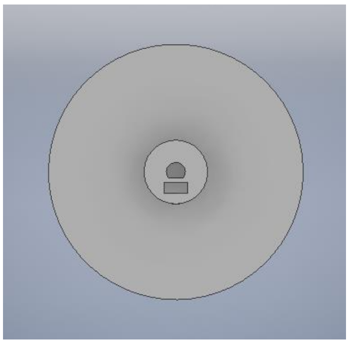

Figure 3.15 Bottom view of the active disk. It is possible to see the two holes used for the insertion of the d-shape connector and the nut.

The other disk, on the other hand, moves only passively and it does not need a system to attach the motor. It is a holed disk (Fig. 3.16) in which a wheel is inserted (Fig. 3.17). The wheel attaches to the disk along its internal lateral surface and it allows the rotation of the disk and the wheel together. Moreover, the wheel is fixed to an underlying structure (Fig. 3.18).
The underlying structure is a small bar that can be moved on the support structure of both disks. In fact, the fundamental characteristic of this second rotational disk is that it can be translated. It is moved away from the active disk to allow the easily insertion of the endoscopic cable and then neared to lock the cable between the two disks and allow a good execution of the movement.

The translation is permitted in this way: the disk and the wheel are fixed to the plastic bar (Fig 3.18). At the extremities of the bar pass two very long screws. The two screws then pass through the support structure of the disks in two slots that run parallel to the long side of the structure (Fig 3.18). Two small nuts, one on each side, are screwed thoroughly when the user want to block the translation and are released a little to allow translation (Fig. 3.21)

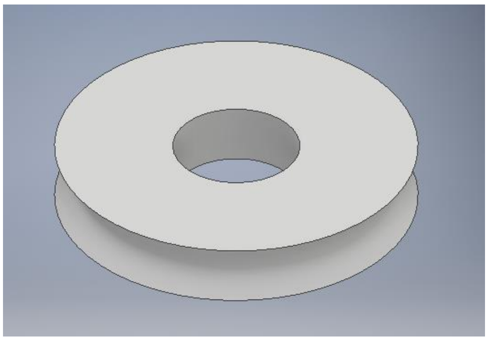

Figure 3.16 Holed passively mobile disk.

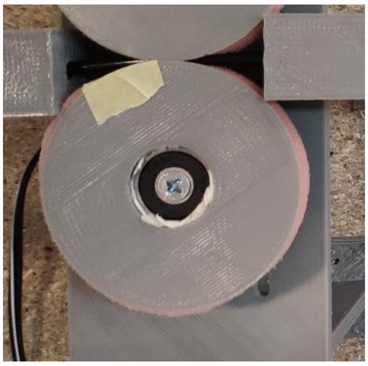

Figure 3.17 Wheel inserted in the central hole of the disk.

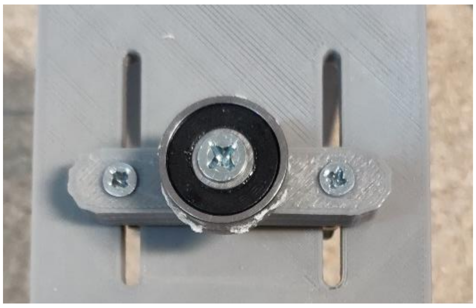

Figure 3.18 The system for the translation of the passive disk. It is possible to see the wheel that attaches to the disk. The well is fixed to a bar. At the extremities of the bar two screws are inserted. The two screws pass to the longitudinal slots of the support structure, allowing the system to translate.

As can be seen from some figures (Fig. 3.14, 3.16) the two disks have a re-entrant lateral surface. It allows the integration with a plastic or rubbery material that can increase the friction between the disks and the endoscopic cable and therefore favour the transmission of the movement. Moreover, it reduces cable wear, as it creates a malleable interface with the disks, no longer hard, like in case of the plastic used for 3D printing. In the experimental test phase, two different materials will be evaluated (one softer and one more rubbery / elastic) and the best will be determined.
The insertion of a softer material was the solution to the problem posed of the easy damage to the cable.

As already mentioned, a support structure is present (Fig. 3.13, Fig. 3.21). It has the main function of locating the two disks the right working height. The right working height is the one at which every movement is fully performed, without any problems of obstruction with the ground.
Moreover, it allows to fix the whole system to a wooden panel to which all the mechanical pieces are bonded.
In addition to the already described functionality of allowing the passive disk translation, it also has the purpose of fixing the motor to it. This is done by exploiting the base of the motor in which the D-shape connector is also present. On this basis there are two screws that can be extracted. The same pattern is reproduced on the structure (Fig. 3.19) with two holes for the screws and one for the D-shape connector. The screws are reinserted by placing the support structure in the middle. It attaches the motor to the system (Fig. 3.21).
The support structure also includes two lateral supports (Fig. 3.20) that have been added to better support the cable, making it easier to enter between two disks and to hold it in position between them. One is located before that the cable pass through the disks and another one just after the disks. The second one also well direct the cable coming out of the disks.

It is important to remember that the technological solutions designed should be able to adapt as easily as possible to other commercial ureteroscopes or endoscopes, as the LITHOS project proposes a solution to various clinical problems. In this case the same device would be adaptable to a multiplicity of instruments. It does not have specifically designed parts for this ureteroscope and the possibility of translating the second disk allows it to adapt to endoscopic cables of different size. The main drawbacks of this solution would be found in all applications: the risk of wear on the cable and the loss of a part of the length of the cable to implement the drag structure.

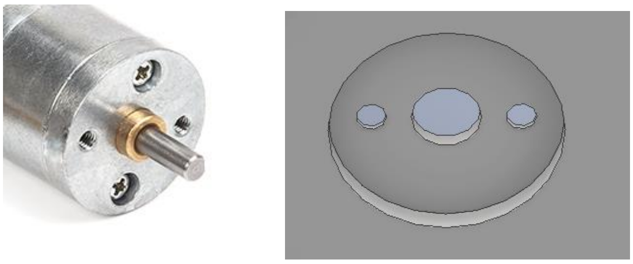

Figure 3.19 The motor base with the removable screws (right), the motor housing structure on the support system with the two external holes for the fixing screws and the internal one to allow the passage of the D-shape connector (left).

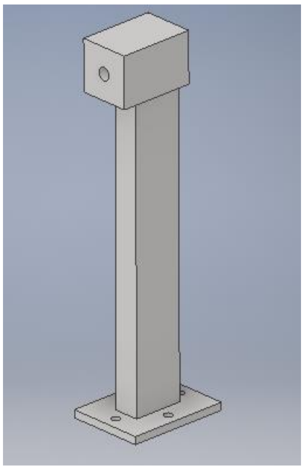

Figure3.20 Lateral support.

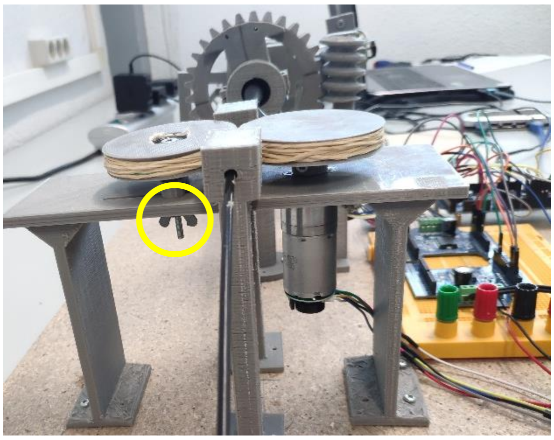

Figure 3.21 Support structure. On the left it is possible to see one of the screws that allow the translation of the passive disk (yellow circle). On the right the motor fixed to the structure.

Figure 3.22 The final structure in which it is possible to see the cable that runs between the two disks, the two disks with integrated an elastic material, the supporting structure and the two lateral supports.

3.2.2 Rotation movement

The main objective of the rotation movement (Fig. 3.23) is to improve the manoeuvrability of the instrument and its use. In fact, a rotation of the instrument reproduces in a rotation of the tip. By rotating the tip, it is possible to align the instrument with a target to help its elimination or favour its visualization or align it with a cavity of the urinary system that the user wants to travel. As mentioned, in the instrument description the tip has four different terminals (Fig. 3.24) (Two working channels of which one can be used for the laser, one led for the illumination, one sensor for the endoscopic images). When the target is found the user must be able to rotate the tip to allow the realization of certain tasks (visualization, capture, destruction) by aligning the right terminal with the target. Moreover, the tip can be deflected just in two direction and it is the fundamental a combination of the rotation movement with the deflection of the tip to move the ureteroscope with dexterity inside the urinary system.

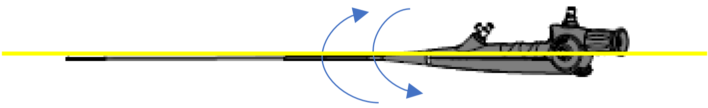

Figure 3.23 Rotation movement around the longitudinal axis (yellow line).

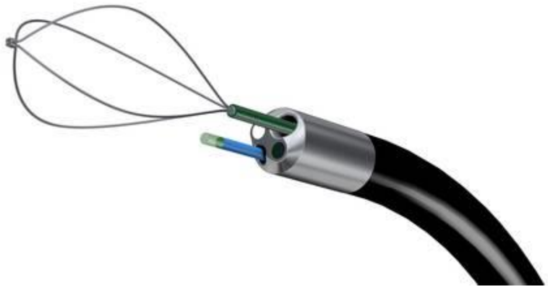

Figure 3.24 Tip of COBRA Ureteroscope. One working channel is used for the basket stone, the other one for the laser. The white terminal is the led. The empty and black terminal is the sensor for endoscopic images recording.

In case of manual control, this movement is performed directly by the surgeon by rotating the instrument with the hand placed on the ergonomic handle. This does not allow a complete rotation of the instrument, but at most 120° in each direction (Rassweiler, et al., 2018). In other literature studies the movement is performed by fixing the instrument to a mechanical arm that rotates and consequently rotates the ureteroscope. Avicenna Roboflex reaches a rotation range of 220 ° to each side, so it can sweep the whole range (Saglam, et al., 2014), while Sheikh Zayed Institute prototype can rotate only 150° to each side (Zhang L. A., et al., 2014, May)
Also in this work, the goal is to achieve a complete 360 ° rotation of the instrument as well as the possibility to rotate it on both sides. This would be an improvement introduced by robotics with respect to the human controlled case.
In addition to the objective concerning the range of motion, it should realize a movement with good precision and maintain a position once it is reached.
Also in this case a schematization of the full system (Fig. 3.25) and a picture (Fig. 3.26) of the result are previously reported. The red arrows of the scheme indicate a links between elements, while the yellow arrows indicate a zoom of a mechanical piece.

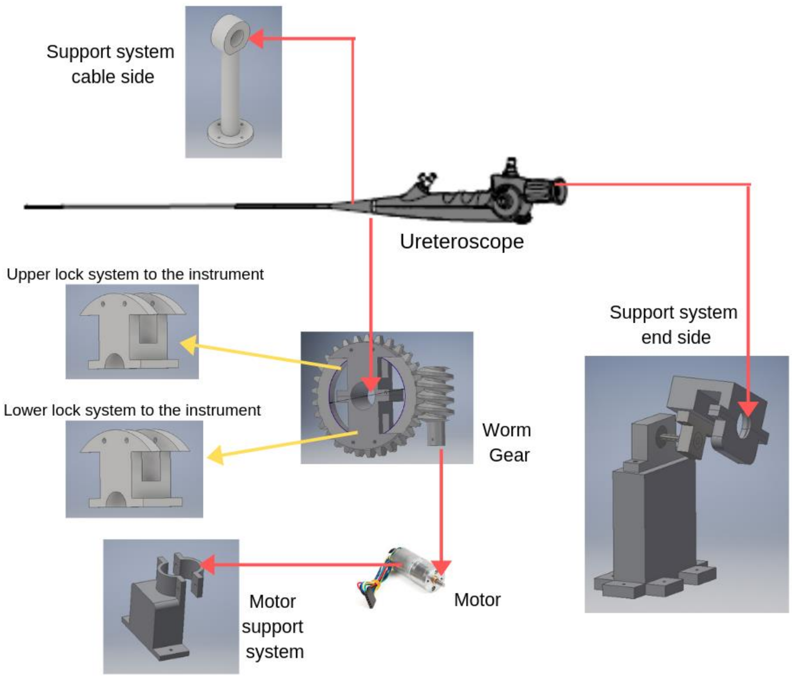

Figure 3.25 Schematization of the technology solution for the rotation movement. It is basically a worm gear system. The gear rotates thanks to the movement of the worm. The gear is constrained with the instrument.

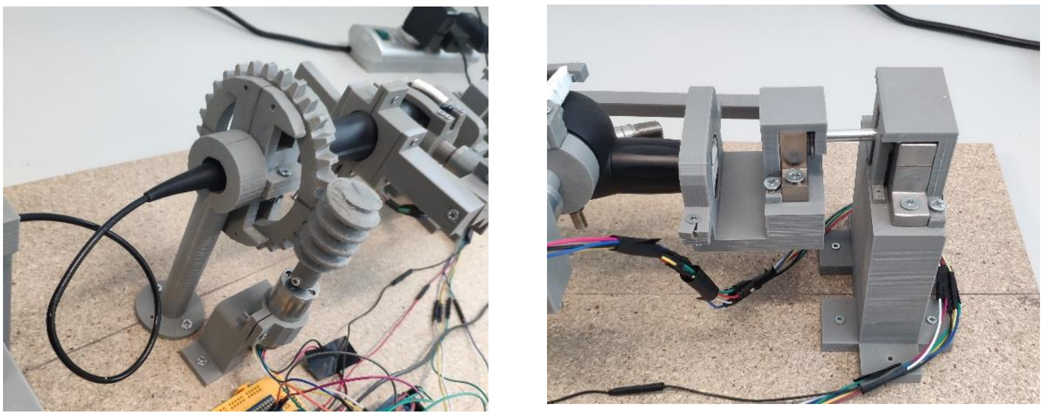

Figure 3.26 The result of the technology solution for the rotation movement.

The basic idea to develop this type of movement was born with the aim of finding a technological solution that allows a complete 360 ° rotation of the instrument. A worm gear system has been developed (Fig. 3.26). The worm is attached to the motor with the same type of solution already implemented in the insertion movement. The gear is instead fixed to the main body of instrument, close to the cable start (Fig. 3.25). It has been located in this area as it was the only one available, as the mechanical part that allows the tip deflection is developed close to the ergonomic handle, where the control lever is located.
The worm rotates thanks to the motor, consequently the gear rotates with it, moving the ureteroscope. This type of solution allows a potentially infinite rotation in both directions, with the only limit imposed by an excessive tangling of the electronic cables that could cause their damage. However, in the use of the instrument, it will be seen how this is a secondary problem and that two complete revolutions are easily achievable in the same direction without any risk of winding.
The worm gear is a strong speed reducer that allows to overcome a great resistance with a small power: what is lost in speed is gained in strength (Eq. 3.1)

$$P = V \cdot F \qquad \text{(Eq. 3.1)}$$

Where P is the total power of the transmission, V is the rotation velocity of the gear, F is the force that the gear can apply. If the velocity is small, the force can increase with a no too high value of power consumption.
It seems an excellent solution for this case where a very high speed is not required, but it required a good accuracy and the ability to move the instrument without a high force.

For the design of this system Autodesk Inventor Design Accelerator function has been exploited. It allows to quickly select the parameters of interest.

In designing the worm gear system two main factors are relevant.

- Transmission ratio: Considering the speeds (revolutions per minute) n_1 and n_2 of the worm (n_1, driving) and of the gear (n_2, conducted) respectively, the transmission ratio (i) can be expressed as:

  $$i = \frac{n_1}{n_2} \qquad \text{(Eq. 3.2)}$$

  Therefore, considering that the user wants to control the rotation as precisely as possible, what is required is as higher as possible transmission ratio, so that many turns of the worm correspond to a few turns of the gear.

- Structure dimensions. It is requested a no too big structure that could cause obstruction problem with the ground.

The main technical parameter that influence these two quantities is the number of gear teeth. More teeth, larger structure and higher transmission ratio.
A higher transmission ratio ensures a more precise movement, but at the same time implies the use of a thicker gear tooting that causes an increase in the spatial dimension of the gear and therefore a greater obstruction. A trade-off between these two factors was necessary to establish the dimensions of the gear. The final worm gear (Fig. 3.19) system has the following characteristics:

- Number of teeth: 30
- Transmission ratio: i=30
- External diameter of the gear: 90 mm

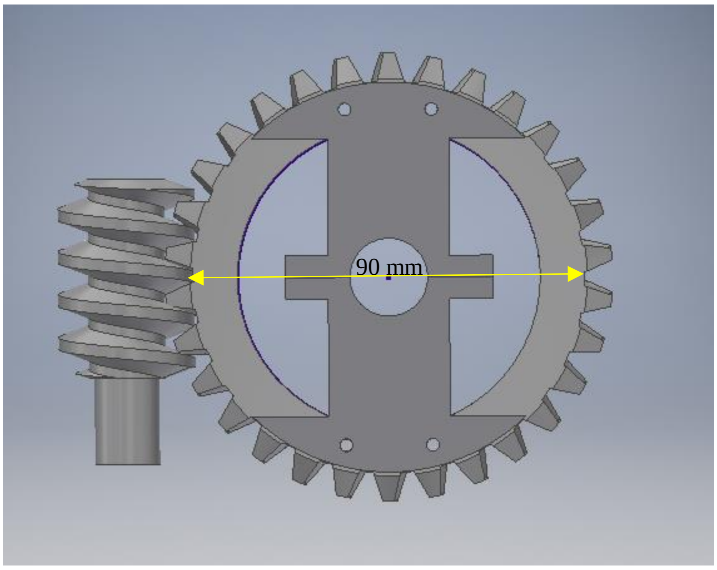

Figure 3.27 The worm gear system. In the central hole of the gear the ureteroscope can pass and be fixed. The bottom part of the worm is the protrusion used for the connection with the motor.

An ad hoc locking system (Fig. 3.29, 3.30) has been designed to fix the gear to the ureteroscope available for this work (COBRA, Richard Wolf). By changing this small detail, the same type of technology would be adaptable to other instruments. The figures 3.29, 3.30 shows the detail of the locking piece that it is replicated identical on the other side and blocks the instrument inside. The two pieces are bonded to the gear (Fig. 3.28) The curved central section has been designed imitating the dimensional features of the part of the instrument into which it would then be attached (Fig. 3.30). The two identical part can be connected thanks to two holes in the bottom part (Fig. 3.30).
The main problem of this locking system is the difficulty that the user encounter in installing and uninstalling the device each time. The two pieces of the lock system are joined together with fours screws and the instrument pass through the central hole. In this way they firmly attach the gear to the instrument. This assembly procedure is particularly tedious and long. In a future clinical application, it would be necessary to develop a lock-unlock system that attaches the instrument to the mechanical parts quickly.

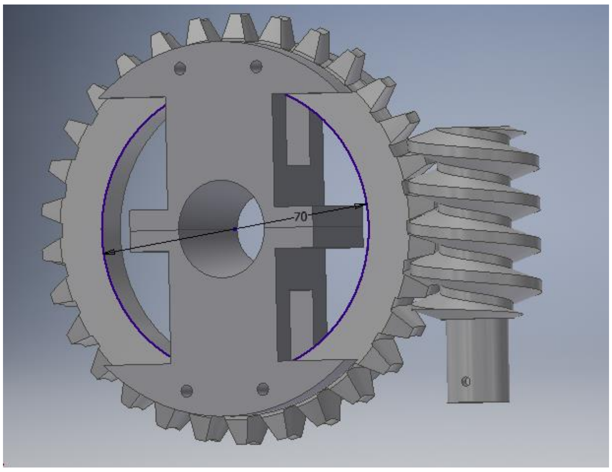

Figure 3.28 A different view of the worm gear, where it is possible to see the two parts of the lock system, mounted on the gear.

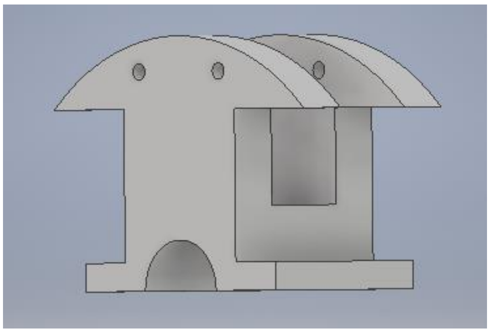

Figure 3.29 One of the two equal parts of the lock system to fix the ureteroscope with the gear. This part is fixed with the gear, that is inserted between the two round parts at the top

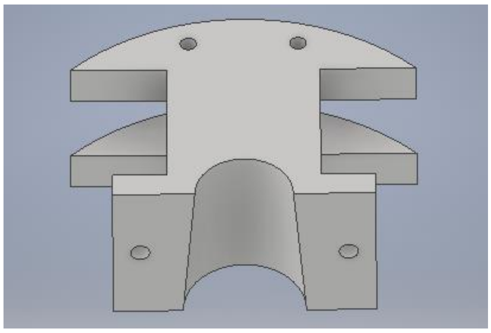

Figure 3.30 One of the two equal parts of the lock system to fix the ureteroscope with the gear. In the bottom part there are two holes, one each side, to connect the two equal parts. The curved central section replicates the ureteroscope geometrical characteristics.

A support for the motor (and the worm, bound to the motor) has been projected. This support uses a different principle with respect the one used in the insertion movement. A clamp divided in two curved pieces is designed. They have the same radial dimension of the motor and when they are closed one to other, they block the motor inside (Fig. 3.31). The left side part is then fixed to the ground, keeping the motor in this location.

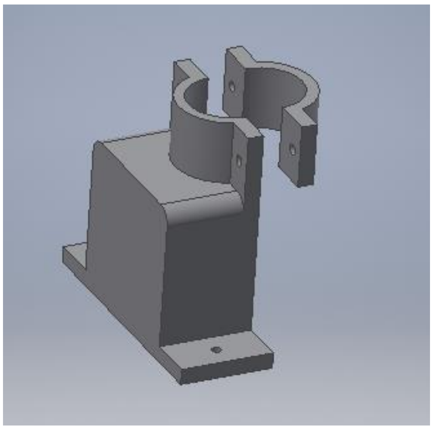

Figure 3.31 Motor support system. The two parts close, blocking the motor and fixing it to the ground.

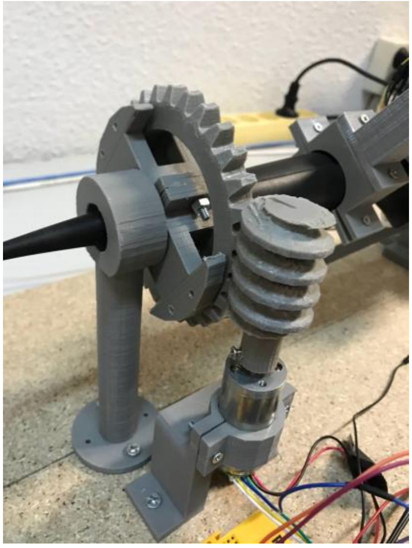

Figure 3. 32 Worm gear system and motor support system. It is possible to note how the system is located near the connection with the endoscopic cable. the first support system necessary, the cable-side one, is observable.

A further element to allow the rotatory movement is the ureteroscopic support. It is divided in two components. A first component located close to the worm gear system (Fig. 3.32, Fig. 3.35) and a second one (Fig. 3.36) positioned at the other end of the instrument, opposite to the tip. This support has the functionality to hold the entire system and cooperates in the rotation of it. In fact, the only gear worm system was not enough to allow movement and ,at the same time, to hold the structure in the right position. To exploit the functionality of the worm gear is necessary that the ureteroscope is fixed, without any possibilities of translation and with the rotation around its axis as only degree of freedom allowed. Just in this situation, by coupling the gear and the worm together, the principle of the worm gear is realized, and the movement is completed. As said, two constraints are needed to keep the endoscope on axis. They are schematized as a cylindrical (Fig. 3.33) and a spherical joint (Fig. 3.34) that, when they are applied together, they just allow the rotation around the axis of the instrument. Thanks to the overall work of these two pieces, the ureteroscope remains aligned and can only rotate. The position of the two elements of the support system has been determined so that the worm and the gear were well coupled.

The first support (Fig. 3.35) is simply a ring inside which the part, close to cable connection, can be inserted and supported. It leaves the system, freedom to rotate on its own axis and to translate.
The second support (Fig. 3.36, Fig. 3.38) is attached to the end of the endoscope thanks to special connection (1, Fig .3.36). This connection is specially designed and adapted to this endoscope. The connection would allow the endoscope to rotate within the connection itself. This movement is not desired. For this reason, it was necessary to introduce a bar (Fig. 3.37) that links this connection to the system which is used for tip deflection which is completely constrained with the body of the ureteroscope. In this way this non desired internal rotation is blocked. The main body (2, Fig. 3.36) of the structure allows the fixing to the ground and the placement of the system to the right working height. Another part (3, Fig. 3.36) is the one that allows the rotation. It acts like a spherical joint. It is composed by a metal tube that is free to rotate inside the upper part of the main body (2) and that is completely constrained to the special connection (1). This tube (3) is aligned with the axis of rotation of the system.

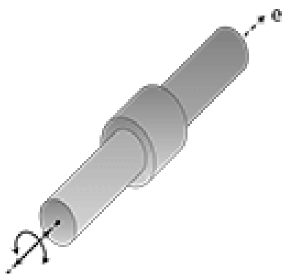

Figure 3.33 Cylindrical joint schematization (Comsol, 2019).

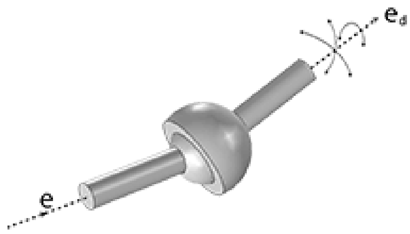

Figure 3.34 Spherical joint schematization (Comsol, 2019).

Figure 3.35 Support system cable-side. The instrument is inserted in the circle hole and can freely translate. It can be schematized in a cylindrical joint.

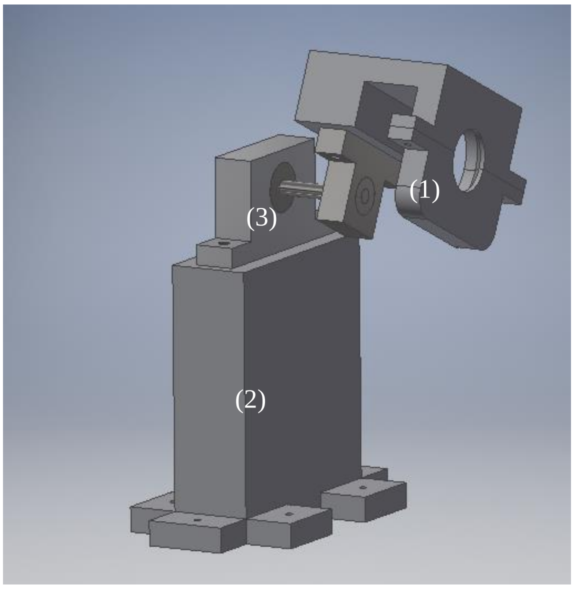

Figure 3.36 Support system end-side. (1) part is used to connect it with the ureteroscope. (2) is used to fix the system to the ground. (3) acts like a spherical joint, allowing the rotation of the instrument.

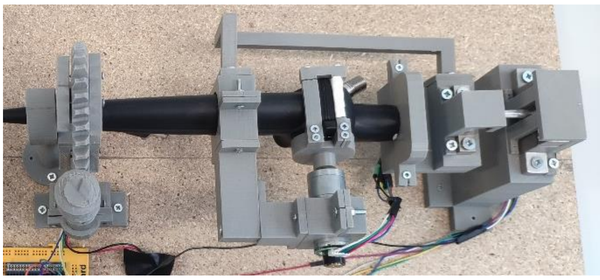

Figure 3.37 Top view of the robot. On the left side the worm gear system, on the right side the second support. In the upper part the bar that connects the second support and the mechanical part for the movement of the tip. This bar blocks the rotation of the instrument inside the connector.

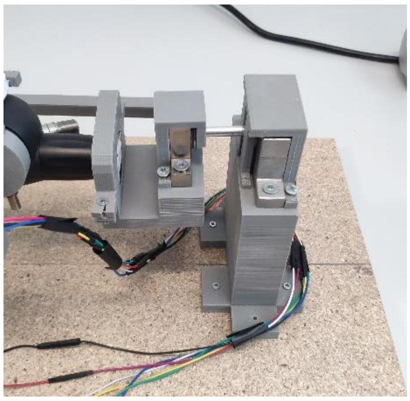

Figure 3.38 Side view of the second support.

This technological solution would be adaptable to different instruments with small modifications in the lock system between the gear and the body of the instrument and in the connection system between the second support and the final part of the instrument. The main drawback of this solution is the difficulty to install / uninstall the instrument each time.
Nevertheless, it achieves the prefixed objective with performances that will be evaluated in the last part of experimental tests.

3.2.3 Tip Deflection Movement

Tip deflection movement (Fig. 3.39) is the third and last fundamental movement. It is essential to move the instrument dexterously in the environment, reaching every part of the desired urinary system. It also allows to align the cable with a target and improve its visualization and its elimination. The tip can be deflected only in two main directions (Fig. 3.40). For this reason, it must be combined with the rotation in order to have a complete range of movement and allow an excellent control of the overall activity of the instrument.

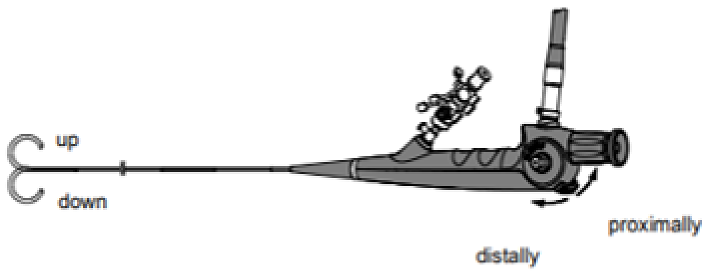

Figure 3.39 Tip deflection movement executed with the control lever located on the handle.

Figure 3.40 Deflection of the tip in just two directions (Richard Wolf, 2019).

In the majority of commercial ureteroscopes the movement of the tip is activated thanks to a control lever, placed on the ergonomic handle (Fig 3.41). Normally the lever moves around a circular structure (Fig 3.39) for a variant range based on the instrument. The lever of the ureteroscope used (COBRA, Richard Wolf) has a range of movement of ±45°, which is mapped in a range of ± 270° of tip deflection.
In case of manual control, the surgeon can easily manage this movement by driving the lever in the two possible directions.
Even in case of a robotic device the most immediate solution is to create a device that can be hooked to this lever, making it move and causing the tip deflection. This structure must not be an obstacle to the movement of the lever, reducing its range of movement. Moreover, it should allow good accuracy of movement, comparable to the human one, and it should remain stable in a position once it is reached.

Figure 3.41 Control lever located close to the ergonomic handle. It is also possible to see the circular structure around which the lever can move (Richard Wolf, 2019).

In other studies, the approach is similar. They build a system that operates directly on the lever. Zhang et al. created a pulley system to allow this movement, driven by a single motor (Zhang L. A., et al., 2014, May). In Avicenna Roboflex a lever actuation system is created directly on the mechanical arm to which the ureteroscope is attached (Saglam, et al., 2014).

Also in this case, a schematization of the full system (Fig 3.42) and a picture (Fig 3.43) of the result are previously reported. The red arrows of the scheme indicate a links between elements.

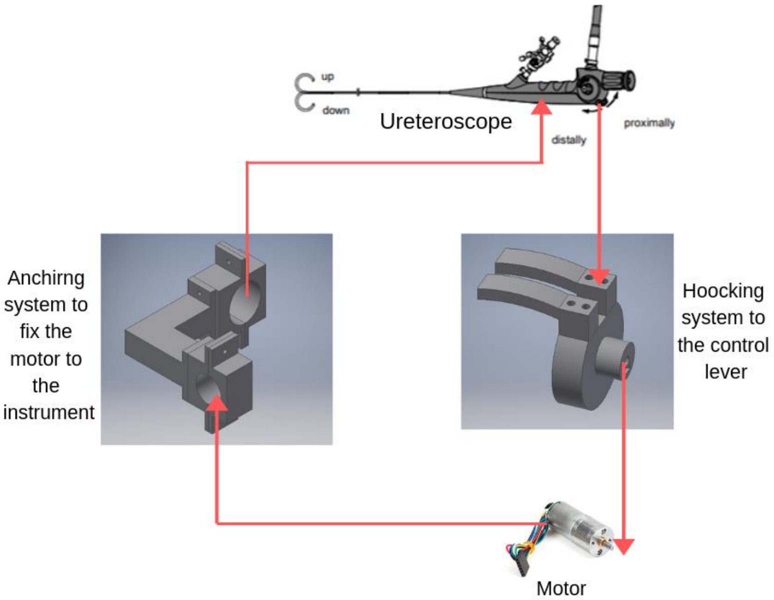

Figure 3.42 Schematization of the technology solution for the tip deflection movement. It is basically a hooking system that moves the control lever of the instrument.

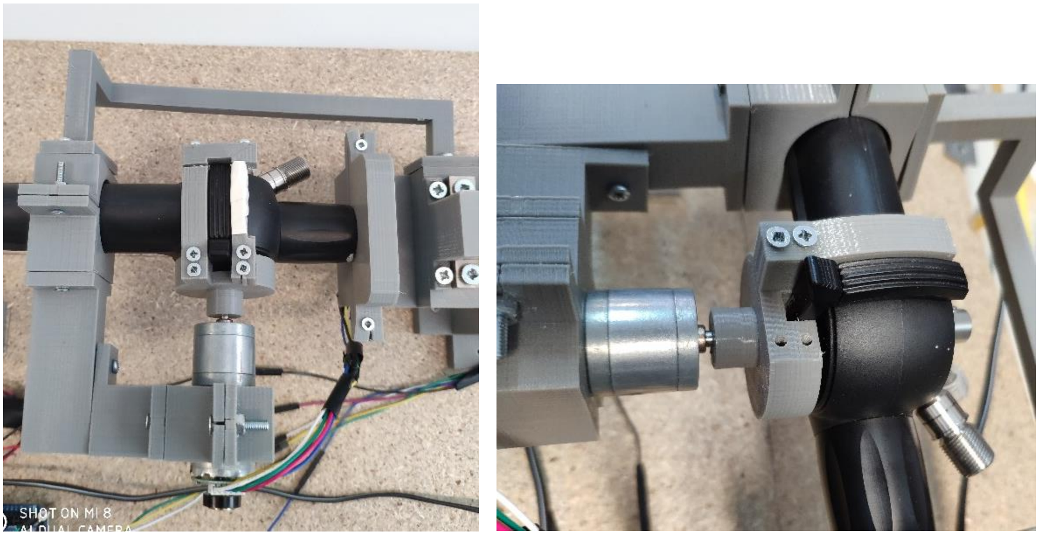

Figure 3.43 The result of the technology solution for the tip deflection movement.

In this work a specific main piece was designed (Fig. 3.44). It must hook to the control lever and allow its movement. A motor must then be attached to it, to allows the rotation of this specific piece and therefore the rotation of the control lever. Furthermore, a system must also be designed (Fig. 3.45) to keep the motor in position and anchors it to the endoscope. All these pieces will then rotate with the ureteroscope. Compared to the other two movements the entire mechanical part, including the motor, moves with the endoscope. It may cause an imbalance, as the motor (Weight 95 g (Pololu, 2019)) and the entire support structure are located on the same side of the instrument, causing a slight imbalance towards this side (a small problem related to it will be found in the experimental analysis). The mechanical hooking piece (Fig. 3.44) was designed as a circular structure, which mimics the shape of the lateral area of the lever zone (Fig 3.41). Two small lateral bars are then attached in the upper part of the hooking piece as it possible to see in Figure 3.44. They are located in front and behind the control lever (Fig. 3.45). The two lateral bars are then fix one to the other in their opposite ends respect to the one used to attach them to the circular structure (Fig. 3.45). It favours the locking of the lever between the two bars. The two lateral bars have a roundish base that follows the development line of the ureteroscope circular structure. The two bars allow to fix the lever and promote its movement. They have been drawn slightly raised so that they do not touch the circular structure of the ureteroscope on which the lever moves back and forth.
In the circular structure it can be noted the connection system with the motor (Fig. 3.44), which is the same already used for the other movements.

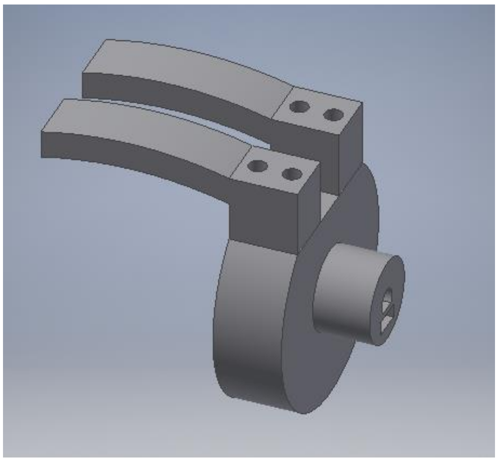

Figure 3.44 Hooking system with the two lateral bars that improve the hooking and push the control lever. It is possible to see the connection system with the motor and the round shape of the base of the lateral bars.

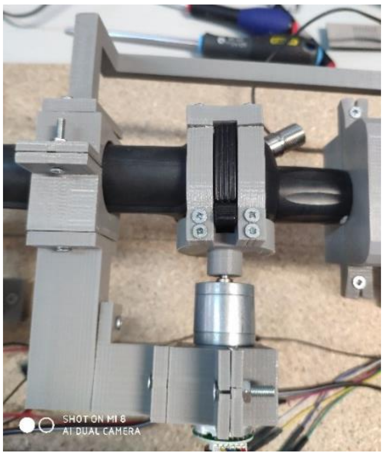

Figure 3.45 Top view of the complete system for tip movement. It is possible to see how the two lateral bars are connected to each other in the end opposite to the one of attachment to the circular construction. Moreover, the L-shaped system that blocks the motor to the ureteroscope.

A motor anchoring system has been designed to constrain the motor to main body of the instrument (Fig. 3.48). It is composed by two locking systems. The first clamps the motor (Fig. 3.46) and the second clamps the endoscopic body (Fig. 3.47). These two are then connected with an L-shaped structure which keep the motor in this location and bound it to the ureteroscope structures. In this way, when the instrument rotates, the motor rotates with it. It is remembered that the only degree of freedom allowed to the endoscope body is the rotation around its axis, but if for some reason it moved or changed his height in hypothetical developments of this prototype, the motor would continue to move with the instrument.

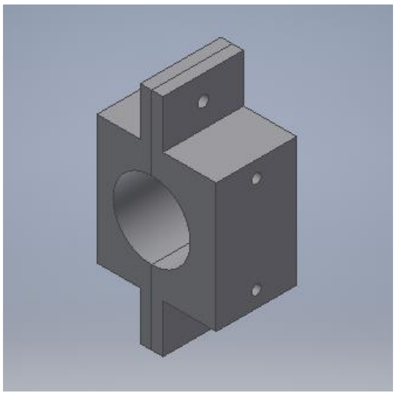

Figure 3.46 Locking system for the motor. The central section is circle with a diameter of 25 mm, like the motor. In the upper part it is possible to see a hole to connect the two-mirroring part. Others two holes are used to connect this part with the L-shape connector.

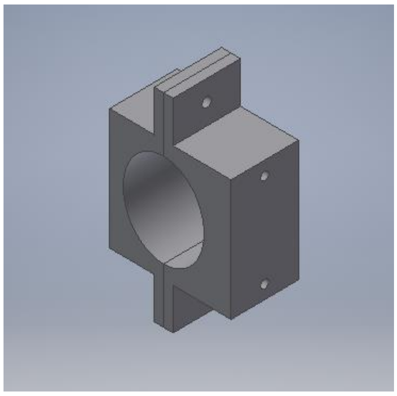

Figure 3. 47 Locking system for the ureteroscope. The central section is oval, the same shape of the instrument body. In the upper part it is possible to see a hole to connect the two-mirroring part. Others two holes are used to connect this part with the L-shape connector.

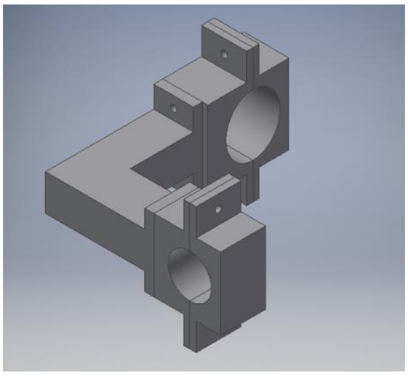

Figure 3.48 Complete anchoring system with the two locking parts and the L-shaped connector.

This system achieves theoretically the objective with performances that will then be judged in the final experimental part. It is a specific system for this ureteroscope, as different parts, such as the circular structure, the bars, the anchoring systems, are constructed by adapting to the specific instrument. Modifying these dimensional details, however, the system could be adapted to other type of commercial endoscopes that are based on the same principle to allow the tip deflection. Two main drawbacks have been noted. The first one the system is slightly unbalanced towards the side where the motor is allocated. The second one it has been created a quite cumbersome structure, binding the motor to the instrument. The main cause for which the instrument must work elevated (axis height 130 mm) is the position of this motor. However, the obstruction level is certainly not exaggerated and does not cause serious problems. The height at which he works is not at all problematic.
In Figure 3.45 it is possible to see this lateral obstruction created by the motor. On the other side a smaller obstruction is generated by the bar used to block the rotary movement of the endoscope with respect to the support connector, described in the previous section.

Chapter 4: Electronics and Control

This chapter will deal with the control and management system of the device. Firstly, the hardware, the physical and electronic parts will be discussed and then the firmware, that allows the control and the communication of the hardware specific elements, will be explained.
It is important to introduce the functionalities and objectives that the control system must implement in order to better understand the choice of the various elements.
The fundamental objectives to be achieved are:

- Activation of the motors to allow all the desired movements of the ureteroscope using a controller that the user can manage from a comfortable and convenient position.
- Creation of a graphic interface in which the user can monitor velocity and position data of the motors.

At the hardware level, a micro controller, a control system and a personal computer are required. They have different objectives, achieved with the firmware:

- The micro-controller deals with:
    - receiving data regarding the activation of the motor from the PC.
    - activating and deactivating the 3 motors according to the received data from the PC.
    - receiving data produced by the encoders
    - processing and sending the data from the encoders to the PC to obtain information about position and speed.

- The control system (3DMouse) deals with:
    - allowing the user to manage the different movements.

- The PC deals with:
    - reading the data concerning the movements from the control system (3DMouse).
    - sending the data concerning the movements to the micro-controller.
    - receiving data of position and velocity from the microcontroller.
    - creating a graphical interface to plot the received data of velocity and position.

At the firmware level, two different codes have been developed, one for the management of the microcontroller functions and one for the management of the PC activities.

Figure 4.1 shows a detailed schematization of all the elements and the data transmitted of the system, that will be described hereafter.

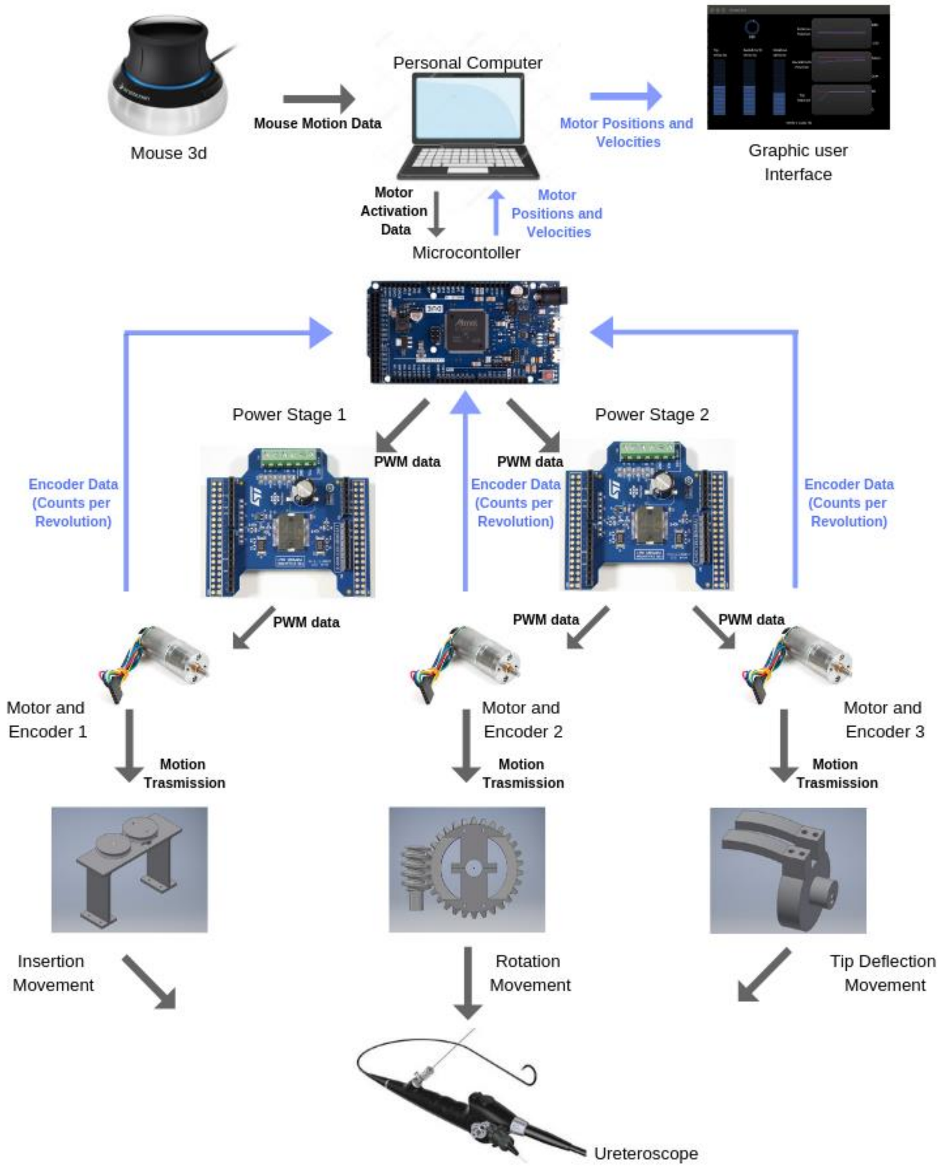

Figure 4.1 Schematic Representation of all the system elements and the data transmitted between them.

4.1 Hardware

The following section describes the hardware needed to manage the motors and consequently the movements of the device.
The hardware should achieve the following main objectives:

- Allow the user to control the movement of the implemented device, satisfying the initial specifications of range of motion and precision.
- Activate and deactivate the motors according to the commands received from the control system.
- Transmit and collect the signals from the motor encoders and the control system.

A microcontroller has been used to directly supply the motors and control their movement in two possible directions, with different velocities. Furthermore, a control system is necessary to allow the user to control times and modalities of motor activation.
In this work, both hardware elements communicate with a personal computer. A firmware will allow the communication between the hardware elements and the personal computer. In the firmware section, the continuously data exchange between them will be described.

4.1.1 Electronic Hardware

This section describes the electronic tools used for the realization of the proposed objects. The fundamental elements that compose the electronic system are:

- 1 Arduino Due, which incorporates the microcontroller Atmel SAM3X8E.
- 2 X-NUCLEO-IHM04A1, dual brush DC motor drivers based on the H-bridge L6206 expansion for STM32 Core
- Cables for connections.

The Arduino Due (Fig. 4.2) is the fulcrum of the electronic control system. It is an Arduino board based on the Atmel SAM3X8E ARM Cortex-M3 CPU equipped with 54 digital input and output pins and 12 analog pins. It is also equipped with 3 output pins that provide 5V and 5 output pins that provide ground that can be easily used for powering motors or power stages. The Arduino Due card works at 3.3V and it has a flash memory of 512 kB and clock speed of 84 MHz. It also provides two types of USB ports that allow connection with the PC. Both will be exploited. In particular, a native USB port will be used as a serial port for sending and receiving data and a programming port that will be used to load the firmware onto the device. The native port is introduced in this board to enable the Arduino to emulate different USB devices and allow a high-speed serial communication. These ports also allow the power supply to the microcontroller (Arduino, 2019). These characteristics make it a good board for the management of large-scale projects, that require several connections and that need discrete computing power. In this case, the microcontroller will have to perform several operations of sending, receiving and computing data, as well as continuously activation and deactivation of the motors. It is important to emphasize that this work is not focused on the evaluation of different control techniques based on different microcontrollers and different programming environments. Certainly, Arduino is an excellent system for this first prototyping phase, in which a detailed level of control, that Arduino could not provide, is not required. Further improvements are possible from this point of view, but the Arduino Due is a good solution to achieve the goals set in this work.

Figure 4.2 Arduino Due Board. (Arduino, 2019).

In cooperation with the Arduino it is necessary to use a power stage for the motor control, in this case composed by 2 X-NUCLEO-IHM04A1 (Fig. 4.3). They are dual brush DC motor expansion board that can drive two bipolar DC motors or four unipolar DC motors. For this reason, two expansion boards are used to control the three motors. They allow to control the direction and the velocities of the motors through an H-bridge circuit. They are connected directly to the Arduino (Tab. 4.1)

They are equipped (Fig. 4.4) with a power supply connector through which it is powered and attached to the electric current with a maximum voltage of 50 volts. It has four motor phases connectors, two for each motor that allow the activation of the motor in two possible direction thanks to an H-bridge system. (St, 2019)

The H-bridge is a circuit that allows to apply the load voltages in two directions and therefore to make the current flow in the two possible ways so that the motor can turn clock and counter clock wise. Depending on the level of voltage and current set, the motor can run at different powers and turn at different velocities.

The PWM (pulse width modulation) technique is used to control the transistor of the H-bridge. It is based on the modulation of the duty cycle of a square wave that allows to obtain real intermediate values between the digital values of 0 and 1 and therefore adjust the motors power.

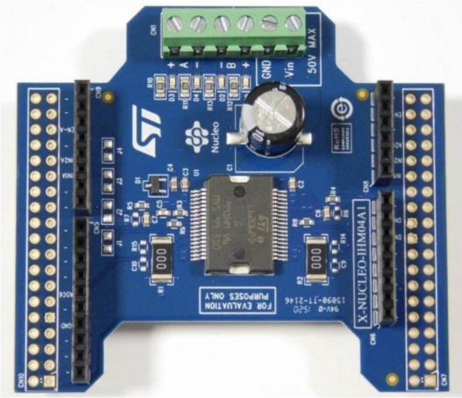

Figure 4.3 Power Stage, X-NUCLEO-IHM04A1, dual brush DC motor drivers based on L6206 expansion for STM32 Core (St, 2019).

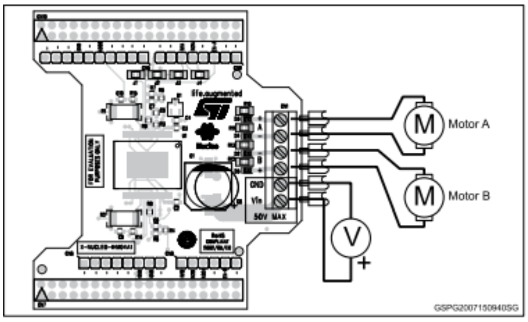

Figure 4.4 Schematic representation of the motor drivers. In the right part it is possible to see the connections with two motors and with the power supply system. (St, 2019)**.**

It is also important to introduce the connections necessary for the management of the motor to better understand the use of all the cable exploited at the hardware level.
The gearmotors with encoder are equipped with six cables of six different colours and functions (Fig. 4.5). The cables connections between the motor and the electronics system are summarized in Table 4.1.
Two cables (red and black) are used for the bipolar control of the motor. They will be connected to the motor phases connector of the power stage, and according to the current flow direction, the motor runs in the two possible ways with different velocities.
Two cables (green and blue) are necessary for the positive (between 3.5V and 20V) and ground power supply of the encoder. They will be connected to the pins of the Arduino that supply 5V (positive pole) or that supply GND (ground pole).
The last two cables (yellow and white) are used to transmit the signal produced by the encoder. They send signals 1 and 0 alternately when the motor position changes. The two outputs are square waves from 0 V to Vcc approximately 90 ° out of phase. The frequency of the transitions relates the speed of the motor, and the sequence of the transitions relates the direction. They are connected to two digital interrupt pins of the Arduino. The operation of the signal and its evolution will be described in more detail in the description part of the firmware.

Figure 4.5 The upper part of a motor with the encoder and all the cable needed for motor management (Pololu, 2019).

Additional connections are needed between the expansion board and the Arduino for the system operation (Fig. 4.6). Each H-bridge has:

- An enable pin that allows the activation of a motor control. This pin is connected to a high fixed digital pin of the Arduino.
- Two input pins that receive the PWM signal produced by the Arduino. For this reason, they are connected with Arduino digital pins that generate the PWM signal.

In addition, each expansion board has a ground pin that connects to GND pin of the Arduino.
All these connections are summarized in Table 4.2.

Colour	**Function**	**Connections**
Red	Motor power, positive pole	Motor connection +, power stage
Black	Motor power, positive Negative	Motor connection -, power stage
Green	GND encoder	GND Pin, Arduino
Blue	Vcc (3.5-20 V) encoder	5 V Pin, Arduino
Yellow	Encoder output A	Digital Pin, Arduino
White	Encoder output B	Digital Pin, Arduino

Table 4.1 Connection between the motor and the electronic system.

Pin Power Stage	Function	Pin Arduino
Enable A	Activation control motor A	Digital pin, fixed high
Input1 A	PWM Control motor A, direction 1	Digital Pin, generating PWM signal
Input2 A	PWM Control motor A, direction 2	Digital Pin, generating PWM signal
Enable B	Activation control motor B	Digital pin, fixed high
Input1 B	PWM Control motor B, direction 1	Digital Pin, generating PWM signal
Input2 B	PWM Control motor B, direction 2	Digital Pin, generating PWM signal
GND	Ground	Pin GND

Table 4.2 Connection between the power stage and the Arduino Due.

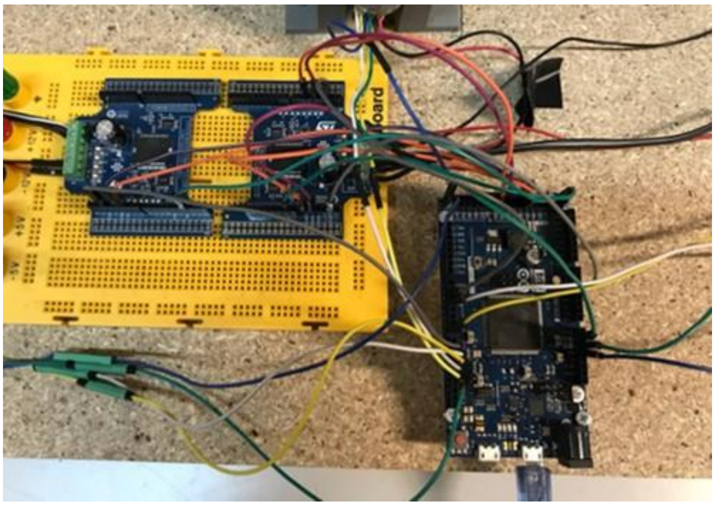

Figure 4.6 The Arduino Due connected with two expansion boards for motor driving.

4.1.2 Control System Hardware, 3D mouse

This section describes the second fundamental element of the hardware: the control system that allows the user to control and move every element of the system, comfortably seated in an ergonomically advantageous position and potentially far from the operating area to avoid contact with x-ray machines.
The choice of the control system in this type of work fell was a 3D mouse (SpaceMouse Compact, 3d connexion, Boston, USA) (Fig. 4.7). As for electronics, the aim of this work was not to design and develop a specific control system with the best performances but use an approachable and commercial device that could ensure good performance in this first prototyping phase. For this reason, further developments would certainly be needed from this point of view.
The choice was first based on laboratory availability. In fact, this type of control had already been used in a virtual reality simulator for flexible ureteroscopy developed by the laboratory where this work was carried out (Peral Boiza, 2018). This virtual simulator, that perfectly enters the context of the work described here, had been tried by some surgeons, reporting positive feedback about the use of a control solution based on a 3D mouse. Moreover, other studies in literature (Zhang L. A., et al., 2014, May) have used this kind of approach in some phases of the work.

Figure 4.7 SpaceMouse Compact, 3d connexion, Boston, USA (3dconnexion, 2019).

The 3D mouse is a device normally used for 3D navigation with 6 degrees of freedom. It consists of a fixed underlying part and a movable controller cap. The base is in brushed steel that allows device stability for precise 3D navigation. The controller cap can be pushed or pulled completely, can be rotated to the right or to left and can be tilted in one direction. It also owns two lateral buttons (3dconnexion, 2019).
The purpose was to associate a type of mouse movement for each type of robot movement. An approach that could be as intuitive as possible for the user was used (Tab. 4.3 and Fig. 4.8). The movements association was:

- The right and left rotation of the mouse cap to rotate the endoscope.
- Back and forth inclination of the mouse cap to perform the insertion and retraction movement of the endoscopic cable.
- The right and left inclination of the mouse cap to perform the tip deflection movement.

The possibility of accelerating and decelerating one of the movements using the two lateral buttons was also introduced. It was decided to accelerate and decelerate the rotation movement of the system. This choice was made based on some trials performed on the robot. The rotation movement is the one with a larger range. For this reason, accelerating its execution could be useful to pass quickly to two different points. It is also useful to slow down to perform a more precise movement when the desired zone has been reached. A more in-depth discussion about which movements should be introduced the possibility of changing the execution speed will be done in the experimental test results chapter. It is in fact expected that other movements can be accelerated or decelerated by improving the control system. The same firmware technique could easily be used in other cases without further complications.

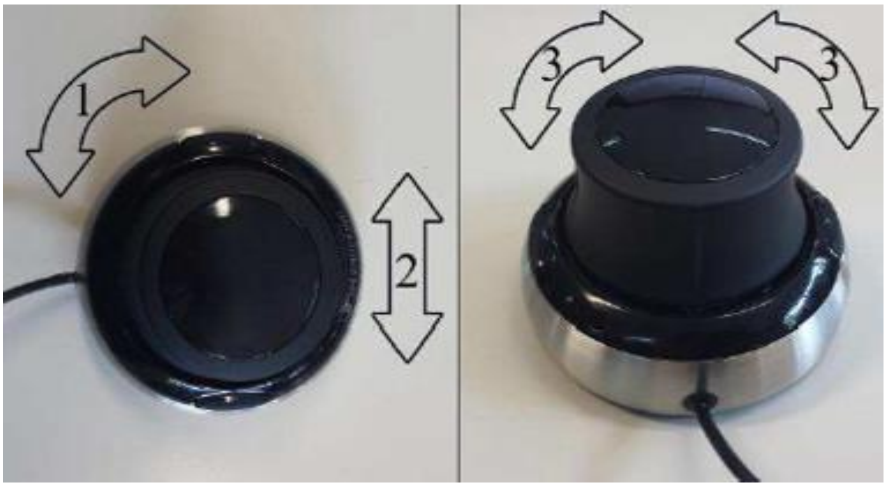

Figure 4.8 The movement of the 3Dmouse used to perform the system motion. 1: rotation of the cap to rotate the ureteroscope; 2: Back and forth inclination to insert and retract the cable; 3: Right and left inclination for the tip deflection.

Robot Movement	Mouse Movement
Rotation of the instrument	Right and Left rotation of the controller cap
Insertion/retraction of the cable	Back and forth inclination of the controller cap
Tip Deflection	Right and Left inclination of the controller cap
Acceleration/Deceleration rotation	Lateral buttons

Table 4.3 Association between mouse and robot movements.

In the following figures (Fig. 4.9 and Fig. 4.10) the full system is reported. It is possible to see all the mechanical pieces used for the movement of the robot, the electronic hardware and the 3DMouse for the user control of the device. It is important also to underlay the presence of a personal computer. The personal computer is the link element between the 3D mouse and the electronic hardware. The mouse, in fact, sends its data to the PC, where they are elaborated and sent to the Arduino. The firmware developed on the PC allows the communication between the element and the data transmission and computation, as reported in the schematic (Fig. 4.1). On the personal computer the values of position and velocity of the motor can be monitored thanks to the graphic user interface.

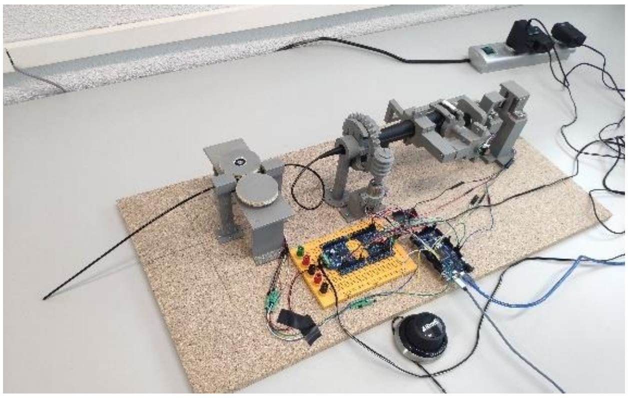

Figure 4.9 Full system.

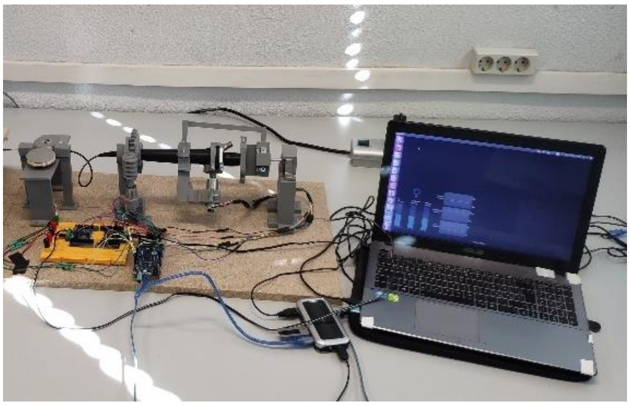

Figure 4.10 Full System with the Personal Computer.

4.2 Firmware

The following section will describe the firmware developed for the control of the robotic system. The firmware should allow the communication and the data transfer between the hardware elements of the system (3D Mouse, PC, and a microcontroller), the activation of the motors in accordance with the user's wishes and the creation of a graphic interface on the PC screen for the plotting of data about position and velocities of the motors.
Two software were needed:

- Arduino IDE: is a specific software to program Arduino microcontrollers. It was chosen because the microcontroller exploited is an Arduino Due and in this prototyping phase it is not required a deep control that Arduino would not give to the user. Arduino IDE is an intuitive and easy to use platform for a high-level programming, that may be acceptable for this phase. The firmware developed in Arduino IDE is loaded on the Arduino board and takes care of managing all the functions that the microcontroller must perform.
- Chai3D: is an open source C ++ programming software, optimized for the introduction of haptic effects on robots. As mentioned, the introduction of haptic effects is not an objective of this work. Nevertheless, this would be one of the first potential innovations that could be introduced in this kind of device. Moreover, the virtual simulator for flexible ureteroscopy, developed by this laboratory (Peral Boiza, 2018), introduces haptic effects and it has been fully programmed in Chai3d. A further possible development could be the connection of the robotic system implemented in this work with the virtual simulator. For these reasons it was decided to use Chai3d as a development environment. Chai3d should take care of all the functions required by the PC, among which the reception of the data from the 3D mouse and the elaboration of a graphical interface for the user.

Before the description of the two firmware, it is important to remember the objectives that each of the two codes must achieve.

Arduino has the following objectives:

- Data collection from the encoder.
- Calculation of the motor position and velocity, from the data sent by the encoder.
- Sending of position and velocity data to Chai3D.
- Reception from Chai3D of the data necessary to control the direction and power of the motors.

- Management of the PWM for the activation of the motors, in accordance with the data received from Chai3d.

Chai3d has the following objectives:

- Connection with the 3D mouse, receiving data about the user actions.
- Processing of the 3D mouse data.
- Sending data to Arduino for the control of the motors.
- Receiving motor position and velocity data from Arduino
- Creation of a graphic interface, for the representation of position and velocity values.

As it can be seen from the intended objectives, a continuous data exchange between the two firmware must be performed to manage the functioning of the device. The data transfer is represented by the arrows in Figure 4.1 and Figure 4.11. The black arrows represent the data flow that goes from the 3DMouse to the motors and blue arrows represent the data that go from the motor encoders to the graphic user interface. For the realization of these objectives it was necessary to create a continuous bidirectional communication protocol between the two software. A small summary scheme is also reported here (Fig. 4.11).

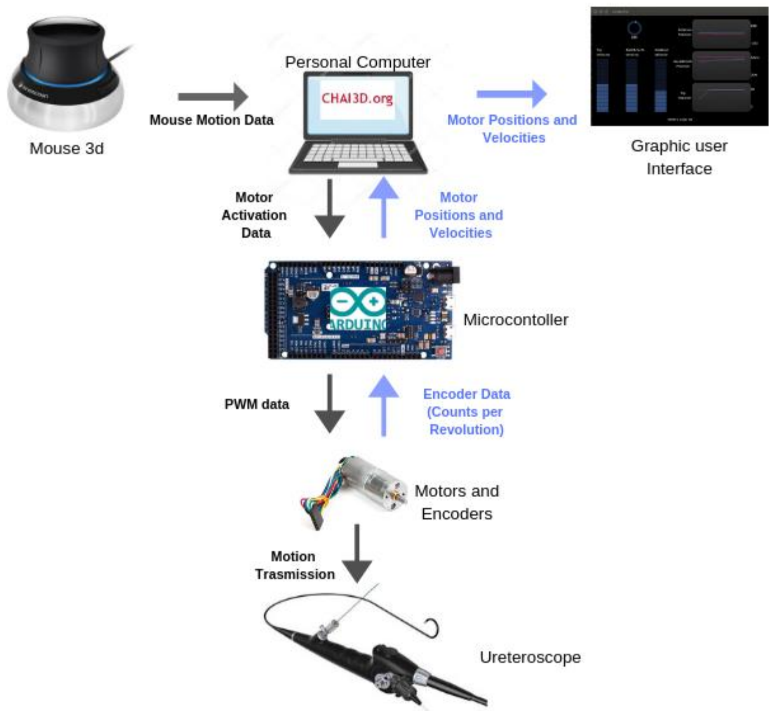

Figure 4. 11 Small schematization of the elements involved and the data transfer

4.2.1 Arduino Code

In this section the general functioning of the Arduino Code and the details of the implementation of all the functions necessary for the intended objectives will be described. Many functionalities are managed using an interrupt handler, also known as an interrupt service routine (ISR), that is a call back subroutine in an operating system whose execution is triggered by the reception of an interrupt. Interrupts can be the occurrence of a hardware event or each sampling period. Interrupt service routine are useful for making things happen automatically in microcontroller programs and can help to solve timing problems. For an easier management of timers for ISRs, it has been used the *duetimer* library which is a fully implemented timer library for Arduino Due by Ivan Seidel (GitHub, 2019) .
In case of the Arduino Due, the SAM3X8E CPU has 3 timer counters (TC). Every timer counter contains 3 channels. Every channel has its own counters and interrupt handler that are independent of other channels. In other words, each channel can be considered as a separate "timer” and is like having 9 separate timers.
The general idea of the code is to create some functions that deal with the various necessary functionalities and that are activated as ISR. In this way it is easier to have a control of the system timing. Furthermore, the use of faster and light computational functions is recommended when working with several ISRs, so that another ISR does not start before the end of the previous one.
The following functions will be implemented.

- A function that will collect the encoder data, and it will be activated every time the encoder sends a data.
- A function that will calculate position and velocity data based on the encoder data and save them in a global variable.
- A function that will take the data from the global variable about position and velocity and send it to Chai3d.
- A function that will read the data received from chai3d and save them in a global variable.
- A function that will use the data saved in the global variables from Chai3d to activate the motors.

Data collection from encoder

In this device three motors have been used, and each of them is equipped with a magnetic encoder, which allows to obtain data about the position and the power of the motors. The procedure that will be described for the collection and processing of this data is the same for each encoder.

As previously mentioned, the encoder data is transmitted via two cables (yellow and white). These two cables can transmit one bit each, so a value of 0 or a value of 1. The encoders integrated are 48 Counts per revolution in quadrature. It means that they record 48 counts for each complete revolution of the input shaft. Every step (1/48 of round of the shaft) one of the two bits changes, alternately. They create a cycle of variation of the two bits which, based on the order it evolves, allows to have information about the rotation direction of the motor. The two bits always change in one order or in exact opposite one, as shown in Table 4.4 and Table 4.5. They vary as square waves signals 90° out of phase. Based on the order of variation of the bits, the direction of motor is determined. Order 1 implies a counter clockwise rotation, order 2 implies a clockwise rotation. At this point until the direction of rotation changes, the position value continues to increase / decrease according to the direction. If there is a change in this direction, this value starts to decrease / increase in the opposite way.

	Step 1	**Step 2**	**Step 3**	**Step 4**	**Step 5**	**Step 6**	**Step 7**	**Step 8**
Bit 1	1	1	0	0	1	1	0	0
Bit 2	0	1	1	0	0	1	1	0

Table 3.4 Variation of bits for each motor step in order 1.

	Step 1	**Step 2**	**Step 3**	**Step 4**	**Step 5**	**Step 6**	**Step 7**	**Step 8**
Bit 1	1	0	0	1	1	0	0	1
Bit 2	0	0	1	1	0	0	1	1

Table 4.5 Variation of bits for each motor step in order 2.

This function is implemented in the Arduino Code through the activation of an ISR every time a change is registered in one of the two pins (Fig. 4.12). In both cases the *ENCODER_count* function is activated.

```
attachInterrupt(digitalPinToInterrupt(pinEncoder1), ENCODER_Count1, CHANGE);
attachInterrupt(digitalPinToInterrupt(pinEncoder2), ENCODER_Count1, CHANGE);
```

Figure 4.12 AttachInterrupt activate the function ENCODER_count as an interrupt every time the pinEncoder changes.

The *attachInterrupt* function is defined in an initialization function in which first the position and velocity values are reset, and the two pins of the Arduino are set as input pins in order to be able to receive data.

The *ENCODER_count* function reads the two pins, and saves them in a variable *ENCODER_cStateEncoder* (Fig. 4.13)

```
//Workout what the current state is.
char chanA = digitalRead(pinEncoder1);
char chanB = digitalRead(pinEncoder2);

//2-bit state.
ENCODER_cStateEncoder1 = (chanA << 1) | (chanB);
ENCODER_cStateEncoder1 = ENCODER_cStateEncoderOld1;
```

Figure 4.13 This code read the two pins and save them in a state encoder variable.

Then it checks that the new encoder pin status is valid:
-The XOR operation with the previous pin state should not result 11 (=*INVALID*), that would imply that both have changed.
-The new pin state should be different from the previous one, that would imply that neither of them has changed (Fig. 4.14)

```
//Entered a new valid state.
if (((ENCODER_cStateEncoder1 ^ ENCODER_cStateEncoderOld1) != INVALID) &&
    ( ENCODER_cStateEncoder1 != ENCODER_cStateEncoderOld1 )) {
```

Figure 4. 14 It verifies that new status is valid, so that just one of the two pins has changed.

.

It updates a *change* variable through the operation in Figure 4.15. *PREV_MASK* has a value of 01 and *CURR_MASK* has a value of 10. It is possible to verify how the result of the operation is always zero if it is rotating clockwise and 1 in the counter clockwise case. If the result of this updating operation is 0, change takes a value of -1.

```
//2 bit state. Right hand bit of prev XOR left hand bit of current
//gives 0 if clockwise rotation and 1 if counter clockwise rotation.
change = (ENCODER_cStateEncoderOld1 & PREV_MASK) ^ ((ENCODER_cStateEncoder1 & CURR_MASK) >> 1)

if (change == 0)
  change = -1;
```

Figure 4.15 The updating variable change takes a value of 1 or -1 according with the motor rotation direction.

An *ENCODER_lCounterEncoder* variable updates by +1 or -1 depending on the direction of rotation. This is the motor counts value that will be the fundamental data that will be used for the performance study in the experimental phase.

Position and Velocity Updating

The position values are already fully calculated thanks to the *ENCODER_count* function.
For what concern the velocity values, they are calculate every predetermined period, thanks to the use of an interrupt service routine activated in the encoder initialization function. The ISR is activated every *ENCODER_SPEED_CALCULATION_SAMPLING_PERIOD ·1000* μsec. The sampling period can be managed by changing this constant. The ISR activates the *ENCODER_CalcSpeed* function. (Fig. 4.16)

```
Timer4.attachInterrupt(ENCODER_CalcSpeed1);
Timer4.start(ENCODER_SPEED_CALCULATION_SAMPLING_PERIOD * 1000);
```

Figure 4.16 Function to activate the ISR that calculate the motor velocity.

This function exploits the last two values of *CounterEncoder* and calculates a first order discretized derivative based on two position values. These are the actual position and the position value when the last speed calculation was executed, they are so separated in time by the sampling period.
The two values are subtracted and then divided by the sampling period. It is like subtract two position and divide for a period of time. Clearly, if the positions have a bigger difference between them, the motor is rotating at a higher speed. In this way it is obtained a velocity value in motor counts per microsecond. It is much more significant to get value a motor counts per second. For this reason, the subtraction result is multiplied by 1000, which corresponds to dividing by the entire sampling period and multiplying by 10^6, passing from microseconds to seconds. It is important to note that at the end of the function the value of *CounterEncoderOld* is updated, in order to use it as the previous value in the next velocity computation (Fig. 4.17).

```
void ENCODER_CalcSpeed1 ( void )
{
  ENCODER_lSpeed1 = ( ENCODER_lCounterEncoder1 - ENCODER_lCounterEncoderOld1 ) * 1000 /
  ENCODER_SPEED_CALCULATION_SAMPLING_PERIOD; //Secs in a mSec / num of mSecs of int

  ENCODER_lCounterEncoderOld1 = ENCODER_lCounterEncoder1;
}
```

Figure 4.17 Function to calculate the velocity value. The result obtained is in counts per second.

The position and velocity values are automatically kept updated each time a step of the input shaft occurs and for each set sampling period.

The *pos_vel_update* is an ISR function is used to update the global variables of position and velocity to be sent to Chai3D.
Pos_vel_update calls the functions *ENCODER_GetCount1* and *ENCODER_GetCountInSpeedInterval1*, which return the last values of position and velocity calculated as previously seen. It is done for each motor/encoder (Fig. 4.18).

```
void pos_vel_update(){

Pos1     = ENCODER_GetCount1();
Speed1   = ENCODER_GetCountInSpeedInterval1();


Pos2     = ENCODER_GetCount2();
Speed2   = ENCODER_GetCountInSpeedInterval2();


Pos3     = ENCODER_GetCount3();
Speed3   = ENCODER_GetCountInSpeedInterval3();
}
```

Figure 4.18 ISR function to update the global variable of velocity and position.

Data Sending to Chai3D

As previously stated, the communication between the two firmware is a serial communication. The serial transmission is a communication mode between digital devices in which the bits are transferred along a communication channel one after the other, and they arrive sequentially to the receiver in the same order in which the sender transmitted them. It is a type of communication that can be easily implemented in the Arduino and Chai3d and therefore it can be exploited in this first prototyping phase. The native USB port is used for this communication, which should ensure better performance when many data are processed. To start the serial communication, it is necessary to use the begin function (Fig. 4.19).

```
SerialUSB.begin (115200); //native USB port.
```

Figure 4.19 Function to open the serial USB port in Arduino.

It is important to note that in case of the native port the baud rate value shown in brackets is not relevant. The USB port will work at its speed which depends on various factors, type of port, USB type, cable etc. The native Arduino Due port allows communication up to 480Mbps.

An ISR is created to send the data. This function creates a string in which all the values of position and velocity are concatenated. The values of position and velocity sent are the ones saved in the global variable by the *pos_vel_update* function. Chai3D will take care of the interpretation and separation of the data of the string. In this way float data can be sent. In fact, it is possible that the velocities values are not integers. The string is anticipated by a start byte (A), this will allow the receiver to know when a new data packet has arrived.
Thanks to the *SerialUSB.println* function this package is loaded on the serial port. (Fig.4.20)

```
void send_data() {
  tosend = " "; //clear the string for a new input
  tosend = 'A';
  tosend.concat(Pos1);
  tosend.concat(' ');
  tosend.concat(Pos2);
  tosend.concat(' ');
  tosend.concat(Pos3);
  tosend.concat(' ');
  tosend.concat(Speed1);
  tosend.concat(' ');
  tosend.concat(Speed2);
  tosend.concat(' ');
  tosend.concat(Speed3);

  SerialUSB.println(tosend):
}
```

Figure 4.20 Send data function.

Data Reading from Chai3D

Data is also read via serial communication. It is performed by an ISR function called *read_data* (Fig. 4.21). This function checks if data are available (*SerialUSB.available ()*) on the serial port to be received. If they are available, the *SerialUSB.readBytes* function reads 3 bytes. As the code has been set, Chai3D always sends 3 bytes, each one dealing with the management of a motor. These 3 bytes are read as a string. Thanks to the *toCharArray* function, 3 binary 8-bit arrays are created (*sub[]*). They are ready to be interpreted for motor management. *Sub[]* are the global variables exploited by the motor control functions.

```
void read_data () {
  if (SerialUSB.available() > 0)
  {
    SerialUSB.readBytes(buff, 3);
    inString = buff;
    inString.toCharArray(sub, 4);
  }
}
```

Figure 4.21 Read data function.

Motor control

Before describing in detail the functions for the motor activation and deactivation, it is important to introduce the type of motor control data that Chai3D sends to Arduino. For each of the three movements Chai3d sends a byte composed as follows:

- First bit: 1 if movement in direction A is activated, 0 if not.
- Second bit: 1 if movement in second direction B is activated, 0 if not.
- Third bit: 1 if lateral button A for acceleration/deceleration is pressed, 0 if not. This only if the possibility of accelerating and decelerating that movement is contemplated.
- Fourth bit: 1 if lateral button B for acceleration/deceleration is pressed, 0 if not.
- Fifth and Sixth Bits: Empty, Reserved.
- Seventh and Eighth bit: movement identification code (01: Tip, 10: Rotation, 11: Insertion).

The 3 bytes are continuously sent to the Arduino which, based on the identification code activates, deactivates, accelerates or decelerates the motors. The 3 bytes are always sent in the same order: The first one for the tip deflection, the second one for the rotation movement, the third one for the insertion/retraction movement.

Therefore, Arduino should read the identification code of each byte to understand to what motor the information is destined. Arduino, subsequently, takes care of control motors accordingly to the other bits.

This first phase is managed by the ISR *motor_activaction* function (Fig. 4.22). It checks that the 2 most significant bits correspond to the correct identification code for each movement, to then activate the *control* function.

If the identification code is not correct (maybe data has been lost in the communication) , the corresponding motor is switched off. The *motor* constant selects the motor to be controlled (in the example the first) the

MOTOR_SetVoltage function sets the motor voltage and turns it off when it sets a zero value. The *MOTOR_SetVoltage* function will be described in detail later.

```
void motor_activation() {

  if (sub[0] >> 6 == 1)

  {
    controll();
  }
  else
  {
    motor = 1;
    MOTOR_SetVoltage(0);
  }
```

Figure 4.22 Motor activation function. It reported just the example of checking of the first byte. The same structure is used for all the others.

The *control* function (Fig. 4.23) selects firstly the motor that it will drive (e.g. *motor*=1, tip deflection). Then it checks the first two bits: if they are 01, then it activates the rotation in direction A, if they are 10, it activates it in opposite direction. Otherwise, if they are 00 it turns off the motor. This control operation is done through bitwise operations. The value set with *MOTOR_SetVoltage* function is the one considered optimal after experimental evaluations.

```
void controll(void)
{
  motor = 1;
  if (sub[0] & 0x1)
  {
    MOTOR_SetVoltage(3);
  }
  if (sub[0] & 0x2)
  {
    MOTOR_SetVoltage(-3);
  }
  if ( ((sub[0] & 0x1) == 0) && ((sub[0] & 0x2) == 0 ))
  {
    MOTOR_SetVoltage(0);
  }
}
```

Figure 4. 23 The control function.

The *control1* and *control3* functions (tip deflection and insertion movement) work in the same way, not providing the possibility of accelerating or decelerating the motor. The only difference is found in the *control2* function. It controls the rotation movement and therefore provide the possibility of being accelerated.
The idea about the acceleration/deceleration control is here reported:
Every time a button is pressed the motor accelerates/decelerates keeping the same rotation direction. One of the two button causes acceleration and the other deceleration, depending on the rotation direction. Until the rotation direction is not changed with the mouse cap, it is possible to accelerate and decelerate the motors with the two buttons but without changing the rotation direction. When the direction of rotation (with the mouse cap) is changed, the power is reset to a base value ($\pm$3 V). At this point until the rotation direction doesn't change another time, it is possible to use the buttons to accelerate and decelerate. What first accelerated now decelerates. Each time the direction of rotation changes, the power resets to the standard value and the functionality of the two button is inverted. The reset value could be $\pm$3 V depending on the mouse cap movement way. The goal is that when the user is turning the mouse cap to the right, the right button causes acceleration, and the left button decelerates. The opposite occurs if the user is rotating the cap to the left. Each time a button is pressed again, after being released, a change in speed is caused. Keeping the button pressed leads to a unique increase in speed. The increase or decrease is unitary for each button press. The motors used have a nominal voltage of 12 V, so all the integer values between -12 and +12 can be supplied to them.
In the firmware, this functionality is implemented in the following way: A variable *u_m* represents the power value (in V) to be given to the motor.
When the code checks which direction of rotation is activated, it first checks if this direction is the same direction as the previous movement. If it is the same, the value of *u_m* does no change. If the direction is different, *u_m* is reset to $\pm$3 V.
The *last_side* variable is used to keep in memory the direction of the previous movement (Fig. 4.24)

```c
void control2(void)
{
  motor = 2;
  if (sub[1] & 0x1)
  {
    if (last_side != 1)
    {
      last_side = 1;
      u_m = +3;
      MOTOR_SetVoltage(+u_m);
    }
    else
    {
      MOTOR_SetVoltage(+u_m);
    }
  }
```

```c
if (sub[1] & 0x2 )
{
  if (last_side != 2)
  {
    last_side = 2;
    u_m = -3;
    MOTOR_SetVoltage(u_m);
  }
  else
  {
    MOTOR_SetVoltage(u_m);
  }
}
```

Figure 4.24 First part of the control2 function. It is controlled the rotation side and it can be reset the power value.

If no motion directions are activated (first two bits equal to zero) the motor is turned off, but without changing the value of *u_m*. In this way if the user resumes the movement in the same direction of the previous one it will be performed with the previous power (Fig. 4.25)

```c
if ( ((sub[1] & 0x2) == 0) && ((sub[1] & 0x1) == 0 ))
{
  MOTOR_SetVoltage(0);
}
```

Figure 4.25 Second part of control2 function. It allows to turn off the motors without changing the value of *u_m*.

The third and fourth bits are then checked. These bits are dedicated to acceleration/deceleration and they have a value of 1, when the corresponding button is pressed. If these values are 1 the variable *u_m* is increased or decreased, depending on which of the two is being pressed. It also uses a flag (*acc*). Only if it has a value of 1, it is possible to vary the value of *u_m*. *acc* is set to zero each time a button is pressed and returned to 1 just when both buttons have been released. It allows that a unique button press implies a unique variation of the *u_m* value (Fig. 4.26).

```
if ( (sub[1] & 0x4) && (acc == 1) )
{
  acc = 0;
  u_m = u_m + 1;
}
if ( (sub[1] & 0x8) && (acc == 1) )
{
  acc = 0;
  u_m = u_m - 1;
}
if ( ((sub[1] & 0x4) == 0) && ((sub[1] & 0x8) == 0 ))
{
  acc = 1;
}
```

Figure 4.26 Third part of the control2 function. It checks the 3rd and 4th pin to change the motion power. A unique pression of the button allow a unique variation of the power, thanks to the flag *acc.*

MOTOR_SetVoltage is the function exploited to activate the motors and control their power. This function requires as input a float value, that is the power at which the user wants to move the motor.
At the beginning of the function this value is normalized, dividing the input value with the maximum power voltage that the motor could tolerate (*MOTOR_MAX_VOLTAGE*=12 V). If the result of the normalizing operation is bigger than 1.0 or smaller than -1.0, it means that the user has inserted a non-valid value, so it is relocated in the limits. In this way *f_voltage* could be between -1 and 1 At this point, according to the sign of *f_voltage*, the rotation direction is defined, updating the variable *u_dir* (Fig. 4.27).

```c
void MOTOR_SetVoltage ( float f_voltage )
{
  int u_dir;
  /* Normalize */
  f_voltage /= MOTOR_MAX_VOLTAGE;
  /* Check Limits */
  if ( f_voltage > 1.0 )
    f_voltage = 1.0;
  else if ( f_voltage < -1.0 )
    f_voltage = - 1.0;
  /* Set dir */
  if ( f_voltage >= 0.0 )
    u_dir = LEFT;
  else
    u_dir = RIGHT;
```

Figure 4.27 First part of the function to set the motor voltage. The power input value is normalized, located in its limits and the rotation direction is determinate.

The function *PWMC_SetDutyCycle* is then used to set the duty cycle value of the PWM control. Each motor has two pin that can exploit, one for each direction. In this example (Fig. 4.28), if the rotation direction is clockwise (left) the pin 0 is disabled, and the pin 1 is activated. This pin provides a PWM signal with a period that vary according to the value of *f_voltage,* so the power value that the user sets.

```c
if (motor == 1)
{
  if ( u_dir == LEFT )
  {
    PWMC_SetDutyCycle (PWM, 0, 0);
    PWMC_SetDutyCycle (PWM, 1, (uint16_t) (((float) uPWMPeriod) * fabs(f_voltage)));
  }
  else
  {
    PWMC_SetDutyCycle (PWM, 0, (uint16_t) (((float) uPWMPeriod) * fabs(f_voltage)));
    PWMC_SetDutyCycle (PWM, 1, 0);
  }
}
```

Figure 4.28 Second part of the motor set voltage function. According to the movement direction and the motor selected a different channel is activated to provide PWM signal. The PWM has a duty cycle that varies with the power value given in input.

All the pins that must provide a PWM signal are digital pins that are configured in the function *configure_PWM_HW*.
In this function the pwmc.h library is exploited. It is a library that allow a better control of the PWM in case of an Atmel Core. It allows to choose and enable a

channel that the user wants to use as a PWM signal generator. It is possible to set a value of prescaler, value that divided by the PWM frequency. Changing the prescaler value, it is possible to obtain different frequency. It is then possible to set the period of the PWM, and consequently the frequency. In the configuration function all these fixed parameters are set, while the duty cycle, that it is the variable that really controls the power of the motor, it sets each time in the *MOTOR_SetVoltage* function.

4.2.2 Chai3D code

This section will describe in detail the most significant parts of the Chai3D code. As previously said, Chai3D is a C++ development environment, designed as a platform framework for computer haptics, visualization and interactive real-time simulation. ChaiI3D is an open source framework that supports a variety of commercially-available freedom haptic devices and makes it simple to support new custom force feedback devices.
Many of these capacities of simulation and force feedback are not exploited in this work. Nevertheless, one of the first improvement that may be introduced, is the application of haptic feedback and the use of the robot in a virtual reality. For this goal just a modification of the Chai3d code would be necessary. This is the main reason because the PC controller code has been developed in Chai3D.
A Chai3d code is normally composed by a main section where the simulation world is created. In this world objects, sentences or widgets like the ones exploited in this work can be inserted. It is also possible to set up some cameras and lights to render the world. Furthermore, a device with haptic properties can be created and its characteristics defined. In this section it is also possible to open communications with other devices, in this case, the 3DMouse and the Arduino.
The simulation is then based on a thread or loop. There are two main loops, the graphical loop that updates continuously the graphic characteristics of the created world, and the haptic loop, which normally deals with managing the feedback forces and haptic properties of objects. Other threads can be created specially to develop functions that must be repeated continuously during the firmware operation.
According to the objectives that must be developed, in the main section the world will be created and all the widgets for plotting the position and velocity data will be inserted. Furthermore, the communication with Arduino and the Mouse3D will be opened. On the other hand, loops and threads will be exploited to receive position and velocity data from Arduino, update the widgets based on these data, read and process the data received from the 3DMouse to create the 3 bytes that control the 3 motors, send these bytes to Arduino through serial communication.

3D mouse communication and data elaboration

To open the communication with a new device, connected to the PC via USB, it is necessary to develop a procedure based on two fundamentals functions: *open()* and *ioctl()*.
In the main section of the code the communication is configured (Fig. 4.29)
The *open()* function establishes the connection between the device and a file descriptor (f3d). A file descriptor is an indicator, normally used in Unix operating systems, that allows the access to a file or other input/output resources. The *open()* function will return a file descriptor (an integer) for the named file that is the lowest file descriptor not currently open for that process.
As input, it requires the path to follow to find the device (*fname*). Moreover, some options regarding the opening of the file can be defined. In this case it uses *O_RDWR* to be able to read and write on the file, and *O_NONBLOCK* which prevents the blocking of the code if the device is not present.
Thanks to the while loop, different paths, in which the 3D mouse could be located, are examined.

```
int i = 0;
char *fname = NULL;
struct input_id ID;
// find the SpaceNavigator or similar device
fname = (char *)malloc(1000 * sizeof(char));
while (i < 32)
{
    sprintf(fname, "/dev/input/event%d", i++);
    f3d = open(fname, O_RDWR | O_NONBLOCK);
```

Figure 4.29 Opening the connection with the 3D mouse and creation of the file descriptor.

If a device is found, the file descriptor takes a positive value, just in this case the *ioctl()* function is exploited.
The *ioctl()* function manipulates the device parameters. In particular, many operating characteristics may be controlled with *ioctl()* requests. The first argument *(f3d)* must be a file descriptor. The second argument is a device-dependent request code. The third argument is an untyped pointer to memory. In this case EVIOCGID allows to find information about device identify. The third argument is a pointer to an input_id structure, where it is possible to save the information extracted from the device. If the ID information (ID.vendor and ID.product) of the connected device are correct, so the right device (3DMouse) is in use, the connection is created.
Two global fundamental variables are used. The variable *axes[]* in which the movement of all the 6 degrees of freedom of the mouse are saved, and the variable *button[]* in which button status is recorded. These are the arrays in which the

information about the actions performed by the user with the 3Dmouse, will be allocated.
Another fundamental global variable is the *input_event* structure that allows to manage the types of events that can occur and their intensity. Important events that can occur with the 3DMouse are the movement of the cap in one of the possible ways, or the pression of one of the laterals buttons.
The capabilities or features of each device can be determined through the event interface, using the request code EVIOCGBIT in *ioctl()* function (Fig. 4.30). This function allows to determine the types of features supported by any particular device, for example, whether it has keys, buttons or neither of them. The EVIOCGBIT *ioctl()* takes four arguments. In this case, f3d argument is the file descriptor; 0 is a special type of features to return request, indicating that the list of all feature types supported should be returned, *size of()* shows the upper limit on how many bytes should be returned; and *evtype_bitmask* is a pointer to the memory area where the result should be copied. The return value is the number of bytes copied. Here all the event type that can occur are defined.

```
ioctl(f3d, EVIOCGBIT(0, sizeof(evtype_bitmask)), evtype_bitmask);
```

Figure 4. 30 *Ioctl()* function to obtain information about the events that occur.

In the haptic loop (Fig. 4.31) it is now possible to monitor continuously the occurrence of these types of event. Now that the communication with the device is open, it is possible to use the function *read()* to take data directly from the device. It necessary to define the file descriptor, where the data are saved (*&ev*) and how many data are read. What is read from the 3D mouse is firstly the event type:
EV_KEY when a button is pressed, EV_ABS if a movement of the mouse cap is performed.
The *ev.code* is then read, so which buttons or which movements are performed and the *ev.value*, so the intensity of the event. Thanks to these two data it is possible to allocate the correct intensity (*ev.value*) of a movement in the correct box(*ev.code*) of the array, which corresponds to that movement.
The array *axes[]* and *button[]* are continuously updated in a synchronized way with the occurrence of events and they are ready to be interpreted to obtain the bytes to be sent to Arduino.

```
int n = read(f3d, &ev, sizeof(struct input_event));
if(n >= sizeof(struct input_event))
{
  switch (ev.type)
  {
    case EV_KEY
      buttons[ev.code] = ev.value;
      break;

    case EV_ABS:
      axes[ev.code] = ev.value;
      break;

    default:
      break;
  }
}
```

Figure 4.31 Read function in the haptic loop to update the global variables with the new data from the events that occur.

Three special functions have been implemented to treat these data, one for each movement. The main goal of these functions is to create a byte, containing all the information about the movement, as explained in the previous section. 2 bits (LSB) for the movement direction, 2 bits for acceleration/deceleration, 2 bits reserved, and 2 bits (MSB) for the ID code of the motor to which the information is destinated.

It is important to specify how the data produced by the 3DMouse are treated. The 3DMouse provides for each movement an integer variable value that can be negative or positive based on the direction of the movement. This value has a higher absolute value if the movement with the 3dMouse is performed by the user more in deep. In this work it was decided not to exploit the different intensities that the 3DMouse could provide according to its degree of depth of a movement. This decision was taken because in real use, the range of motion that can be performed with the mouse cap is actually very small, and difficulties in adjusting the movement to stop it at different depths have been recorded. For example, it would have been possible to implement a technique for what if the cap movement is performed slightly, the motor moves slowly, while if it is executed in full, the motor moves quickly. This would be easy to implement at the firmware level, thanks to the data collection system created here, but difficult to perform in the manual mouse control. For this reason, when the value exceeds a threshold level means that the user is moving the mouse in that direction and the motor is activated. The power of the movement is not adjustable through a more or less deep control of the mouse cap. The movement occurs or does not occur. A not too low threshold has been set in order not to detect small caps movements, probably committed by mistake.

The three functions created deal with the management of the three movement. Each one a different movement. Exactly like the Arduino code, the functions for the tip deflection and for insertion movement have the same setting, not introducing the possibility to accelerate the movement, while the rotation one is slightly different.
The three functions are located in the haptic loop, and they are call back just after the updating of the values of the *axes[]* and *button[]* variables. It implies that any data that is collected is immediately processed and prepared for sending. These functions produce a global variable, *sent_value[]*, which will be sent. This variable is an array of char. Each element of the array is one of the bytes that describes one of the motors.
The function first checks the element of the array *axes[]* corresponding to that movement (e.g. in case of tip deflection the corresponding axis is the number 4). If this value is greater than the threshold, the two MSBs indicating the ID of the motors are activated correctly (01 in case of tip deflection), all other bits are set to zero, and the first bit representing the movement direction A is activated. The same operation is performed if the negative threshold is exceeded but the second bit is activated instead of the first, that represents movement in the direction B. In the event that neither of the two thresholds is exceeded, the last two bits are set to zero (Fig. 4.32). These types of bit activation and deactivation operations are easily managed thanks to the bitwise operation “and” and “or”.

```
void flex_deflex_endoscope()
{
 if(axes[4] < -threshold)
   {
  sent_value[0] |= 0x40;
  sent_value[0] &= 0xFD;
  sent_value[0] |= 0x2;
   }
else if(axes[4] > threshold)
   {
  sent_value[0] |= 0x40;
  sent_value[0] &= 0xFE;
  sent_value[0] |= 0x1;
   }
else
{
sent_value[0] &= 0xFC;
}
```

Figure 4.32 Example of a function to update the variable to send to Arduino.

In the rotation movement case, the possibility of accelerating or decelerating the motor is added. The same firmware technique could be implemented in other movements, for future development in which the possibility of changing the execution power of other movements is contemplated.
The first part of the code works exactly in the same way as the one for the other movements and it deals with pull up/down the first two bits, dedicated to movement in the two possible directions.
The second part manages the activation of the third and fourth bits, those for acceleration (Fig. 4.33).
The setting is the same as the previous one. If a button is pressed, the ID is activated, the first acceleration bit is activated and the second is deactivated, or vice versa. It is possible to access this type of operation only if the Boolean variable *button_press* variable is false. The variable changes to false only when both buttons have been released. In case that a button is keeping pressed and the user also press the other one no actions are performed. Therefore, it prevents the creation of problems of uncontrolled pulling up/down of the bits if by mistake the user press both buttons together. To perform a new button action, both buttons need to be released first.
At this point, the variable *sent_data[]* is ready to be sent to Arduino and to be interpreted.

```
if ((button_press1== false) && (buttons[256]==1))
{
button_press1= true;
sent_value[1] |= 0x80;
sent_value[1] |= 0x4;
sent_value[1] &= 0xF7;
}
else if ((button_press1== false) && (buttons[257]==1))
{
button_press1= true;
sent_value[1] |= 0x80;
sent_value[1] |= 0x8;
sent_value[1] &= 0xFB;
}
else if ((buttons[256]==0) && (buttons[257]==0))
{
button_press1= false;
sent_value[1] &=0xF3;
}
```

Figure 4. 33 Code to manage the third and fourth bits for the changing of motor power in case of rotation movement.

Data Sending to Arduino

To be able to send and receive data to the Arduino it is necessary, as in the previous case, to connect the two hardware devices. This is done thanks to a function, specifically created, *open_port*, that is called back in the function specifically created to read the data of the code (Fig. 4.34)
This function uses the *open* function exactly how it was done to open the communication with the 3DMouse. A file descriptor is opened, and it is fundamental for the data sharing. The options provide in the function *open* guarantee the possibility of writing and reading on this device. If the communication is not opened correctly and so the device is not found on the indicated path, an error message is displayed. *Fcntl* is a function that manipulates the file descriptor allowing an accurate management of the file descriptor. In this work no particular options are used, at the contrary each flag is set to zero, but a more accurate study of the system's communication protocol would require the use of this function to improve communication.

```
int open_port(void)
{
  fd = open("/dev/ttyACM0", O_RDWR | O_NOCTTY);
  /* wait for the Arduino to reboot */
  usleep(500000);
  if (fd == -1)
  {
    perror("open_port: Unable to open /dev/ttyCOM0 - ");
  }
  else
    fcntl(fd, F_SETFL, 0);
printf ("%s \n", "Open");
  return (fd);
}
```

Figure 4.34 Open port function to communicate with the Arduino.

Once the communication with Arduino has been opened the data can be sent. They are sent continuously in the haptic loop, after the functions that modify the three bytes sent are called back. Therefore, in the haptic loop, first the data from the 3DMouse are read, then they are elaborate and finally they are sent. This process ensures that each data read is then sent to Arduino.
The function used for sending data is the *write* function (Fig. 4.35). It takes as inputs the file descriptor, the data packet to be sent and the number of bytes to send. It writes these data on the serial communication port, returning the number of the bytes sent or -1 in the event of a communication error.

```
int wr_result = write(fd, &sent_value, 3);
```

Figure 4.35 *Write* function to send data to Arduino.

Data Receiving from Arduino

For the data receiving process, a thread is created. It deals specifically with the reading and processing of the Arduino data. A thread of execution is a sequence of instructions that can be executed concurrently with other sequences in multithreading environments. The thread is composed of a first part of setting, which is run only once. In this phase some variables are defined, and the serial communication is opened, as mentioned above, through the *open_port* function.
After that, a *while()* loop is present. It is the part of the function that is repeated every time the code enters the thread. (Fig. 4.36)
The *read* function takes care of reading the data. It receives as inputs the file descriptor, a buffer where to allocate the data and the number of bytes to save.
At this point this buffer (*b_read*) is copied into another (*b_read2*), excluding the first byte, which , if the reading has been correctly read, should be an "A". It represents a start byte and it carries the information that a new data has arrived.
If this value is "A", the buffer with just the data (*b_read2*), without the starting byte, is processed. The *strtod* function allows to convert strings into double: It scans the string and converts a series of chars into a single double until it finds a white space that represents the end of the number. This data is saved in six support variables and printed on the screen. They are the position and velocity data and it may be useful for the user to have a numerical feedback of them on the PC monitor. The support variables then update the global variables *MotorOnePosition, MotorOneVelocity* ... which will deal with the updating of the graphic interface created.

```
while(1)
{
     int n = read(fd, b_read, 100);
         if( n==-1) break;
         if( n==0 )  continue;
   strcpy(b_read2,b_read+1);

       if (b_read[0]== 'A')
       {
       d1=strtod(b_read2,&pEnd);
       d2=strtod(pEnd, &pEnd);
       d3=strtod(pEnd, &pEnd);
       d4=strtod(pEnd, &pEnd);
       d5=strtod(pEnd, &pEnd);
       d6=strtod(pEnd, NULL);
       }
```

Figure 4.36 Repeated code in the read thread. The motor data are read and elaborated

Graphic User Interface Creation and updating

The graphic user interface has the main goal to plot the data of position and velocity taken from the encoders and then elaborated by Arduino and sent to Chai3D. The data plotting should be synchronized with the mouse actions and with the motors activation or the delay should be minimum that the user can not notice it. A brief deepening of this problem will be discussed in the experimental chapter. The graphic user interface has been created thanks to some widgets that Chai3D makes available. The widgets are created and set in the main section of the code. In this section, their characteristics can be defined: the position of the object in the world, its size, its level of transparency and its range of value accepted. (Fig. 4.37)

```
scopeOne = new cScope();
camera->m_frontLayer->addChild(scopeOne);
scopeOne->setLocalPos(350,50);
scopeOne->setSize(200,100);
scopeOne->setRange(+100,-900);
scopeOne->setSignalEnabled(true, true, true, false);
scopeOne->setTransparencyLevel(0.7);
```

Figure 4.37 Example of a part of the firmware to create a widget and set its characteristics.

Subsequently, they are continuously updating in the graphic loop of the code, using the global variable updated by the read thread and the *setSignalValues* function (Fig. 4.38). The graphic loop, as aforementioned, is specifically used to update the graphical features of the world created in Chai3d. The widgets used in this work, are not the only ones available, and the final objective of the work was not to create the best graphic user interface, but just a first idea, that could be improved in future developments.

```
scopeOne->setSignalValues(MotorOnePosition);
```

Figure 4.38 Example of a part of the firmware to update values of a widget.

Three main widgets have been used to plot the data. (Fig. 4.39)

- Scope. It is a line that continues to move forward, rising and falling in a range based on the value it is recording. It is used to represent the position of each motor. After the experimental phase the displacement ranges for each movement has been set as the limit for each scope
- Level. It is a vertical bar composed by different horizontal levels. The levels can be turned on or off. This widget is used to represent the velocity of the motor. The faster is the velocity in direction A, the more levels will be switched on, the faster is the velocity in direction B, the more levels will be switched off. As mentioned, the only velocity that can have different powers is the one of the rotation movement. In its level bar the switching on and off the various levels can be appreciated, while for the other two movements, the bar is all switched on when it rotates in direction A, all switched off when it rotates in direction B and in the middle when the motor is off.
- Dial. It is a rotation widget, composed by a pointer turning in a circle. The pointer follows the movement of the rotation of the ureteroscope. It starts its movement in a vertical position in the upper part of the circle and then it rotates on the right or left according to the rotation of the instrument.

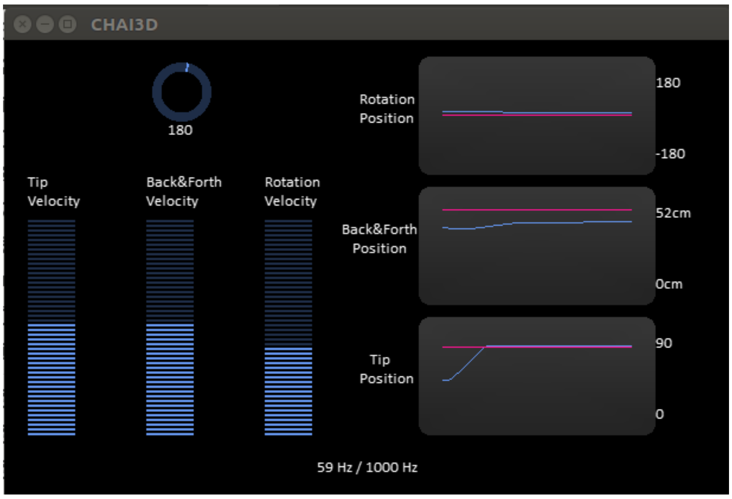

Figure 4. 39 The graphic user interface. On the right side it is possible to see the three scope to plot the position data, on the right of each scope the limits for each movement is reported. On the left the levels to plot the velocity are reported. In the upper part the dial to represent the rotation position.

Thanks to the two firmware described the main functionalities, set as objectives, have been realized. Testing the device, it has been observed how it provides a good communication between the elements and a real time data transfer that guarantees that when the user moves the 3DMouse the motor immediately moves, and the data are reported in the GUI. Further improvements of these codes will surely be necessary, in order to have a better control of the timing, to ensure the absence of lag, to insert new features. Some possible developments will be described in the last chapter of this document.

Chapter 5: Experimental Tests and Results

In this section of the document the experimental tests, conducted with the robot device completed in its hardware and firmware, will be described. The results of these experiments will be then reported with the mechanical and firmware variations that they caused. The final goal of this phase of the work is to verify the realization of the main objectives proposed at the beginning of the work. These general objectives require a cooperation between the two main part of the work, the mechanical part and the electronic one. To create the prototype now tested, many tasks have been carried out. These tasks are sub-objectives usually concern just a part of the work. They have been verified with trials during the creation of the robot. Some examples of these sub-objectives can be the creation of a mechanical part to provide a movement, the creation of a firmware to make the hardware elements communicate in the right way, the creation of a firmware to develop a GUI. All these realized tasks now collaborate to test and achieve some higher-level objectives.
These main objectives are here reported.

- Movement range: for each of the three movements a predetermined range of movement must be performed
    - Insertion / Retraction movement: considering an overall length of the urinary system of about 50 cm (about urethra 20 cm in men, shorter in woman, about 5 cm of bladder, about 25 cm of ureter) (Wikipedia, 2019), the ureteroscope should realize the objective of reaching the final part of the system and the kidney area. For this purpose, the cable of the ureteroscope should travel a stretch of about 50/55cm.
    - Rotation range: the entire rotation range of 360° around its longitudinal axis must be travelled.
    - Deflection range: it is necessary to exploit the whole range of possible movement of the control dials that is used to perform the deflection of the tip. The control dials should travel 90°.

- Precision of movement: it should be comparable or improved compared to the case that the movement is performed directly by the user.

- Stability of the position reached: the ability of the device to maintain a position once reached, is evaluated.

- Global movement: Being able to move with dexterity in an environment that represents human urinary apparatus, reaching certain targets in a time comparable to the case that the endoscope is controlled manually

Firstly, it is described how the objectives will be verified.
For what concerns the movement range, in case of the insertion/retraction movement this length will be estimated thanks to some measurement tools (calibre). For the other two movements it will be tested that the desired range can be travelled despite the use of mechanical piece to control the instrument.

A more trouble computation is required to obtain data about movements precision. The main goal is to obtain a measure in a unit of measure easily interpretable and associated with the corresponding movement. It requires:

- A measurement in centimetres for the insertion / retraction movement, that will represent the minimum advancement that the ureteroscopic cable can perform.
- A measurement in degree for the rotation, that will represent the minimum rotation the instrument can perform around its longitudinal axis.
- A measurement in degree for tip deflection, that will represent the displacement of the control lever which is then mapped into a deflection of the tip. The precision of the movement of the lever and not of the tip itself is monitored for reasons of simplicity, since the motor moves the lever directly and the data exploited in this work are fully extracted from the motor encoders. Furthermore, the tip of the instrument is severely damaged and does not respond to the lever controls. For this reason, every evaluation concerning the tip deflection has been made on the lever, which should then map on the tip deflection according to the characteristics of the ureteroscope.

The measure that is supplied by Arduino, extracted from the encoders, is in motor counts. It is the basic measure from which much information will be obtained. The motor counts are the value provided by the encoders, that they exploit to measure how much the motor have rotated and in which direction. An in-depth description about how this value can be obtained at the firmware level, is reported in the second section of chapter 4. The motor counts collected by each encoder are printed on the Pc monitor. In this way, it is easier to perform all the measures needed.
The encoders provide 48 counts for each full revolution of the input shaft. Therefore, it is enough to divide the motor counts by 48 to obtain the revolutions of the input shaft. Conversely, if it was required to compute the revolution of the output shaft it necessary to divide this quantity by 4741,44. The gearbox ratio

must also be considered, as explicated at the beginning of the chapter three of this document.
A full revolution of the output shaft (4741,44 motor counts) correspond to:
- A full rotation of the active disk for the insertion movement.
- A full rotation of the worm for the rotation movement.
- A full rotation of the hooking piece to the control lever for the tip deflection movement.

This precision measure in motor counts will be obtained in the same way for all the movements with the following procedure:
1. With the use of the 3D mouse, the user performs an action with the mouse cap as small as possible, but enough to cause an actual movement (e.g. the mouse is rotated the least possible to obtain a minimum rotation of endoscope).
2. The test is repeated several times (41 times).
3. The motor counts data is recorded for each attempt.
4. An average value is calculated, and it can be considered the estimate of the accuracy of the movement in motor counts.

This measure represents the number of motor counts that are recorded by the encoders with a movement as precise as possible of the 3DMouse.
It now necessary to convert this value in the unit of measure required. In order to obtain that, it is possible to create a ratio between a predetermined range of that movement and the motor counts necessary to travel this range. The range will be measured in the desired unit of measure to the numerator and in motor counts in the denominator. In this way, multiplying the precision in motor counts for this ratio, a precision in the desired unit of measure will be obtained.
This range must travel several times and an average value of the range in motor counts will be computed. The choice of the range travelled, and the number of trials performed will be discussed in the analysis of each single movement.

$$Precision(cm\ or\ °) = \frac{Range(cm\ or\ °)}{Range(motor\ counts)} \cdot Precision(motor\ counts)$$

(*Eq. 5.1*)

As regards the precision value that it can be considered acceptable, it was not possible to measure accurately the human precision in performing the movements due to the absence of instrumentation. The human precision could have been a good value for comparison. These values have therefore been estimated based on the conditions in which the robot will work and the skill that a surgeon could have in managing a particular movement. The estimate of each acceptability value will be described in the section dedicated to the specific movement.

Another characteristic that will be evaluated is the stability of the instrument once stopped, so the ability to maintain a position. In case of manual control, this goal is very complex to perform. In fact, the surgeon costs a lot of effort to maintain a position once it is reached, and small movements will always be present in human control. Keeping a desired position can facilitate the surgery, for example by stabilizing at a precise point near the kidney stone and then destroying it with a laser. This task is evaluated by reaching some random positions with the 3DMouse, stopping, and releasing the controller. Once the controller is released, the position data ,displayed on the pc, are monitored, and it is evaluated how much these values change.

These first three characteristics of the system will be evaluated at different power level at with which the movement is executed. The aim is to find an ideal work power for each movement and discuss the utility of introducing the possibility of accelerating each movement. Other specific technical characteristics of each movement have also been varied and the results compared. More details in the sections dedicated to each specific movement.

The last task that will be evaluated is about the global movement that the user can perform with the prototype.
To realize this task a low fidelity model of the urinary system has been built. The low fidelity model was designed by the University of Toronto for surgical training and it was replicated in this work. Many studies have evaluated good skill improvement with a training with this model. Moreover, it has a cost about $20, which is much less than the $3,700 required to purchase the high-fidelity bench model. (Wignall, Cadeddu, Pearle, Sweet, & McDougall, 2008) (Matsumoto, Hamstra, Radomski, & Cusimano, 2002). For these reasons it was evaluated as a good model to perform some initial tests. The Toronto University low fidelity ureteroscopy model consisted of Penrose drain, inverted cup, molded latex in portable plastic case and two embedded straws approximately 8 mm in diameter as substitutes for urethra, bladder dome, bladder base and bilateral ureters, respectively(Fig. 5.1, Fig. 5.2) (Matsumoto, Hamstra, Radomski, & Cusimano, 2002)
The test performed consists in locate some target that the user must reach with the robotized ureteroscope and with the manual control of the ureteroscope and the operation times are compared. Three targets will be placed for each ureter (one in the beginning, one in the middle and one in the end). It is expected that it will be difficult to carry out this phase of the work because, as said, the instrument tip is damaged and does not rotate when the lever moves. Nevertheless, the experimental set up has been built and the test procedure decided.

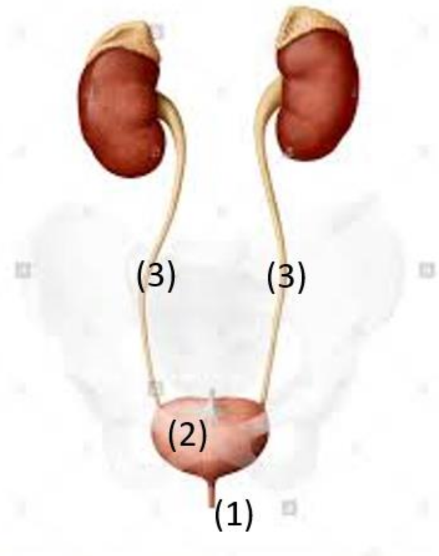

Figure 5.1 Urinary system. 1: Urethra, 2: Bladder, 3: Ureters.

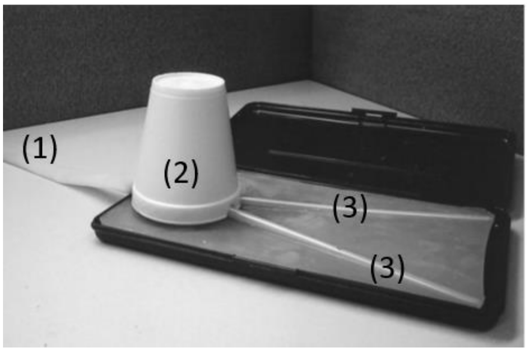

Figure 5.2 The Toronto University low fidelity ureteroscopy model. 1: Urethra, 2: Bladder, 3: Ureters (Matsumoto, Hamstra, Radomski, & Cusimano, 2002).

Each movement experimental tests and results will be now described in detail. This experimental analysis has also led to find some system problems, especially in its mechanical part. The encountered problems have been analysed and possible solutions and improvements have been proposed.

5.1 Insertion/Retraction movement

In this section it will be described how the length of the ureteroscope cable, and the movement accuracy have been measured. The results will be then discussed, and the stability of the movement evaluated.
Two main features of the system have been changed and they cause different results:

- Motor Power, this characteristic will be studied for each movement. The maximum power at which the motor can work is 12 V. Powers of 5 V, 6 V, 7 V will be evaluated for this movement. Powers below 5 V will not be evaluated as they are not enough powerful to perform the full range of movement without the human intervention. In fact, it will be explicated that, with the drag system designed, there is the risk of having endoscopic cable jamming. It will be seen, with many practical trials, that these jamming cannot be solved without human intervention at a power smaller than 5V. Powers greater than 7 V lead to too little precision in movement control. For this reason, they have not been considered.

- Disk Material. This second variable is specific for this type of movement. It is the material used around the disks. It should be remembered that the lateral surface of the drive disks is concave, in order to allow the insertion of a material that can lower the mechanical wear and increase the friction between the cable and the disk to facilitate the drag. A soft/spongy material and a rubbery/elastic material will be tested.

5.1.1 Movement Range

In this first section it will be described the computation of the full movement range and the estimation of the ratio $\frac{range\ (\,in\ cm\,)}{range\ (in\ motor\ counts)}$ useful to then compute the movement accuracy. The length of the cable is not influenced by the power or the disk material.
The target length that the ureteroscope cable should travel is about 50/55 cm, considering an overall length of the urinary system of about 50 cm (about urethra 20 cm in men, shorter in woman, about 5 cm of bladder, about 25 cm of ureter). The total length of the cable is 68 cm, and the less length is lost, the better the result is. As already discussed, in any type of robotic solution and not, for the control of this instrument, a part of the cable will not be used.
The maximum range is computed when the cable is fully extended outside the drag structure for the insertion movement. The distance is measured in centimetres between the last point of the lateral support structure and the tip of the cable (Fig. 5.3)

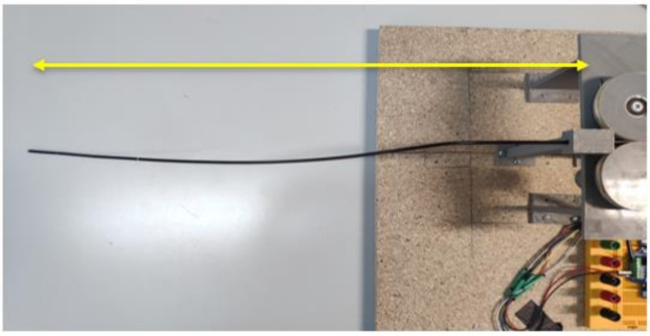

Figure 5.3 Maximum extension of the ureteroscopic cable.

The cable has been placed on a wood board, located at the same height of the starting point of the cable, so that it is perfectly parallel to the ground (Fig. 5.4). Then it is extended as more as possible and fixed in a perpendicular way to the short side of the wooden table. A calibre has been used to measure the length of the cable in extension. The calibre also helps to get the perpendicularity (Fig. 5.5). 5 measures have been performed to obtain an average final value. For each measurement the cable is re-extended and re-fixed, since an error in this procedure cause variation in the measures.

Figure 5.4 The cable located at the right height. It is the same height of the hole of the lateral support, that is the point from where the measure is performed.

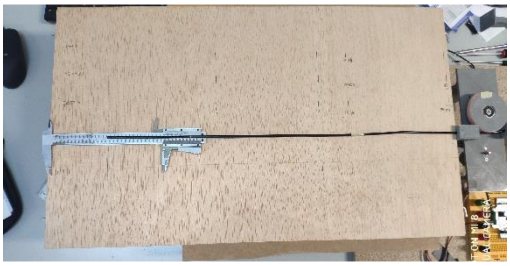

Figure 5.5 The cable extended and positioned in a perpendicular way thank to the use of the calibre. Then the cable is fixed, and the measure is performed.

The final result is summarized in Table 5.1

Insertion full Range	**Average Value**	**Range**	**STD**	**N° of tests**
	51,48 cm	[51,35cm-51,61cm]	0.102 cm	5

Table 5.1 Insertion/retraction full range data.

It can be said that the goal is not fully achieved. To improve this range the size of the drag structure could be reduced. It is not possible to further bring the structure closer to the origin of the cable, as it requires a space to be able to wrap without getting damaged (Fig. 5.6).

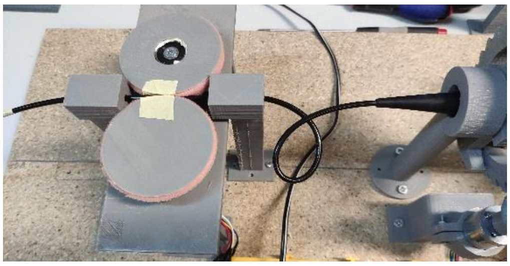

Figure 5.6 It is possible to see the little space between the cable principle and the drag structure. It causes difficulty in the cable drag and bending of it potentially harmful.

In this phase a first weakness of the drag structure was found. In fact, if this structure is placed too close to the cable principle, the cable itself presents more problems in rolling up. It must also be rolled up forcing its movement and causing possible damage on the cable. Relocating the structure far from the cable connection would solve this problem but would cause more loss in the cable length range. This problem becomes weightier in male patients whose urethra is longer. It would be necessary to use ureteroscopes with longer cable in order to best use this technological solution. Further improvement would be to make this structure smaller. Another idea to avoid damaging the cable would be to create a collection system for it. This would also contribute to solve other problems that will be introduced later. This collecting structure should however rotate with the instrument to allow the cable to rotate when the instrument rotates.

Once computed the total movement range in centimetre, it was necessary to evaluate the motor counts necessary to travel this stretch.
In this way it is possible to compute the ratio between the range in centimetre and the range in motor counts, that allow to estimate the precision value in centimetre. Motor counts is the basic information provided by the encoders. 48 motor counts correspond to a revolution of the input shaft of the motor. 4741.44 motor counts correspond to a full revolution of the output shaft, that for this movement correspond to a full rotation of the active disk.
11 tests were performed, in which the motor counts required to fully extend the cable from a rolled position were measured and 11 tests in which the motor counts required to completely roll up the cable from the extended position were measured. Clearly different results were found between the first and the second kind of test. The results are summarized in Table 5.2 and in Figure 5.7 and Figure 5.8. This test was performed with a motor power of 5 V and with a soft material, but a similar behaviour was noted also with other powers.

Total Range	**Cable Rolling up**	**Cable Extending**
Average (motor counts)	12420,92	15534,75
Range (motor counts)	[11304-13663]	[12659-19926]
STD (motor counts)	629,66	2484,31

Table 5.2 Data about motor counts to extend and roll up the cable for the total range at 5 V and with a soft material.

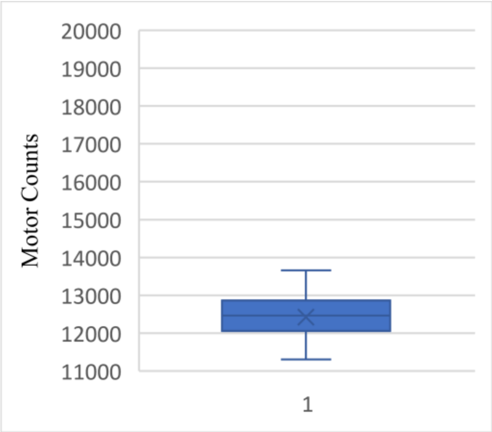

Figure 5.7 Box Plot Total Range Cable Rolling up.

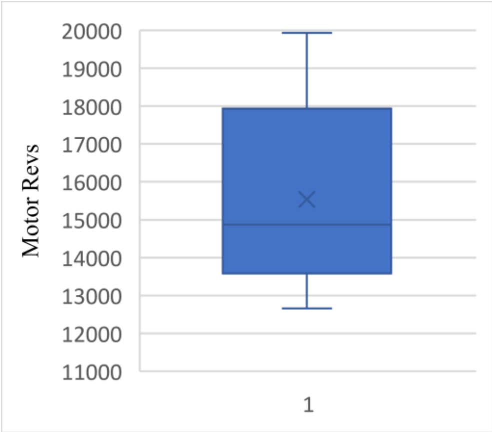

Figure 5.8 Box Plot Total Range Cable Extending.

It can be seen how the cable extending requires on average many more motor counts to be performed and with a much greater variability. This is due to the fact that in some cases the cable in the extension phase can get jammed, requiring more motor counts to unlock it. This occurs at the end of the extension phase (Fig. 5.9). No blocking events have been recorded in the rolling up phase.

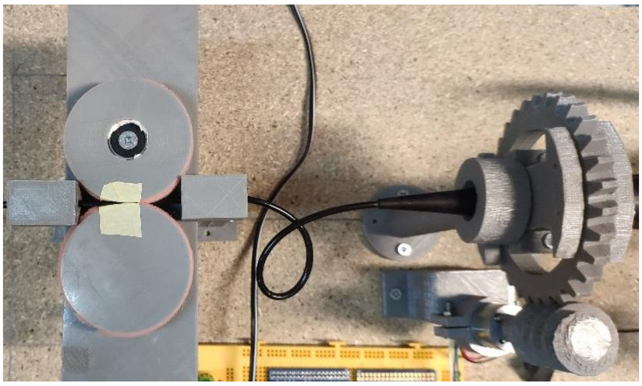

Figure 5.9 An example of jammed cable in the extension phase.

Due to the presence of this difference between extension and rolling up range, the complete section cannot be used to compute the ratio necessary to obtain the movement precision in centimetres. It is in fact necessary to use a length that is always travelled by a similar number of motor counts in both directions of movement. For this reason, it has been a chosen a shorter section of the cable,

called partial range. It should exclude the problematic part of the cable near the connection with the instrument and it should be as long as possible.
This segment has been chosen and measured exactly with the same method used to measure the total range. The result is reported in Table 5.3.

Partial Range	**Average Value**	**Range**	**STD**	**N° of tests**
	35,328 cm	[35,28cm-35,44cm]	0.067 cm	5

Table 5.3 Insertion/retraction partial range data.

Also in this case, 11 tests in each direction have been performed to compute the motor counts necessary to travel this segment. The power supplied was 5 V and a soft material was used. The data are summarized in the Table 5.4 and in the Figures 5.10 and 5.11.

Partial Range	**Cable Rolling up**	**Cable Extending**
Average (motor counts)	7393,00	7403,18
Range (motor counts)	[7312-7448]	[7199-7984]
STD (motor counts)	42,440	199,86

Table 5.4 Data about motor counts to extend and roll up for the partial range the cable at 5 V and with a soft material.

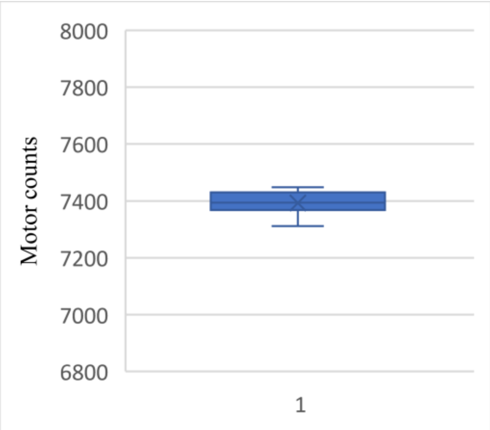

Figure 5.10 Box Plot Partial Range Cable Rolling up.

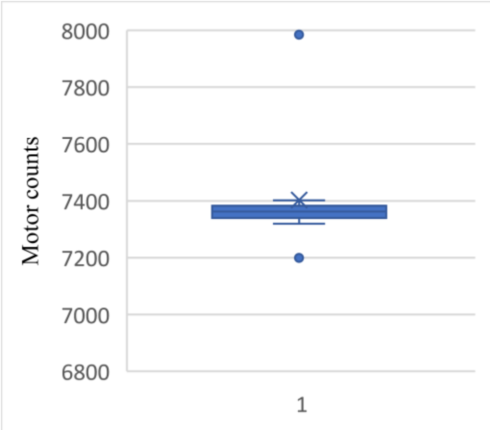

Figure 5.11 Box Plot Partial Range Cable Extending.

It is possible to note from the box plots and from the data a behaviour much more similar between the movement in the two directions. Some values of outliers are recorded in case of rolling up but are just two values. Moreover, it must be considered that the range of the vertical axis of the box plot is much smaller than in the previous case. Comparing the number of motor counts necessary to complete the partial range (Fig. 10 and Fig. 11) and the total one (Fig. 5.7 and Fig.

5.8), there is a large difference between the two directions of movement in the total range, while a behaviour much more similar for the partial range is noted. So, it is possible to consider the two movement directions with the same behaviour for the partial range and so this range acceptable for the calculation of the ratio.
For example, in this case with 5 V power and a soft material the ratio will be $0{,}004775\ \frac{cm}{motor\ counts}$. It is important to say that as value of partial range in motor counts has been considered the total average between the extending and the rolling up movement direction, that in this case is: 7398,09 motor counts (range [7199 motor counts-7984 motor counts], std 141,086 motor counts).

The different values of motor counts to travel the range, varying the motor power or the disk material will be now analysed. It is important to note that the full range in centimetre previously measured cannot vary for the motor power or the material used. It is now a fixed quantity that could vary just changing some mechanical parts of the system. On the opposite, the values computed in motor counts can vary, causing differences in the ratio and in the precision value that will be computed. The disk can act in a different way on the cable varying the power or the material, the motion transmission can change, causing a variation of the total motor count necessary to travel the range.
Before discussing in detail, the differences in the range (in motor counts) and therefore in the ratio obtained varying the disk material and the power voltage, it is important to describe some qualitative behaviours that have been found testing the two materials.

- The soft/spongy material has a lower friction on the cable. It allows the cable to rotate with less difficulty. In fact, a second problem introduced by the designed drag system was found in the rotation of the cable, when the user rotates the entire system. In this phase the cable and the tip must rotate with the instrument. On the contrary, it has been seen that the cable can get stuck between the two disks due to high friction and causing a difficulty in following the rotation of the instrument in the first phase. It brings to a dephasing between the rotation of the instrument and the tip. With the soft/spongy material, thanks to the lower friction, this problem is less evident. On the contrary, in the drag phase, this material has less force on the cable, causing higher jamming problems in the final part of the extension phase. Moreover, the material used was much more fragile and the continuous drag of the cable on it caused its damage.
- The rubbery/elastic material causes more evident problems in the rotation action. The response to the rotation of the cable with respect to the main structure is slightly delayed. This due to the higher friction that blocks the cable inside the disks in a first phase. On the other hand, in the drag phase is much better and there are no problems of material damage.

Data are now reported for different material and powers. These objective data influence the choice of the best material together with the qualitative ones previously reported.

These graphs represent the difference between the average number of motor counts necessary to perform a movement in the extension direction and in the rolling up direction, for a complete range (Fig. 5.12) or for a partial range (Fig. 5.13). This difference is calculated for all the materials and the powers. For each test 11 trials were performed for the extension phase and 11 for the rolling up phase. The two averages were then calculated and subtracted one from each other. In these graphs it is possible to note how for the material 1 (soft/spongy) cause big differences between the extension movement and the rolling up when the complete range is travelled, for any tested power. These differences lower a lot for the material 2 (rubbery/elastic) and become negligible by increasing the power of movement. For the partial range there are no significant differences for either of the two materials. This confirms that this segment is the best for calculating the accuracy of this movement.

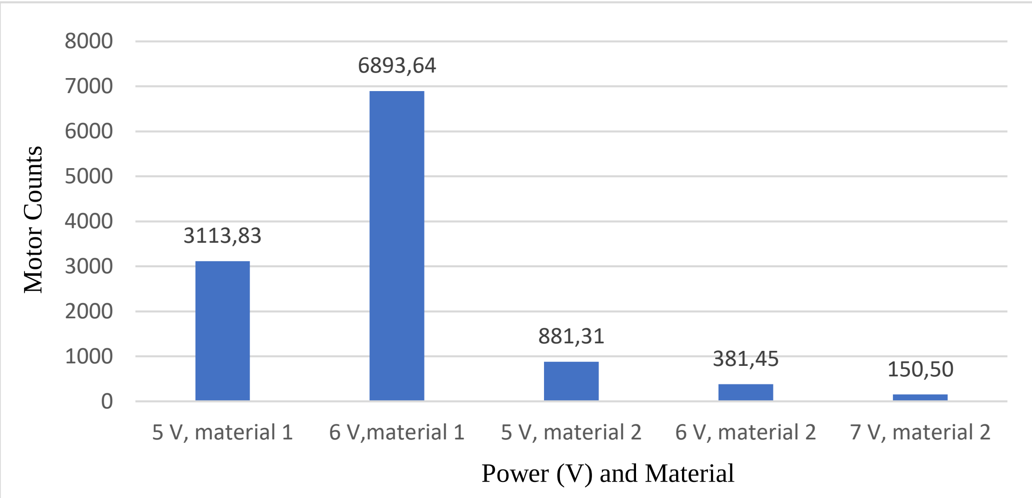

Figure 5.12 Difference of motor counts for extending and rolling up movement for the complete range.

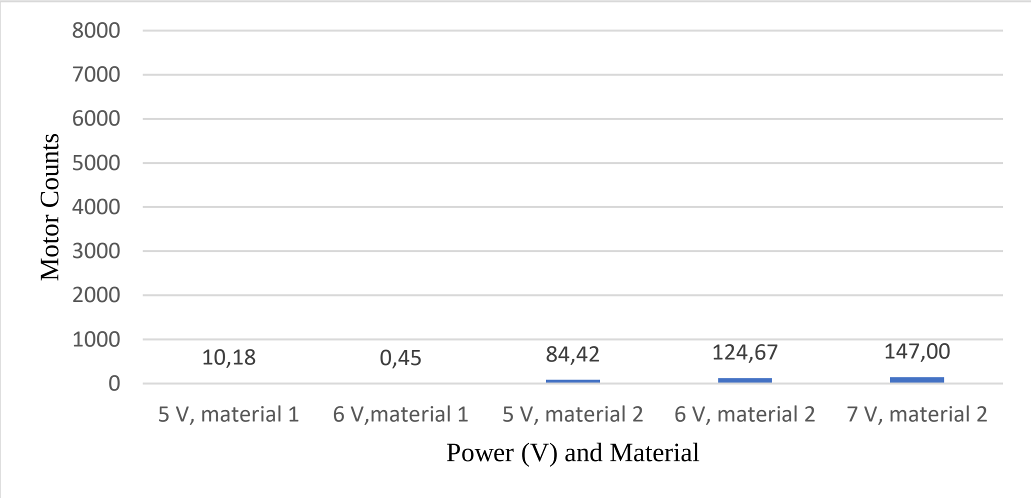

Figure 5.13 Difference of motor counts for extending and rolling up movement for the partial range.

It is possible to see that the behaviour of the device in the drag phase is much better with the rubbery/elastic material. Moreover, this material did not present problem of damaging and the problem found about the dephasing in rotation is a however present also with the use of the soft/spongy material. For these reasons a rubbery/elastic material has been chosen for the final version of the prototype. A more detailed analysis with additional materials would be necessary in future developments.

Two graphs about the variation of the range (in motor counts) in extension and rolling up phase using the rubbery/elastic material and varying the power are here reported.
The first one (Fig. 5.14) represents the total range and the second one (Fig. 5.15) represents the partial range. It would be desired that the motor always travels the same length with the same motor counts, despite the different speed. In this case, this performance is not evident with percentage variations up to 17.7%, (13277,08 motor counts (range [14327 mot counts-12149 mot counts], std 598,90 mot counts) at 7 V power vs 10751,23 motor counts (range [11972 mot counts-10163 mot counts, std 433,23 mot counts) at 5 V power), normalizing the difference for the higher value recorded. A possible cause of this variation could be in the different behaviour that the cable assumes in the rolled state. It could roll up in a different way each time with jamming problem causing variations.
It is possible to note a behaviour trend: as speed increases, it requires more motor counts to perform the complete movement. This leads to a second explanation concerning this variation. At higher speeds it is possible to have a slip of the disks

on the cable and therefore a less efficient transfer of motion while at lower speeds the disk slides less on the cable and transfers the motion better.
Much smaller differences have been found in the partial section where the problematic part is excluded with a maximum percentage difference, recorded in extension phase of, of 4.62 % (7801,83 motor counts (range [8815 mot counts-7587 mot counts, std 330,2670637 mot counts) at 6 V power vs 7180,75motor counts (range [7919 mot counts-6985 mot counts], std 242,87 mot counts) at 5 V power), normalizing the difference for the higher value recorded in the total range in order to obtain a percentage difference comparable with the previous one.
It confirms again the better result obtainable in calculation of the ratio using this part. Improvements and further experimental tests are necessary in order to obtain a more stable behaviour also for the complete range.

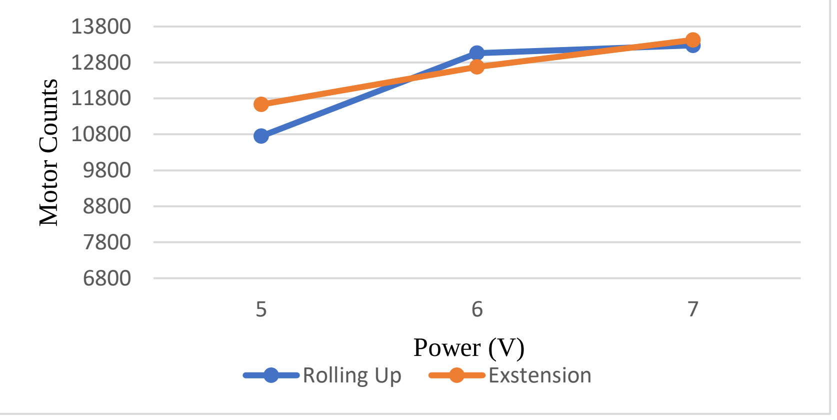

Figure 5.14 Motor counts necessary to travel the complete range in the two directions, varying the motor power.

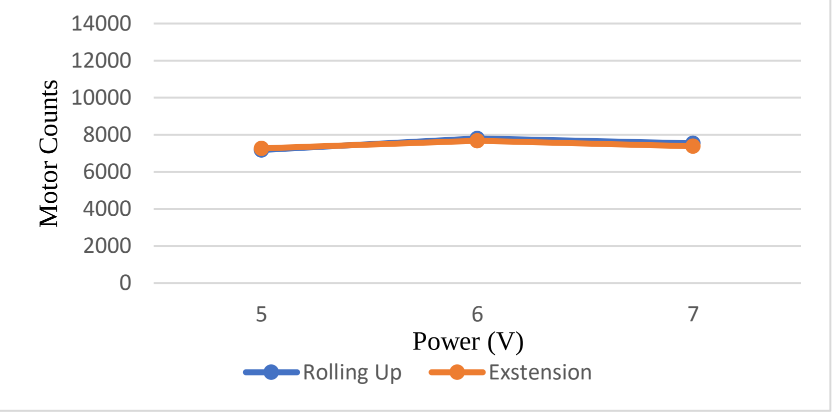

Figure 5.15 Motor counts necessary to travel the partial range in the two directions, varying the motor power.

5.1.2 Movement Precision

Before describing how the precision of the insertion movement have been computed and its variation according to the material used and the power applied, it is necessary to estimate a precision value that can be considered acceptable for this movement. As said, it was not possible to measure the precision with which the surgeon performs these actions. For this reason, it was necessary to estimate this value based on the ability to control the instrument that the surgeon has and based on the goal he/she must perform with this movement.
As mentioned in the mechanical chapter, the surgeon controls the insertion movement by pulling or pushing the terminal part of cable. It surely assures a good precision in the execution of this movement.
It was also considered the overall length of the channel that the cable must travel (about 50/55 cm) and that the target, around which it must move and be positioned, is a kidney stone that have a medium size around 1 cm in diameter. (Rassweiler, et al., 2018)
Based on this information, a range of acceptability of minimum movement of half size of a kidney stone was estimated, so 0.5 cm. It seems to be a value comparable to the human precision. In fact, it is difficult for the surgeon to move the cable with a precision in the order of millimetres.
For the calculation of the precision as previously explained, as small as possible movements have been performed with the 3DMouse cap, in this case by tilting the cap back and forth. 41 tests have been executed by tilting the cap forward and 41 tests by tilting the cap back and the motor counts that are performed have been recorded. The data of the test done with 5 V power and with a soft/spongy material are reported here. Similar behaviour is encountered in all cases. The main purpose is that there is no difference in the average motor counts values performing the forward and backward inclinations. The results are summarized in Table 5.5 and in Figures 5.16 and 5.17. It is possible to note a similar distribution and a very similar average value between the two directions. At this point the total average of all the tests (82) is calculated and this value is multiplied by the ratio obtained previously. In this way a centimetre precision measurement is obtained.
In this case a total average value of 105,91 motor counts (range [21 motor counts-183 motor counts], std 35,42 motor counts). The precision in the right unit of measure is:

$$105{,}91\ motor\ counts\ \cdot 0{,}004775\ \frac{cm}{motor\ counts} = \ 0{,}5058\ cm$$

This test is performed in a central section of the cable where there are no jamming problems. For most of the working activity the cable is in this state and the calculation of precision here is certainly more reliable.

Precision	Tilt forward	Tilt back
Average (motor counts)	105,63	106,20
Range (motor counts)	[155-47]	[183-21]
STD (motor counts)	25,34	43,56

Table 5.5 Data about motor precision, tilting the cap back and forth with a power of 5 V and a soft/spongy material.

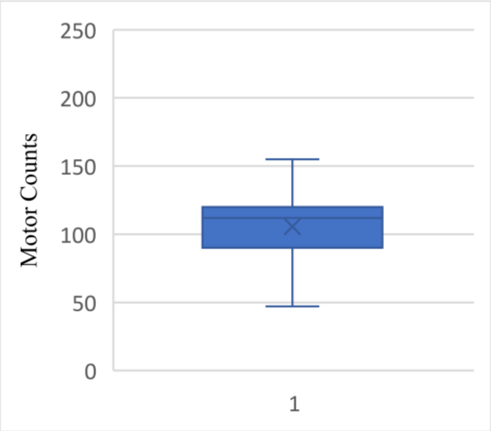

Figure 5.16 Box Plot of precision movement tilting the cap forth.

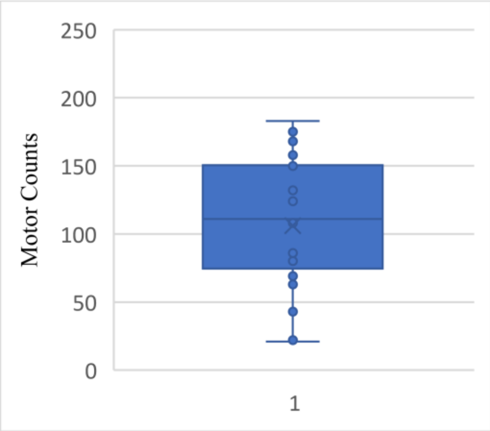

Figure 5.17 Box Plot of precision movement tilting the cap back.

It now reported a graph (Fig. 5.18) and a Table (Tab. 5.6) that summarize all the test, varying the power and the material. It is possible to note that the material does not influence in a significant way the precision, in fact the two line are almost perfectly superimposed.

On the contrary, as expected, the power strongly influences the movement precision. Just using the minimum possible power voltage of 5 V the precision value computed is close to the acceptable one.

Precision	Soft Material	Elastic Material
Power 5V	0,506 cm	0,519 cm
Power 6V	0,751 cm	0,734 cm
Power 7V		0,920 cm

Table 5.6 Precision data for each material and each power.

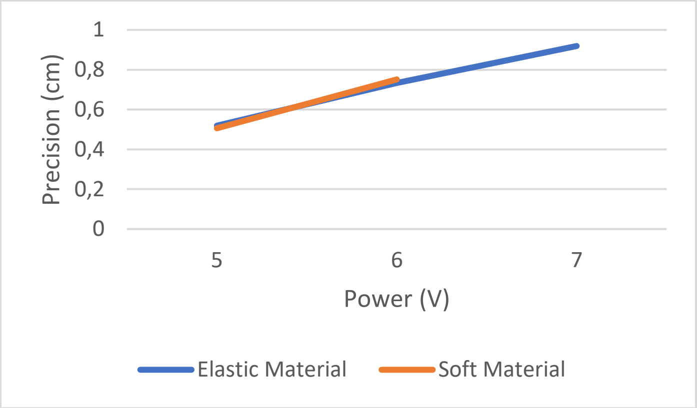

Figure 5.18 Precision trend varying the disk material and the motor power.

The precision value for a power of 7 V and using a soft material was not computed, as the material was too damaged to be used. The similar trend for the two materials can be noted, anyway.

5.1.3 System Stability and Final Comments

For what concern the system stability no critical points were found for this of movement. Every time the controller was released, the cable kept its position and the motor counts, printed on the Pc screen, did not change. Qualitatively and at a high level it is possible to say that the goal of stopping the device in a desired location is reached for this movement.

Some conclusions about the analysis performed on this movement: Some problems were encountered in the execution of it, especially in the final part of the extension phase. The cable often risks jamming and damage. As said, a cable collection system could be a solution to this problem but complicating the mechanical of the system.
Further analyses are certainly necessary about the material used. Neither of them has a perfect behaviour. The elastic one has been chosen, ensuring better performance, especially for the drag phase.
In the firmware development of this movement the possibility of accelerating or decelerating is not contemplated. However, it has been seen how an increase in power ensures more constant range of motion and less difference between the two directions of movement, especially for the complete range (Fig. 5.11). Higher power also ensures a more rapid and immediate solution to the jamming problems encountered. On the contrary, a lower power would be necessary to perform the movement with greater precision. The lowest power studied in this work (5 V)

ensures a precision value at the limit of acceptability. Lower power values would not allow the whole range to be performed without human intervention. Therefore, the possibility of accelerating this movement should be introduced in future developments. In this way it is possible to move the cable quickly for long ranges, solving jamming problems, and then decelerate when it is close to the target and move it with greater precision. The power could also decrease below the value of 5 V, ensuring even greater precision according to the trend found (Fig. 5.17)

5.2 Rotation Movement

In this section, it will be described how it was verified that the full range can be travelled, the estimation and calculation of the accuracy and the evaluation about system stability.
The only variable that will be taken in account is the motor power. Powers of 2V, 4V,5V,6V will be evaluated. Powers smaller than 2 V generate a too slow movements, that the user would not apply and so not interesting for this study. Powers higher than 6 V would cause too fast movement and so too small accuracy.

5.2.1 Movement Range

In this first section it will be described the evaluations done about the full movement range and the estimation of the ratio $\frac{range\ (\ in\ degree\ )}{range\ (in\ motor\ counts)}$ useful to then compute the movement accuracy. The possibility to perform the full range required is not influenced by the motor power.
The target range that the instrument should travel in rotation it 360°. Thanks to the mechanical technology developed and described in chapter 3, this range can easily be travelled. The worm gear system does not have any type of block. It is possible to continue to turn the worm and consequently the gear potentially to infinity in any direction. The only limit can be imposed by the tangling of motor cables that manage the movement of the control lever. This motor is constrained to the instrument and turns with it and consequently also the cables turn with it (Fig. 5.19). However, this movement has been tested in many trials and no significant problems of cable rolling have been found, at least up to two complete rotations in each direction (1440°). This value goes much further than the intended goal which can therefore be considered absolutely achieved, thanks to this technology. The maximum tested values are reported in Table 5.7, values higher than these can be reached.

Rotation full range	Max rotation tested rotating clockwise	Max rotation tested rotating counter clockwise	Target Range
	+720°	-720°	[-360°; +360°]

Table 4.7 Data about maximum value of rotation tested.

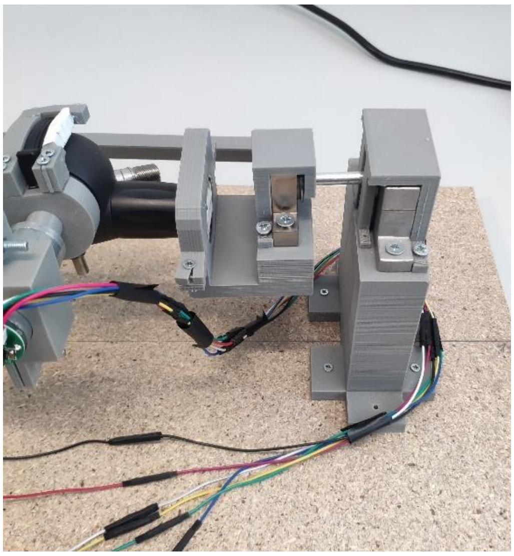

Figure 5.19 The cables of the tip defection motor that can tangle around the instrument and limit the rotation.

It was then necessary to measure the total amount of motor counts necessary to perform this movement. Moreover, it was monitored the motor counts necessary to perform only 90°, a quarter of the full range. This partial range was measured for two main reasons:

- Travelling the full range is really time spending, above all at low motor power. Measuring the partial range allow to perform a higher number of tests in less time.
- It was studied if the different sections of the full range are executed in the same way, at the same speed. For this reason, each quarter was evaluated by monitoring the speed value and the execution time.

The goal would be to have sections that are always travelled in the same way and that are completed with about a quarter of the motor counts needed to complete the full range.
For what concerns the motor counts to compute the full range, 5 tests have been performed rotating the instrument clockwise and 5 rotating the instrument counter

clockwise. The results are reported in Table 5.8. The time to perform the full range was also measured in order to evaluate difference in velocity to perform a direction or the opposite one. The average number of motor counts to compute the full range in the two direction and the time are very similar. The same behaviour has been recorded for other power with no significant difference between the two cases.

Full Range	Clock Rotation	Counter Clock Rotation
Average (motor counts)	107825,4	107769,6
Range (motor counts)	[107771-107895]	[107708-107821]
STD (motor counts)	50,12	49,00
Average Time (sec)	90	88,8
Range Time (sec)	88-92	87-91

Table 5.8 Data about motor counts to perform the full range in rotation at 4 V.

There is no significative difference between the two ranges. It is therefore possible to calculate the total average of all the 10 tests and use it to calculate the ratio between the range in degrees and the range in motor counts. A value of $0{,}003339 \, \frac{degree}{motor\ counts}$ has been computed at 4 V.

To measure the partial sections, the instrument has been rotated starting from a position established as the initial of the gear (Fig. 5.20, Fig. 5.21) (it is the position such that the control lever is facing upwards). The following rotation have been performed, each one 5 times:

- 90 degrees counter clockwise from the initial position.
- 90 degrees clockwise from the lateral position to report it to the initial position
- 90 degrees clockwise from initial position
- 90 degrees counter clockwise from the lateral position to report it to the initial position.

The data regarding the 4 V case are summarized in Table 5.9.

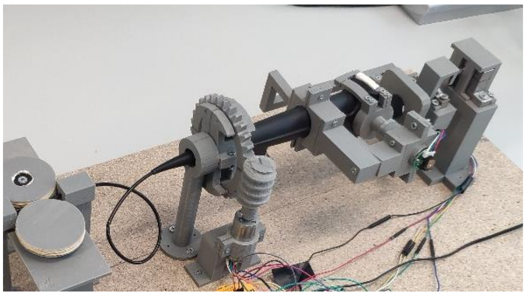

Figure 5.20 Initial position of the device with the control lever facing upwards.

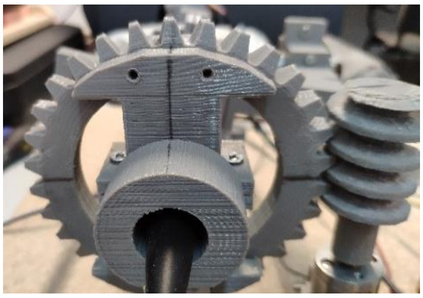

Figure 5.21 Initial position of the gear. The 90° sections are marked.

90° Range	Clockwise from initial pos	Contraclockwise from lateral pos	Contraclockwise from initial pos	Clockwise from lateral pos
Average (motor counts)	26492,8	26489,4	28041,6	27696,0
Range (motor counts)	[25425-27152]	[25385-27072]	[26872-28866]	[26744-28872]
STD (motor counts)	724,04	727,60	865,96	1027,26
Average Time (sec)	20,34	20,80	23,48	21,10
Range Time (sec)	[19,7-21,0]	[20,3-21,5]	[23-24,4]	[20,5-21,5]

Table 5.9 Data about motor counts and time to perform 90° range at 4 V.

The main difference has been found in the contraclockwise rotation from initial position. This section is covered on average with a similar number of motor counts compared to other cases, but in a much longer time. This means that the section has been travelled with a much lower speed. On the graphic user interface, it is possible to monitor a value of speed normally lower for this particular part.
This phenomenon has been studied also for the others motor powers. A significative case is the one with lowest power (2 V). The same data for 2V power are reported in the following table (Tab 5.10)

90° Range	Clockwise from initial pos	Contraclockwise from lateral pos	Contraclockwise from initial pos	Clockwise from lateral pos
Average (motor counts)	26876,33	26868,33	27191,33	27333,33
Range (motor counts)	[26726-27003]	[26674-27031]	[27032-27488]	[27210-27490]
STD (motor counts)	140,00	180,59	257,16	142,95
Average Time (sec)	43,77	45,93	57,78	46,14
Range Time (sec)	[43,3-44,1]	[45,5-46,4]	[57,25-58,5]	[45,9-46,31]

Table 5.10 Data about motor counts and time to perform 90° range at 2 V.

In this case it is also possible to see how the range does not significatively change. On the contrary the travel time is up to 14 secs higher, causing a significant change in travel velocity.
Analysing higher powers, a decrease in this phenomenon has been noted (Fig. 5.22). In this graph is reported the average time of the three similar sections and the average time of the slower section. The differences decrease at higher powers.

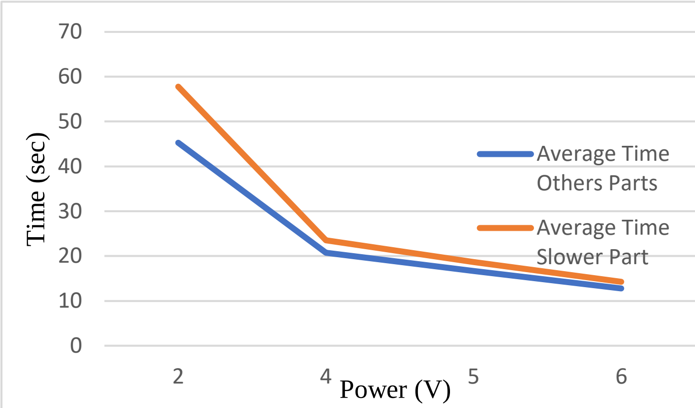

Figure 5.22 Average time to perform the slower section vs Average time to perform the other sections, varying the power.

This phenomenon is probably due to the not perfectly system balancing. As said, the motor that control the tip deflection is constrained to the instrument. It implies that the side where the motor is positioned will certainly be heavier than the opposite side where a slight sidebar is located (Fig. 5.23).

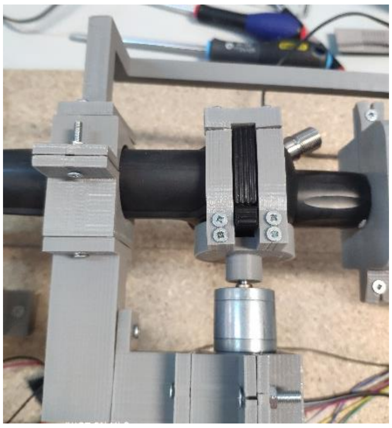

Figure 5.23 Unbalancing of the system. The motor size is much heavier with respect the opposite one.

When the rotary movement must lift the motor, as in the contraclockwise starting from the initial position case, a higher gravitational force must be won. When the motor instead is moved downwards the force of gravity helps this movement and allows a higher speed of movement.

Clearly at lower powers the motor applies a lower force on the motor and therefore the differences between the two cases are much more marked (Fig. 5.22). These differences tend to disappear at higher powers, where the same gravitational force must be won but a much higher force is applied.

As shown in the Figure 5.24, for each power there are no particularly significant differences in the motor counts to travel each section. In this graph the motor counts of the three similar sections and the motor counts of the slower section have been compared. No significative difference has been pointed out. In this way it is possible to mediate all the motors counts for each section in order to find a smaller range that can be used to calculate the ratio. The goal of this smaller range, as said, is to perform more tests in the same time.

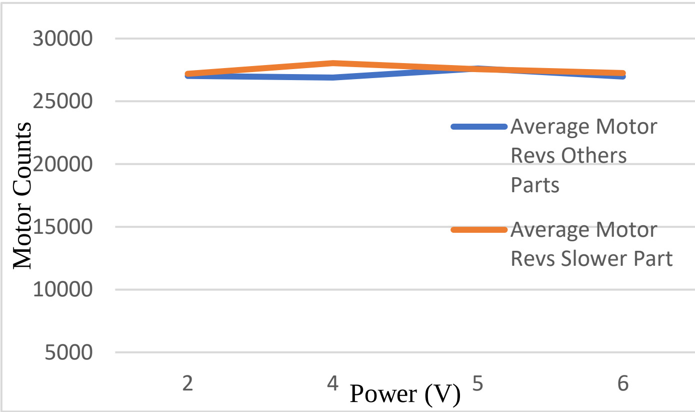

Figure 5.24 Average motor counts to perform the slower section vs Average motor counts to perform the other sections, varying the power.

Finally, the following graph (Fig. 5.25) shows the trend of the 90 ° average range in motor counts (between all the sections) and the complete 360 ° range as the power varies. Compared to the insertion movement there is a much more stable trend. Power is a variable that has a little influence on the motor counts needed to travel a section and this was the objective to achieve.

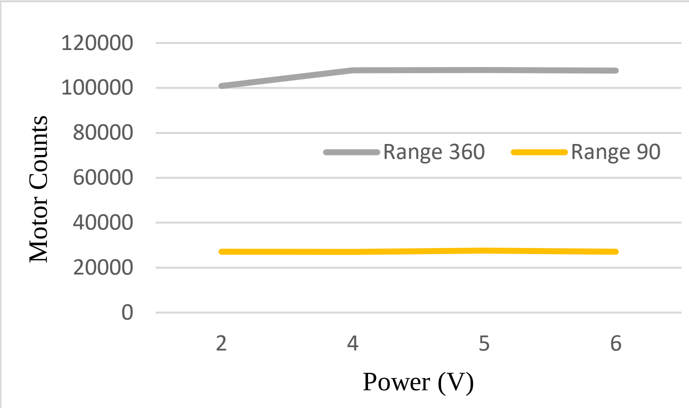

Figure 5. 25 Trend of the two-range varying the motor power.

5.2.2 Movement Precision

Also for this case, it is important firstly to define a precision range that can be considered acceptable. It has been considered how the surgeon control this movement in case of manual control, the ability he/she could have in accurately controlling this movement, and the working conditions in which this movement is performed. As said, the possible range of movement is ±360 °. The surgeon controls the instrument through the ergonomic handle, turning the instrument to the right or left. The precision that it could have does not seem to be optimal through this type of control. It is not easy to move it grade by degree through this kind control. The goal to be achieved is to rotate the tip to better align the different channels with the target. An acceptable range of around 0.5 ° has been estimated. This is a precision value that would probably go beyond the human one.
For the calculation of the precision as previously explained, as small as possible movements have been performed with the 3DMouse cap, in this case by rotating the cap to the left and to the right. 41 tests have been executed for each direction and the motor counts have been recorded. The data of the test done with 4 V power are reported here. Similar behaviour is encountered in all cases. The main purpose is that there is no difference in the average motor counts values performing the right and left cap rotation. The results are summarized in Table 5.11 and in Figures 5.26 and 5.27. It is possible to note a similar distribution and a very similar average value between the two directions. At this point the total average of all the tests (82) is calculated and this value is multiplied by the ratio obtained previously. In this way a degree precision measurement is obtained.
In this case a total average value of 112,98 motor counts. (range [32 motor counts-205 motor counts], std 38,25 motor counts).

The precision in the right unit of measure is:

$$112{,}98\ motor\ counts\ \cdot 0{,}00334\ \frac{degree}{motor\ counts} = \ 0{,}3774°$$

This test is performed around the initial positions of the instruments, but all the position could be use. No problematic positions have been found in the trials with the rotation movement.

Precision	Rotating Right	Rotating Left
Average (motor counts)	115,26	110,69
Range (motor counts)	[39-205]	[32-188]
STD (motor counts)	42,14	34,28

Table 5.11 Data about motor count, rotating the cap to the right and to the left with a power of 4 V.

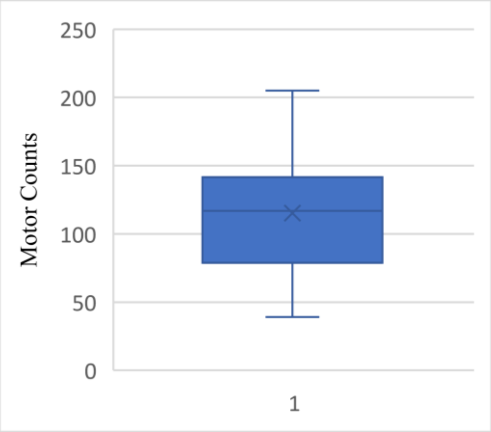

Figure 5.26 Box Plot of precision movement rotating the cap to the right.

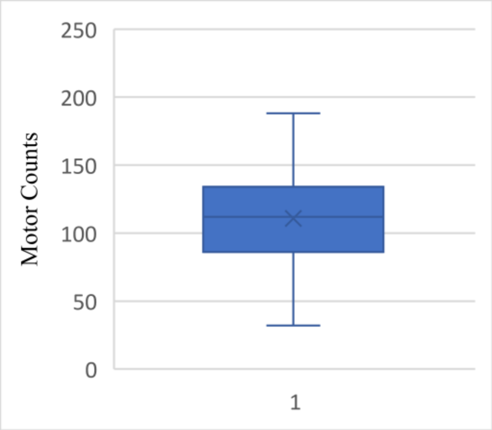

Figure 5. 27 Box Plot of precision movement rotating the cap to the left.

The precision values have been calculated using the 360° range and the 90° range. The results are shown in Table 5.12 and in Figure 5.28. There is no difference between the accuracy calculation with the two ranges. It allows to conclude that it is possible to use a smaller range (of 90°) to perform these types of tests, obtaining more results at the same time and therefore more reliable.

Precision	90° Range	360° Range
Power 2V	0,213°	0,228°
Power 4V	0,373°	0,377°
Power 5V	0,491°	0,503°
Power 6V	0,600°	0,604°

Table 5.12 Data about the precision computed with the two ranges, varying the motor power.

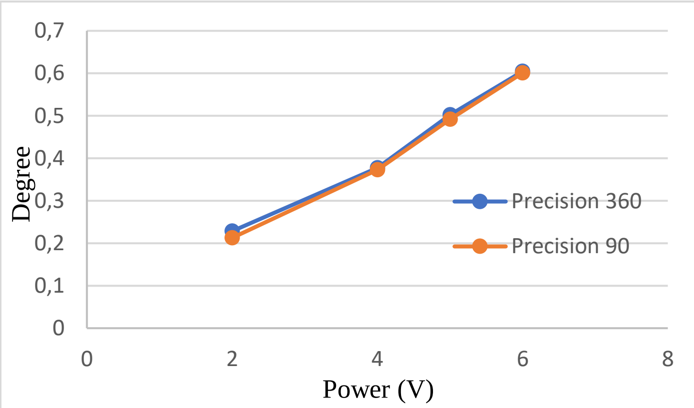

Figure 5.28 Precision trend computed with the two ranges, varying the motor power.

It is possible to see that precision value is higher augmenting the motor power, as expected.

5.2.3 System Stability and Final Comments

For what concern the system stability no critical points were found for this of movement. Every time the controller was released, the instrument kept its position and the motor counts, printed on the screen, did not change. Qualitatively and at a high level it is possible to say that the goal of stopping the device in a desired location is reached for this movement.
In general, no particularly critical points were found in this type of movement. The ranges of movement do not change as the motor power varies (Fig 5.25) Improvements could be made in the distribution of the weight of the instrument in order to ensure the same speed and travel times in performing all the sections in which it is possible to divide the gear. Further analysis would be necessary to discover other sections in which this slowed movement is present due to a higher gravitational weight to be won. The possibility of accelerating and decelerating

the rotation is implemented at the firmware level. Also, for this movement it is certainly a useful possibility. The range of 360 requires a high number of motor counts to be driven, so travelling at high speeds becomes necessary if the user want to travel long distances. On the contrary, high speeds do not allow to have a precision that can be acceptable. At the value of 6 V, the maximum studied here, there isn't a correct precision value. Low power values allow extremely precise control of the instrument. For this reason, the acceleration control must be maintained for this movement.

5.3 Tip Deflection Movement

In this section it will be described the procedure followed to evaluate if the controller lever can travel the full range. The full displacement range of the control lever of ±45° can be mapped in a tip deflection range of ±270°.
The computation of the value of precision and its variation with the motor power will be then described. The motor power value considered had been: 1V,2V,4V,6V. Considering that integer value of the motor power has always been used, 1 V is the minimum value that can perform a motor movement. Moreover, power smaller than 1 V do not ensure a full range movement. When the lever is in the part closest to the end of the instrument (Fig. 5.29), it must travel a section in which it moves from bottom to top. Gravity force comes into play in this phase and too low motor power does not allow it to be won. Values higher than 6 V cannot ensure an enough small accuracy.

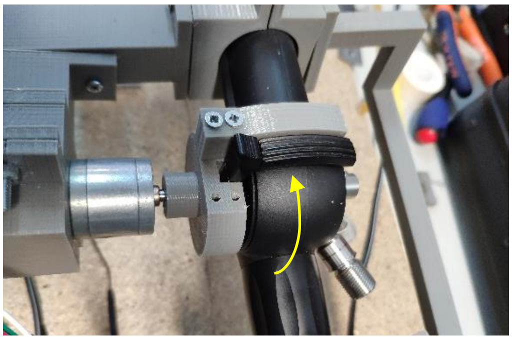

Figure 5.29 The lever is here located at the end of the more "vertical" sector of its range. The yellow line indicates the sector that cannot be well travelled a too low motor power.

5.3.1 Movement Range

In this first section it will be described the evaluations done about the full movement range and the estimation of the ratio $\frac{range\ (\,in\ degree\,)}{range\ (in\ motor\ counts)}$ useful to

then compute the movement accuracy. The possibility to perform the full range required, is not influenced by the motor power.
At first, it was necessary to verify that the mechanical elements placed around the control lever did not in any way limit the range of complete movement of the lever.
Above all the lateral bars are hypothesized as disturbing elements to the complete execution of the range. They may impact with other elements of the ureteroscope and block the movement of the lever. These two lateral bars, however, are mechanically fundamental to well fix the motor to the lever and to ensure its movement.
To verify that the lever can perform complete movement, the range (in motor counts) has been measured in three cases:

- With both the lateral bars (Fig. 5.30),
- Removing the lateral bar instrument end side(right) (Fig. 5.31)
- Removing the lateral bar cable side (left)

If the motor counts needed to travel the full range with the bars and without the bars are the same, it means that the full range of ±45° can be travelled by the lever

Figure 5.30 Control lever with both lateral bars.

Figure 5.31 Control lever without the end instrument side bar.

It is possible to remove only one at a time but without performing other movements. If a lateral bar was removed and a rotation made, the circular structure at which the motor is attached would risk leaving its position. For this reason, they have been removed only in this experimental phase to verify that their presence was not an obstruction to the complete movement.
Data about this experimental test at a 2V power are reported in Table 5.13. The lever has been moved in the two direction for 5 times and the motor values at the extremities of the range have been recorded. For the cases without a lateral bar

just the motor value on the side without bar have been recoded. This value could be the interesting one, because that side now has no possible encumbrances that block the movement. The values with or without lateral bars are then compared.

Full Range	**Motor Counts value left side with bar**	**Motor Counts value right side with bar**	**Motor Counts value left side without bar**	**Motor Counts value right side without bar**	**Total Counts with bar**	**Total Range without bar**
Average Value (Motor Counts)	-200,3	576	-216,67	642,33	776,3	859
Range (Motor Counts)	[-203; -197]	[571;577]	[-219; -213]	[641;643]	[771;780]	[856:862]
STD (Motor Counts)	3,06	1,73	3,21	1,15	4,73	3,00

Table 5.13 Data about motor counts at the extremities of the total range in the cases with and without the lateral bars.

It is possible to see a significative difference between the average value of the total range in case with the bars and without the support. In particular, a higher difference has been found for the right side of the range, the one close to the end of the instrument.
Considering the displacement without the lateral bars as the maximum one of 90° (there are no obstacles), using a proportion it was computed the range with both the lateral bars. A value of 81,338° has been found. This value is far from the objective required.
For this reason, a technical modification has been introduced to solve this problem and achieve the objective of having a full range of ±45° and so a total displacement of 90°.The technical modification consists in reducing the size of the right lateral bar (Fig. 5.32). This piece was in fact seen as the most problematic to reach the full range. The new dimension of lateral support is half of the previous one (0.5 cm) This change does not cause any problems in the execution of the functions to which the lateral supports are dedicated.

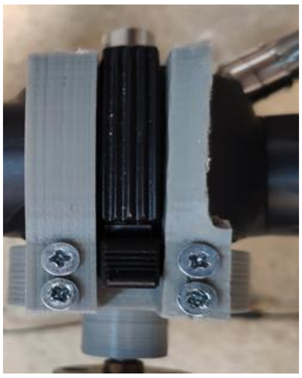

Table 5.32 Technical modification of the right lateral bar.

Data about the experimental tests with the technical modification are reported in Table 5.14. They have been also obtained with a power of 2 V and with 5 tests each side.

Full Range (post technical modification)	**Motor Counts value left side with bar**	**Motor Counts value right side with bar**	**Motor Counts value left side without bar**	**Motor Counts value right side without bar**	**Total Counts with bar**	**Total Counts without bar**
Average Value (Motor Counts)	-211	627,68	-220	649	869	859
Range (Motor Counts)	[-216; -201]	[624,630]	[-224; -218]	[648;650]	[866;873]	[856:862]
STD (Motor Counts)	8,66	3,21	3,46	1,00	3,61	3,00

Table 5.14 Data about motor counts at the extremities of the total range in the cases with and without the lateral bar after a technical modification of the right lateral bar.

Observing the average values of the motor counts necessary to travel the ranges, values much more similar between the two cases have been found.
Thanks to a proportion it is possible to compute the total range in degree. A value of 86,86° has been computed. Value that can be considered much more acceptable compared with the previous one. With a further reduction of the lateral support would be possible to find an almost perfect displacement range.

In the following graph (Fig. 5.33) it is possible to observe the percentage differences between the value in motor counts reached at the end of the left side with and without lateral bars, the value at the end of the right side with and without

lateral bars, and the total range with and without lateral bars. They are represented as the motor power varies. It is evident that the left side has minimal differences for each power applied before and after modification. These small differences are more probably due to a variation in data collection and other external influences than the presence of physical obstacle that blocks movement to the left.
For what concern the movement to the right side, it evident that it is the most relevant side in this problem. This difference decreases thanks to the technical modification applied. However, it stands at higher levels that could lead to assume the presence of a further obstacle to reach the full range. No trend with power can be detected. In any case, the errors reach a maximum of 3.1%, normalizing on the total range.
The total range is the sum of the two errors and records maximum errors around 4%.

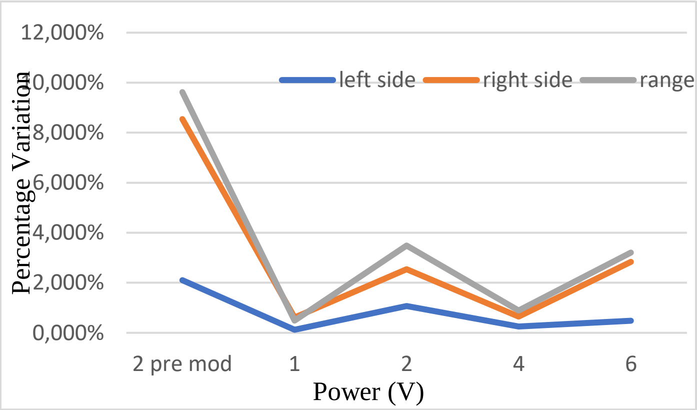

Figure 5. 33 Percentage variations between the case with lateral bar and the case without lateral bar. The left side, the right side and the total range are evaluated. The first value is computed before the tecnical modification of the laterl bar.

It is also reported the total value of the range in degrees (Fig. 5.34 and Tab. 5.15) obtained through a proportion between the motor counts performed with the bars and those performed without bars which correspond to the maximum displacement range of the lever (90 °)
There is a clear improvement in the range value in post technical modification, with values that are between 87 ° and 90 ° degrees. There is no trend that links it with power. The variation in value obtained at different powers is probably due to statistical inaccuracies or other external factors that could influence the motor counts value. It is important to underline that this movement is performed with a very low number of motor counts compared to the other movements. The motor input shaft count is a minuscule distance that can therefore undergo variation even repeating the same test under the same conditions.

Variation of a few motor counts are much more significant in this movement that uses few counts to perform its range.

Power	Range
2 V, pre modification	81,34°
1 V	89,56°
2 V	86,86°
4 V	89,20°
6 V	87,11°

Table 5.15 Lever control movement range varying the power.

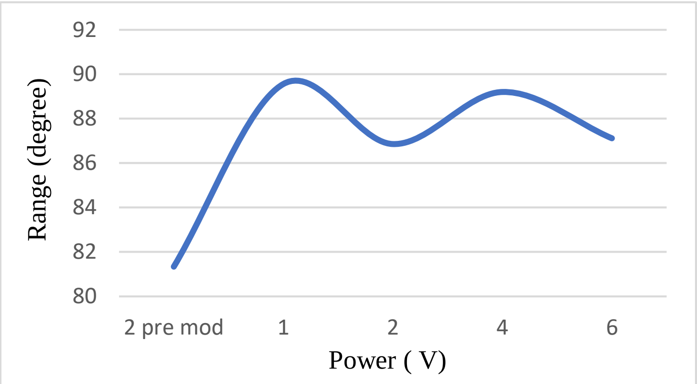

Figure 5.34 Range in degree, varying the power. The first value is computed before technical modification.

Finally, a graph is shown (Fig. 5.35) which describes the variation of the total value of the number of motor counts necessary to travel the full range, varying power. For this type of movement there are no perfectly constant ranges when the power is variated. There are variations up to 16% and a positive trend with increasing power. It is unlikely that the cause of this phenomenon lies in the fact that a longer range is travelled with increasing power. In fact, it has been experimentally tried to move the lever with the use of hands once it reaches the extreme point, but no variation in the motor counts plotted on the PC screen, have been recorded. The variation could be considered non-significant as in absolute terms there is a difference of 161 motor counts which corresponds to 0.034 complete turns of the output shaft. As mentioned, for this type of movement a few motor counts are necessary to complete the whole range. This implies the presence of relatively high percentage changes but a small actual shift.

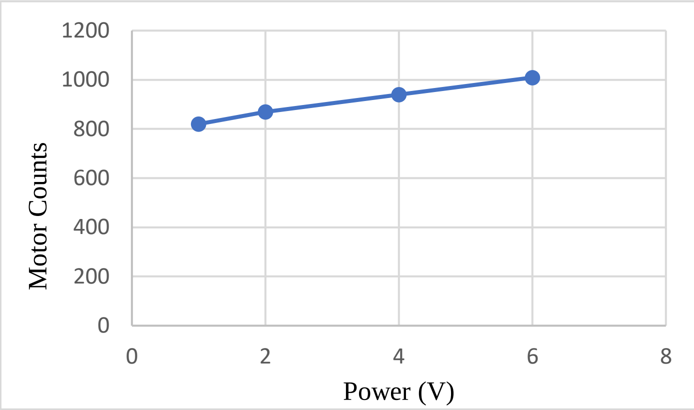

Figure 5.35 Motor counts to perform the full range trend, varying the motor power.

5.3.2 Movement Precision

Before reporting in detail, the procedures for calculating the precision and its results, it is necessary to define a precision value that can be considered acceptable.

At first, it has been hypothesized that if the user manually moves the lever when it is connected to the motor it is possible to record, thanks to the encoders, the movement that the human control cause and therefore the human precision.

Unfortunately, it has been realized that a shift of the lever causes much fewer motor counts if it was moved manually than if it was moved with the 3D mouse. Therefore, the two values cannot be compared. As an example, some ranges are shown in the Table 5.16.

Power	Manual Range	3DMouse Range
1	530 motor counts	816 motor counts
2	528 motor counts	838 motor counts
4	536 motor counts	931 motor counts
6	510 motor counts	977 motor counts

Table 5.16 Average values of the motor counts necessary to perform range in the manual control case and the 3DMouse control case.

For this reason, as for the other two movements, it was necessary to estimate a range of acceptability of precision considering the total range (90°) and the ability that a surgeon could have in controlling this variable through the manual lever. Assuming a non-perfect control that he/she can have on this and the small total range, a value around 5 ° has been considered acceptable.

The same procedure to compute the precision values have been applied also in this case.

As small as possible movements have been performed with the 3DMouse cap, in this case by tilting the cap to the left and to the right. 41 tests have been executed for each direction and the motor counts have been recorded. The data of the test done with 2 V power are reported here. Similar behaviour is encountered in all cases. It is requested no difference between the movement in the two directions. The results are summarized in Table 5.17 and in Figures 5.36 and 5.37. It is possible to note a similar distribution and a very similar average value between the two directions. At this point the total average of all the tests (82) is calculated and this value is multiplied by the ratio obtained previously. In this way a degree precision measurement is obtained.
In this case a total average value of 45,13 motor counts. (range [13 motor counts-85 motor counts], std 16,38 motor counts). The precision in the right unit of measure is:

$$45{,}13\ motor\ revs\ \cdot 0{,}104\ \frac{degree}{motor\ counts} = \ 4{,}67°$$

This test is performed around the central positions of the lever, but all the position far from the ends could be use.

Precision	**Tilting Right**	**Tilting Left**
Average (motor counts)	43,10	47,17
Range (motor counts)	13-85	16-85
STD (motor counts)	14,41	18,09

Table 5.17 Data about motor precision, tilting the cap to the right and to the left with a power of 2 V.

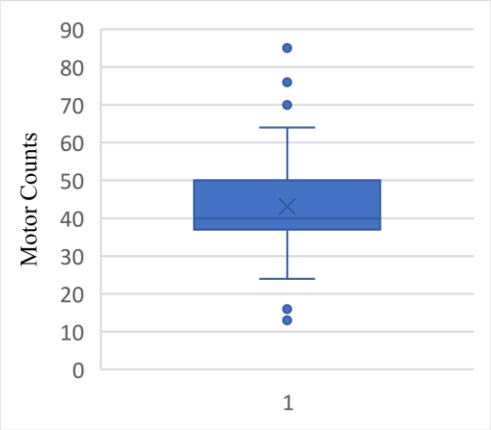

Figure 5.36 Box Plot of precision movement tilting the cap to the right.

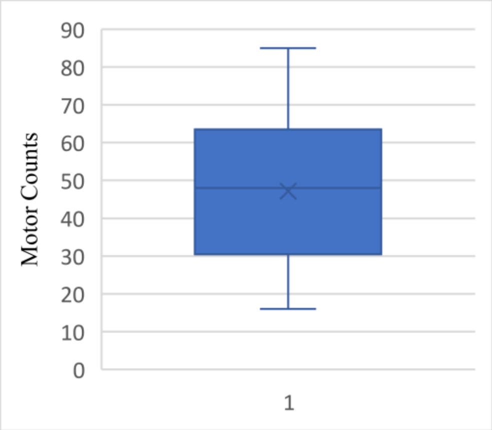

Figure 5.37 Box Plot of precision movement tilting the cap to the left.

The precision values have been calculated for each motor power considered. The values obtained are shown in the Table 5.18 and in the Figure 5.38. A positive trend with increasing power can be found, as expected.

Power	**Precision**
1 V	2,71°
2 V	4,67°
4 V	10,75°
6 V	18,51°

Table 5.18 Precision data for each power.

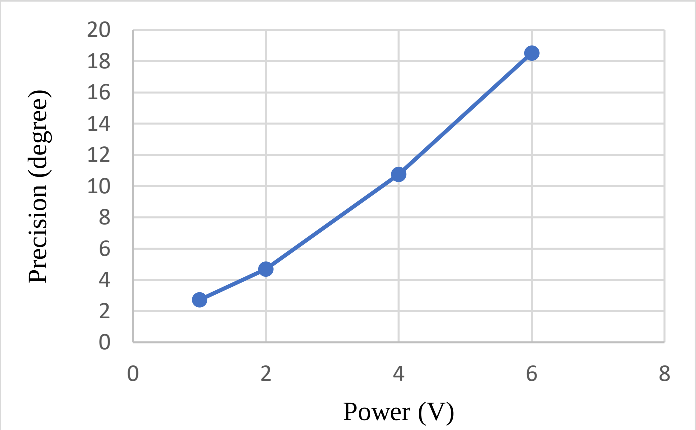

Figure 5.38 Precision trend, varying the power.

5.3.3 System Stability and Final Comments

For the other two movements no problems with stability and ability to keep a position once reached have been found. On the opposite, in this case, this problem was encountered at the extreme points of the range. Travelling the whole range from one end to the other with a continuous movement (keeping the cap tilted in that direction), a value of motor counts is reached. This value decreases if the mouse is released (spring effect) and if the cap is tilted again the motor counts value increase but without returning to the first value. As can be seen from the graph (Fig. 5.39), the instability increases, increasing the power with which the movement is performed. The graph represents four different the percentage variations:

- The difference between the value reached travelling the full range from left to right and the value after realising
- The difference between the value reached travelling the full range from left to right and the value reached after that the cap is tilted again.
- The difference between the value reached travelling the full range from right to left and the value after realising
- The difference between the value reached travelling the full range from right to left and the value reached after that the cap is tilted again.

The percentage values are normalized on the full range in motor counts value.

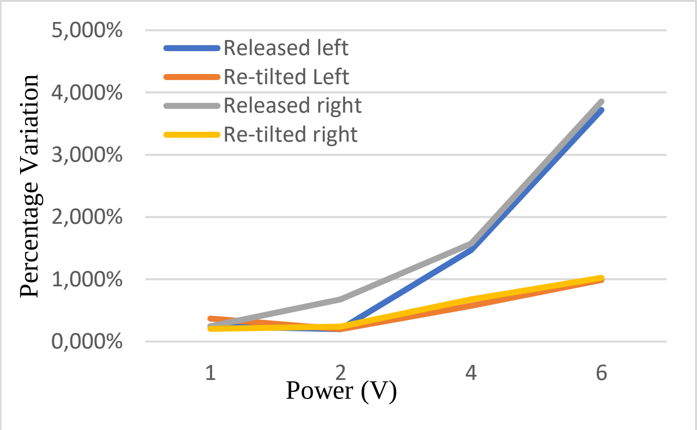

Figure 5.39 Effect of position instability at the ends of the range, varying the power.

There is not a significative difference between this phenomenon, travelling the range in the two possible directions.

This instability effect could certainly create difficulty in the overall control of the instrument. In case that user wants to fix the tip deflection in its extreme values, he/she must keep the cap tilted. A possible solution to this problem could be implemented at the firmware level. If the user tilts the mouse to the right or left for more than a certain time, it means he/she wants to lock it at the extreme point.

So, the Arduino can continue to activate the motor even if the user releases the button and deactivates the motor only when the mouse is tilted again.

In addition to these extreme points, no problematic points have been found in this type of movement. The possibility of accelerating or decelerating the movement is probably not interesting in this case. In fact, the execution range is very small and can be performed quickly even with low motor power. Increasing the power has no positive effects. From powers above 2 V there are no problems to perform the whole range. Increasing the power causes a decrease in accuracy and a higher spring effect just described. A motor power equal to 2 V would ensure accuracy within the range of acceptability without other limits.

5.4 Global Movement

The last task that will be evaluated is about the global movement that the user can perform with the prototype.
As previously introduced, a model of urinary system has been created for this final phase (Fig. 5.40). The model is inspired by the low fidelity model by the University of Toronto (Matsumoto, Hamstra, Radomski, & Cusimano, 2002). The same identical materials are not used due to availability problems but materials with the same characterises. Instead of using a Penrose drainage tube, an elastic tube was used. This tube was cut to the same length as the man's urethra (about 20 cm) and it is 6 mm inner diameter, that is a dimension comparable with the human one. The container, in which it has been built, was 3D printed. As in the original model an inverted cup to model the bladder was used, in this case transparent to be able to see inside, Finally, two straws for the ureters, with an 8 mm of diameter and 25 cm of length, dimensions comparable with the human ureters.
Everything has been fixed to the plastic structure thanks to the modelling paste that dries in the air. Only the tube representing the urethra is free to move.
As expected, the experimental tests on this model have been quite unsuccessful. The tip does not respond to the controls of the lever and it is therefore impossible to have sufficient control to penetrate into the deeper parts of the system, like the ureters. In Figure 5.41 it is reported the final device while it is testing on the model.

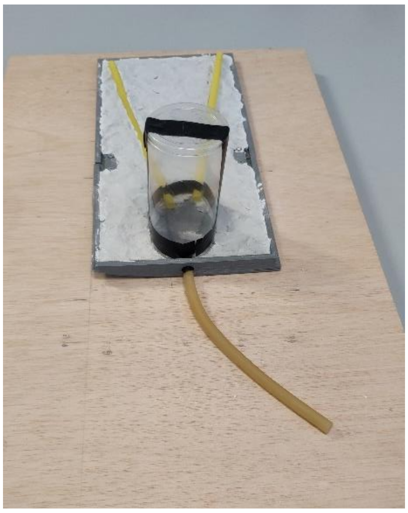

Figure 5.40 The urinary system model implemented based on the idea of the Toronto University Low-Fidelity model.

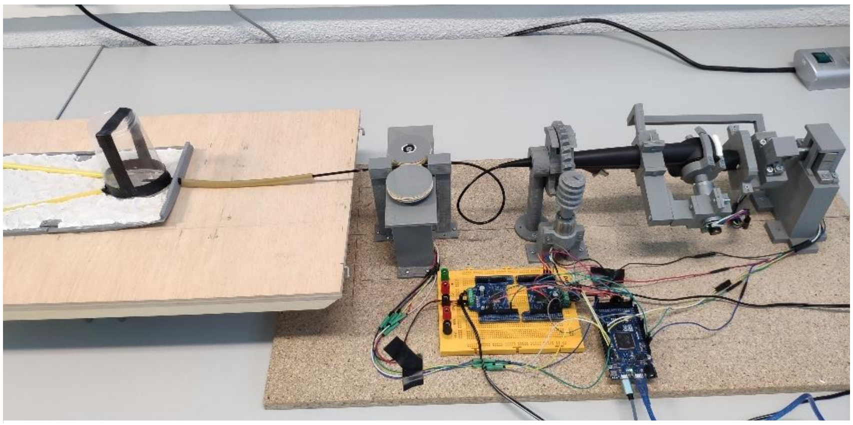

Figure 5.41 The final device during a test on the urinary system model.

Some qualitative considerations have also been made. The control system has some management problems. In fact, the movement of the cap in one direction could erroneously also activate a movement in another direction. It is not easy to clearly separate the different movements of the 3dMouse cap. An improvement in the control system would be necessary, perhaps by switching to two 3DMouse or design a specific control system.

Chapter 6: Conclusions and Future Developments

The thesis work described here represents a potential solution to ergonomic and X-ray proximity problems encountered in flexible urethroscopy applications. The device implemented in fact guarantees the remote control of the ureteroscope from a comfortably seated position, that can potentially be located far from the area of operation.

The device is part of an investigation field in which commercial solutions are still in small numbers, expensive, and not free of defects. The principles with which movements have been developed are certainly an innovation.

The goals set in this work were largely achieved:

The required working range is very close to the objective in case of the insertion movement and tip deflection, while it much better than the required value in case of rotation movement.

For what concerns the precision, compared to the values that have been estimated as acceptable, all the movements approach or realize this goal. Only the insertion movement stands at slightly higher values (0.5 cm vs 0.52 cm) with the minimum motor power that ensures the travel of the full range (5 V). The rotation movement develops a much better level of precision with respect the one that the manual control could ensure, leading to a potential improvement in the execution of the operation.

The stability of the system has been verified for many points of every movement, finding significant problems only in the extreme points of the movement of the lever. It ensures the possibility of stabilizing and stopping the system in most of the points that the cable could travel inside the urinary system. It brings an improvement in the quality of the operation that is not possible in case of human control.

These variables have been studied varying the motor power with which the system moves. It allows to draw some conclusions about the possibility of accelerating and decelerating the movements. It is surely necessary for the insertion movement and for the rotation one, while it is almost useless for the tip movement, as explicated in the respective chapters. Moving the system at a higher speed, in general, causes a decrease in the precision of movement but allows longer ranges to be travelled more quickly and the solution of problems such as the jamming of the cable or the non-perfect distribution of the weights on the instrument.

Problems were found in the global movement test on the model due to a malfunction of the tip movement.

The most problematic technological solution is surely the disks system implemented for cable drag. It presents jamming problems, as mentioned, and the

continuous action on the cable could damage it, being the most fragile part of the instrument.
Improvements or a complete redesign of this technology would be necessary.
At the level of firmware, the fundamental tasks for the realization of the main objectives have been accomplished. A serial communication has been implemented between the different elements of the device that allows the passage of data in real time. With the use of the robot it is possible to notice how the activation response of the motors is immediate with respect to the movement performed with the mouse cap. The updating of the data on the graphic interface is also immediate.
The graphical interface implemented is at a basic level but is updated correctly with data and it well represents what happens on the device.

Improvements in every part of the project are certainly necessary:
Mechanical Part

- Improvement of the cable drag system
    - Study of new materials for the disks that ensure a free rotation of it and a good motion transmission.
    - System dimensions reduction to ensure longer movement range.
    - Study and development of a cable collection system so that it can be rolled up in an orderly manner, reducing the damage on it and the risk of jamming. This system must be able to rotate with the instrument to ensure the rotation of the cable when a rotation is desired.
    - Redesign of the insertion system if the other improvements do not lead to the hoped results. They could be done by acting directly on the structure of the ureteroscope. However, direct control on the cable, that potentially ensures more precise control, would be lost
- Improvement of the tip control system
    - Further reduction in the dimensions of the lateral supports to ensure the execution of the complete movement range.
- Improvement of the Rotation system
    - Improvement of system weight distribution to ensure constant travel times for each section of the movement range
    - Solution of the cable tangling problem.

Control and firmware part

- Improved control system
    - Addition of a second 3DMouse in order to ensure a more precise control and avoid the risks of activating other movements erroneously. An additional mouse would also expand the acceleration management possibilities with two new buttons.

- Design of a new control system specifically created for this type of movement

- Microcontroller
  - Study of alternatives to Arduino control systems that ensure better performance and deeper control.
- Firmware improvement
  - More precise control of timing and ISRs. Tests with different ISRs periods in search of the best solution.
  - Improvement of the communication protocol with the insertion of start, stop and control bytes to avoid the risk of system lag.
  - Implementation of firmware solutions to solve mechanical problems, such as the elastic effect of the lever in its extreme points.
  - Introduction of the possibility of accelerating other movements.
  - Improved GUI with more intuitive widgets and the ability to perform actions directly from here

At a more general level in its future the system will have to:

- be adaptable to different types of ureteroscopes and other types of endoscopes on the market.
- be linked to a multi-functional mechanical arm for a control with a higher number of degrees of freedom
- introduce the haptic feedback
- be connected with the virtual reality system implemented by the laboratory for tests on virtual reality.

Bibliography

3dconnexion. (2019, March 19). Retrieved from Spacemouse_compact: https://www.3dconnexion.it/spacemouse_compact/it/

Aboumarzouk, O. M., Monga, M., Kata, S. G., Traxer, O., & Somani, B. K. (2012). Flexible ureteroscopy and laser lithotripsy for stones> 2 cm: a systematic review and meta-analysis. . *Journal of endourology,* , 26(10), 1257-1263.

Alenezi, H., & Denstedt, J. D. (2015). Flexible ureteroscopy: Technological advancements, current indications and outcomes in the treatment of urolithiasis. *Asian journal of urology*, 2(3), 133-141.

Alivizatos, G., & Skolarikos, A. (2006). Is there still a role for open surgery in the management of renal stones? *Current opinion in Urology*, 16(2), 106-111.

Alletti, S. G., Rossitto, C., Fanfani, F., Fagotti, A., Costantini, B., Gidaro, S., . . . Scambia, G. (2015). Telelap ALF-X–assisted laparoscopy for ovarian cyst enucleation: report of the first 10 cases. *Journal of minimally invasive gynecology*, 22(6), 1079-1083.

Arduino. (2019, March 18). Retrieved from Store Arduino Due: https://store.arduino.cc/due

Atrial Fibrillation Center At Hackensack University Medical Center. (2019, March 6). Retrieved from Niobe Remote Magnetic Navigation: http://www.afnewjersey.com/niobe-remote-magnetic-navigation/

Basillote, J. B., Lee, D. I., Eichel, L., & Clayman, R. V. (2005). Ureteroscopes: flexible, rigid, and semirigid. *The Urologic clinics of North America*, 31(1), 21-32.

Berman, B. (2012). 3-D printing: The new industrial revolution. *Business horizons*, 55(2), 155-162.

Boston Scientific Urology. (2019, March 5). Retrieved from Flexible Ureteroscopy with Dr. Sur, Small Stone Procedure: https://www.youtube.com/watch?v=Yu8dL92_6Z0

Breda, A., Ogunyemi, O., Leppert, J. T., Lam, J. S., & Schulam, P. G. (2008). Flexible ureteroscopy and laser lithotripsy for single intrarenal stones 2 cm or greater—is this the new frontier? *The Journal of urology*, 179(3), 981-984.

Buscarini, M., & Conlin, M. (2008). Update on flexible ureteroscopy. *Urologia internationalis*, 80(1), 1-7.

Cadeddu, J. A., Stoianovici, D., Chen, R. N., Moore, R. G., & Kavoussi, L. R. (1998). Stereotactic mechanical percutaneous renal access. *Journal of Endourology*, 12(2), 121-125.

Cadiere, G. B., Himpens, J., Germay, O., Izizaw, R., Degueldre, M., Vandromme, J., . . . Bruyns, J. (2001). Feasibility of robotic laparoscopic surgery: 146 cases. *World journal of surgery*, 25(11), 1467-1477.

Comsol. (2019, March 12). Retrieved from Multibody dynamics module: https://www.comsol.fr/multibody-dynamics-module

Cook, J. A., McCulloch, P., Blazeby, J. M., Beard, D. J., Marinac-Dabic, D., & Sedrakyan, A. (2013). IDEAL framework for surgical innovation 3: randomised controlled trials in the assessment stage and evaluations in the long term study stage. *Bmj*, 346, f2820.

Coronado, P. J., Herraiz, M. A., Magrina, J. F., Fasero, M., & Vidart, J. A. (2012). Comparison of perioperative outcomes and cost of robotic-assisted laparoscopy, laparoscopy and laparotomy for endometrial cancer. *European Journal of Obstetrics & Gynecology and Reproductive Biology*, 165(2), 289-294.

Dahm, P., Sedrakyan, A., & McCulloch, P. (2014). Application of the IDEAL framework to robotic urologic surgery. *European urology*, 65(5), 849-851.

Desai, M. M., Aron, M., Gill, I. S., Pascal-Haber, G., Ukimura, O., Kaouk, J. H., . . . Moll, F. (2008). Flexible robotic retrograde renoscopy: description of novel robotic device and preliminary laboratory experience. *Urology*, 72(1), 42-46.

Desai, M. M., Grover, R., Aron, M., Ganpule, A., Joshi, S. S., Desai, M. R., & Gill, I. S. (2011). Robotic flexible ureteroscopy for renal calculi: initial clinical experience. *The Journal of urology*, 186(2), 563-568.

Dwyer, M. E., Krambeck, A. E., Bergstralh, E. J., Milliner, D. S., Lieske, J. C., & Rule, A. D. (2012). Temporal trends in incidence of kidney stones among children: a 25-year population based study. *The Journal of urology*, 188(1), 247-252.

Edvardsson, V. O., Ingvarsdottir, S. E., Palsson, R., & Indridason, O. S. (2018). Incidence of kidney stone disease in Icelandic children and adolescents from 1985 to 2013: results of a nationwide study. . *Pediatric Nephrology,*, 33(8), 1375-1384.

Elkoushy, M. A., & Andonian, S. (2011). Prevalence of orthopedic complaints among endourologists and their compliance with radiation safety measures. *Journal of endourology*, 25(10), 1609-1613.

Elmed. (2019, March 7). Retrieved from Avicenna-Roboflex: http://www.elmed-as.com/avicenna-roboflex.html

Ergina, P. L., Barkun, J. S., McCulloch, P., Cook, J. A., & Altman, D. G. (2013). IDEAL framework for surgical innovation 2: observational studies in the exploration and assessment stages. *Bmj*, 346, f3011.

Ernst, S., Ouyang, F., Linder, C., Hertting, K., Stahl, F., Chun, J., & Kuck, K. H. (2004). Initial experience with remote catheter ablation using a novel magnetic navigation system: magnetic remote catheter ablation. *Circulation*, 109(12), 1472-1475.

European Association of Urology. (2019a, March 2). Retrieved from EAU Patient Information-PNL Treatment: ttps://patients.uroweb.org/media-library/kidney-and-ureteral-stones/percutaneous-nephrolithotomy-pcnl/

European Association of Urology. (2019b, March 3). Retrieved from EAU Patient Information-SWL Treatment: https://patients.uroweb.org/media-library/kidney-and-ureteral-stones/shock-wave-lithotripsy-swl/

European Association of Urology. (2019c, March 2). Retrieved from EAU Patient Information-Ureteroscopy: https://patients.uroweb.org/media-library/kidney-and-ureteral-stones/ureteroscopy-urs/

Fanfani, F., Monterossi, G., Fagotti, A., Rossitto, C., Alletti, S. G., Costantini, B., . . . Scambia, G. (2016). The new robotic TELELAP ALF-X in gynecological surgery: single-center experience. *Surgical endoscopy*, 30(1), 215-221.

Fanfani, F., Restaino, S., Alletti, S. G., Fagotti, A., Monterossi, G., Rossitto, C., . . . Scambia, G. (2015). TELELAP ALF-X robotic-assisted laparoscopic hysterectomy: feasibility and perioperative outcomes. *Journal of minimally invasive gynecology*, 22(6), 1011-1017.

Fanfani, F., Restaino, S., Alletti, S. G., Fagotti, A., Monterossi, G., Rossitto, C., . . . Scambia, G. (2015). TELELAP ALF-X robotic-assisted laparoscopic hysterectomy: feasibility and perioperative outcomes. *Journal of minimally invasive gynecology*, 22(6), 1011-1017.

Fuchs, K. H. (2002). Minimally invasive surgery. *Endoscopy*, 34(02), 154-159.

Geavlete, B., Saglam, R., Georgescu, D., Multescu, R., Iordache, V., Kabakci, A. S., . . . Geavlete, P. (2016a). The importance of the ergonomy in robotic flexible ureteroscopy versus standard flexible ureteroscopy . *European Urology Supplements*, 15(11), e1.

Geavlete, P., Saglam, R., Georgescu, D., Multescu, R., Iordache, V., Kabakci, A. S., . . . Geavlete, B. (2016b). Robotic flexible ureteroscopy versus classic flexible ureteroscopy in renal stones: the initial Romanian experience. *Chirurgia (Bucur)*, 111(4), 326-329.

Geraghty, R. M., Jones, P., & Somani, B. K. (2017). Worldwide trends of urinary stone disease treatment over the last two decades: a systematic review. *Journal of endourology*, 31(6), 547-556.

Gidaro, S., Buscarini, M., Ruiz, E., Stark, M., & Labruzzo, A. (2012). Telelap Alf-X: a novel telesurgical system for the 21st century. *Surgical technology international*, 22, 20-25.

GitHub. (2019, March 19). Retrieved from Ivan Seidel/Due Timer: https://github.com/ivanseidel/DueTimer

Guillotreau, J., Gamé, X., Mouzin, M., Doumerc, N., Mallet, R., Sallusto, F., . . . Rischmann, P. (2009). Radical cystectomy for bladder cancer: morbidity of laparoscopic versus open surgery. *The Journal of urology*, 181(2), 554-559.

Harnett, B. M., Doarn, C. R., Rosen, J., Hannaford, B., & Broderick, T. J. (2008). Evaluation of unmanned airborne vehicles and mobile robotic telesurgery in an extreme environment. *Telemedicine and e-Health*, 14(6), 539-544.

Healy, K. A., Pak, R. W., Cleary, R. C., Colon-Herdman, A., & Bagley, D. H. (2011). Hand problems among endourologists. *Journal of endourology*, 25(12), 1915-1920.

Heers, H., & Turney, B. W. ((2016)). Trends in urological stone disease: a 5-year update of hospital episode statistics. *BJU international*, 118(5), 785-789.

Hellawell, G., Mutch, S. J., Thevendran, G., Wells, E., & Morgan, R. J. (2005). Radiation exposure and the urologist: what are the risks? *The Journal of urology*, 174(3), 948-952.

Hesse, A., Brändle, E., Wilbert, D., Köhrmann, K. U., & Alken, P. (2003). Study on the Prevalence and Incidence of Urolithiasis in Germany Comparing the Years 1979 vs. 2000. *European Urology*, 44(6),709-713.

Hubens, G., Coveliers, H., Balliu, L., Ruppert, M., & Vaneerdeweg, W. (2003). A performance study comparing manual and robotically assisted laparoscopic surgery using the da Vinci system. *Surgical Endoscopy and other interventional techniques*, 17(10), 1595-1599.

Jaffray, B. (2005). Minimally invasive surgery. *Archives of disease in childhood 90.5* , 537-542.

Kiemeneij, F., Patterson, M. S., Amoroso, G., Laarman, G., & Slagboom, T. (2008). Use of the Stereotaxis Niobe® magnetic navigation system for percutaneous coronary intervention: Results from 350 consecutive patients. *Catheterization and Cardiovascular Interventions*, 71(4), 510-516.

Klein, J. T., Fiedler, M., Kabakci, A. S., Saglam, R., & Rassweiler, J. (2016). PD18-08 MULTICENTER PHASE II STUDY OF THE CLINICAL USE OF THE AVICENNA ROBOFLEX URS ROBOT IN ROBOTIC RETROGRADE INTRARENAL STONE SURGERY. *The Journal of Urology*, 4(195), e406-e407.

Lee, E. C., Rafiq, A., Merrell, R., Ackerman, R., & Dennerlein, J. T. (2005). Ergonomics and human factors in endoscopic surgery: a comparison of manual vs telerobotic simulation systems. *Surgical endoscopy and other interventional techniques*, 19(8), 1064-1070.

Lee, G. I., Lee, M. R., Clanton, T., Sutton, E., Park, A. E., & Marohn, M. R. (2014). Comparative assessment of physical and cognitive ergonomics associated with robotic and traditional laparoscopic surgeries. *Surgical endoscopy*, 28(2), 456-465.

LinuxJournal. (2019, March 21). Retrieved from https://www.linuxjournal.com/article/6429

Lomanto, D., Wijerathne, S., Ho, L. K., & Phee, L. S. (2015). Flexible endoscopic robot. *Minimally Invasive Therapy & Allied Technologies*, 24(1), 37-44.

Lum, M. J., Friedman, D. C., Sankaranarayanan, G., King, H., Fodero, K., Leuschke, R., . . . Sinanan, M. N. (2009). The RAVEN: Design and validation of a telesurgery system. *The International Journal of Robotics Research*, 28(9), 1183-1197.

Mack, M. J. (2001). Minimally invasive and robotic surgery. *Jama*, 285(5), 568-572.

Maeso, S., Reza, M., Mayol, J. A., Blasco, J. A., Guerra, M., A. E., & Plana, M. N. (2010). Efficacy of the Da Vinci surgical system in abdominal surgery compared with that of laparoscopy: a systematic review and meta-analysis.

Matsumoto, E. D., Hamstra, S. J., Radomski, S. B., & Cusimano, M. D. (2002). The effect of bench model fidelity on endourological skills: a randomized controlled study . *The Journal of urology*, 167(3), 1243-1247.

Mattheis, S., Hasskamp, P., Holtmann, L., Schäfer, C., Geisthoff, U., Dominas, N., & Lang, S. (2017). Flex robotic system in transoral robotic surgery: the first 40 patients. *Head & neck*, 39(3), 471-475.

McCulloch, P., Cook, J. A., Altman, D. G., Heneghan, C., & Diener, M. K. (2013). IDEAL framework for surgical innovation 1: the idea and development stages. *Bmj*, 346, f3012.

Miller, K., Benden, M., Pickens, A., Shipp, E., & Zheng, Q. (2012). Ergonomics principles associated with laparoscopic surgeon injury/illness. *Human factors*, 54(6), 1087-1092.

Nickbrookurology. (2019, March 5). Retrieved from ureteroscopy-semi-rigid: http://www.nickbrookurology.com/

Peral Boiza, M. (2018). *DESIGN AND IMPLEMENTATION OF A VIRTUAL REALITY TRAINING PLATFORM PROVIDEDWITH HAPTIC FEEDBACK FOR FLEXIBLE URETERORENOSCOPY INTERVENTIONS WITH AMINIMALLY INVASIVE SURGICAL ROBOT.*

Peters, B. S., Armijo, P. R., Krause, C., Choudhury, S. A., & Oleynikov, D. (2018). Review of emerging surgical robotic technology. *Surgical endoscopy*, 32(4), 1636-1655.

Pigazzi, A., Ellenhorn, J. D., Ballantyne, G. H., & Paz, I. B. (2006). Robotic-assisted laparoscopic low anterior resection with total mesorectal excision for rectal cancer. *Surgical Endoscopy and Other Interventional Techniques*, 20(10), 1521-1525.

Pololu. (2019, March 11). Retrieved from Product: https://www.pololu.com/product/3219

Prezioso, D., Illiano, E., Piccinocchi, G., Cricelli, C., Piccinocchi, R., Saita, A., . . . Trinchieri, A. (2014). Urolithiasis in Italy: An epidemiological study. *Archivio Italiano Di Urologia E Andrologia*, 86(2), 99-102.

Rassweiler, J., Fiedler, M., Charalampogiannis, N., Kabakci, A. S., Saglam, R., & Klein, J. T. (2018). Robot-assisted flexible ureteroscopy: an update. *Urolithiasis*, 46(1), 69-77.

Remacle, M., Prasad, V. M., Lawson, G., Plisson, L., Bachy, V., & Van der Vorst, S. (2015). Transoral robotic surgery (TORS) with the Medrobotics Flex™ System: first surgical application on humans. *European Archives of Oto-Rhino-Laryngology*, 272(6), 1451-1455.

Richard Wolf. (2019, March 9). Retrieved from https://www.richard-wolf.com/en/

Richard Wolf USA. (2019, 9 March). Retrieved from https://www.richardwolfusa.com/home.html

Roboflexusa. (2019, March 7). Retrieved from http://www.roboflexusa.com/

Routh, J. C., Graham, D. A., & Nelson, C. P. (2010). Epidemiological trends in pediatric urolithiasis at United States freestanding pediatric hospitals. *The Journal of urology*, 184(3), 1100-1105.

Saglam, R., Kabakci, A. S., Koruk, E., & Tokatli, Z. (2012). HOW DID WE DESIGNED AND IMPROVED A NEW TURKISH ROBOT FOR FLEXIBLE URETERORENOSCOPE. *JOURNAL OF ENDOUROLOGY* , (Vol. 26, pp. A275-A275).

Saglam, R., Muslumanoglu, A. Y., Tokatlı, Z., Çaşkurlu, T., Sarica, K., Taşçi, A. İ., . . . Traxer, O. (2014). A new robot for flexible ureteroscopy: development and early clinical results (IDEAL stage 1–2b). *European urology*, 66(6), 1092-1100.

Sari, V., Nieboer, T. E., Vierhout, M. E., Stegeman, D. F., & Kluivers, K. B. (2010). The operation room as a hostile environment for surgeons: physical complaints during and after laparoscopy. *Minimally Invasive Therapy & Allied Technologies*, 19(2), 105-109.

Sas, D. J., Hulsey, T. C., Shatat, I. F., & Orak, J. K. (2010). Increasing incidence of kidney stones in children evaluated in the emergency department. *The Journal of pediatrics*,, 157(1), 132-137.

Scales, C. D., Smith, A. C., Hanley, J. M., Saigal, C. S., & Project Urologic Diseases in America. (2012). Prevalence of kidney stones in the United States. *European urology*, 62(1),160-5.

Simorov, A., Otte, R. S., Kopietz, C. M., & Oleynikov, D. (2012). Review of surgical robotics user interface: what is the best way to control robotic surgery? *Surgical endoscopy*, 26(8), 2117-2125.

Smithers, B. M., Gotley, D. C., Martin, I., & Thomas, J. M. (2007). Comparison of the outcomes between open and minimally invasive esophagectomy. *Annals of surgery*, 245(2), 232.

Sofia, N. H., & Walter, T. M. (2016). Prevalence and risk factors of kidney stone. *Global Journal For Research Analysis*, 5(3), 183-187.

Sorokin, I., Mamoulakis, C., Miyazawa, K., Rodgers, A., Talati, J., & Lotan, Y. (2017). Epidemiology of stone disease across the world. *World journal of urology*, 35(9), 1301-1320.

St. (2019, March 18). Retrieved from X-NUCLEO-IHM04A1: https://www.st.com/b/en/ecosystems/x-nucleo-ihm04a1.html#

Su, L. M., Stoianovici, D., Jarrett, T. W., Patriciu, A., Roberts, W. W., Cadeddu, J. A., . . . Kavoussi, L. R. (2002). Robotic percutaneous access to the kidney: comparison with standard manual access. *Journal of Endourology*, 16(7), 471-475.

Toowoombaurology. (2019, March 4). Retrieved from General Urological Procedures: http://toowoombaurology.com.au/general-urological-procedures/urs/

Türk, C., Petřík, A., Sarica, K., Seitz, C., Skolarikos, A., Straub, M., & Knoll, T. (2016). EAU guidelines on interventional treatment for urolithiasis. *European urology*, 69(3), 475-482.

Wignall, G. R., Cadeddu, J. A., Pearle, M. S., Sweet, R. M., & McDougall, E. M. (2008). Surgical simulation: a urological perspective. *The Journal of urology*, 179(5), 1690-1699.

Wikipedia. (2019, March 9). Retrieved from Urinary System: https://en.wikipedia.org/wiki/Urinary_system

Worcester, E. M., & Coe, F. L. (2010). Clinical practice. Calcium kidney stones. *The New England journal of medicine*, 363(10), 954-63.

Yasui, T., Iguchi, M., Suzuki, S., & Kohri, K. (2008). Prevalence and epidemiological characteristics of urolithiasis in Japan: national trends between 1965 and 2005. *Urology*, 71(2), 209-213.

Zhang, L. A., Khare, R., Wilson, E., Wang, S. X., Peters, C. A., & Cleary, K. (2014, May). Robotic assistance for manipulating a flexible endoscope. *IEEE International Conference on Robotics and Automation (ICRA)*, (pp. 5380-5385). IEEE.

Zhang, L., Khare, R., Wilson, E., Martin, A., Wu, K., Swords, K., . . . Peters, C. A. (2013,June). Mechanical Drive System for Enhancing Flexible Endoscopy: System Concept and Prototype Development. *In The Hamlyn Symposium on Medical Robotics*, (p. 23).